# ADDIS ABABA UNIVERSITY

## SCHOOL OF GRADUATE STUDIES

## COLLEGE OF NATURAL AND COMPUTATIONAL SCIENCES

## SCHOOL OF EARTH SCIENCES

# INTEGRATED GEOPHYSICAL INVESTIGATIONS OF THE CENTRAL MAIN ETHIOPIAN RIFT AND ADJACENT PLATEAUS: AN IMPLICATION TO CRUSTAL STRUCTURE AND MOHO DEPTH DETERMINATIONS

**A THESIS SUBMITTED TO**

**THE SCHOOL OF GRADUATE STUDIES OF ADDIS ABABA UNIVERSITY IN PARTIAL FULFILLMENT OF THE REQUIREMENTS FOR THE DEGREE OF MASTER OF SCIENCE IN EARTH SCIENCES (GEOPHYSICS)**

**BY**

**YEMANE KELEMEWORK**

**ADDIS ABABA UNIVERSITY**

**ADDIS ABABA, ETHIOPIA**

**JUNE, 2016**

**ADDIS ABABA UNIVERSITY**

**SCHOOL OF GRADUATE STUDIES**

**SCHOOL OF EARTH SCEINCES**

This is to certify that the thesis prepared by **Yemane Kelemework**, entitled: **"Integrated geophysical investigations of the central Main Ethiopian Rift and adjacent plateaus: an implication to crustal structure and Moho depth determinations"** and submitted in partial fulfillment of the requirements for the degree of Master of Science in Geophysics complies with the regulations of the university and meets the accepted standards with respect to originality and quality.

Approved by examining committee:

| | Signature | Date |
|---|---|---|
| Dr. Balemwal Atnafu<br>(Head, School of Earth Sciences) | _____ | _____ |
| Dr. Abera Alemu<br>(Advisor) | _____ | _____ |
| Dr. Ameha Atnafu<br>(Co - Advisor) | _____ | _____ |
| Prof. Tilahun Mammo<br>(Examiner) | _____ | _____ |
| Dr. Bekele Abebe<br>(Examiner) | _____ | _____ |

# DECLARATION

I, the undersigned, hereby declare that the thesis entitled with **"Integrated geophysical investigations of the central Main Ethiopian Rift and adjacent plateaus: an implication to crustal structure and Moho depth determinations"** is my original work carried out under the supervision of Dr. Abera Alemu and Dr. Ameha Atnafu and has not presented to any university or institution for the award of any degree or diploma program and all sources of materials used for the thesis are duly acknowledged.

| Name of the candidate | Signature | Date |
|---|---|---|
| Yemane Kelemework | _____ | _____ |

This is to certify that the above declaration made by the candidate is correct to the best of our knowledge and it has been submitted for examination with our approval as university advisors.

| | Signature | Date |
|---|---|---|
| Dr. Abera Alemu<br>(Advisor) | _____ | _____ |
| Dr. Ameha Atnafu<br>(Co - Advisor) | _____ | _____ |

# ABSTRACT

Compilation of newly acquired magnetic and existing gravity, magnetic and seismic data were carried out to examine nature of the crustal structure, probable depth to Moho and density distributions of the crust in the central Main Ethiopian Rift and adjacent plateaus. Data enhancement (filtering) techniques have been applied to the observed gravity and magnetic data in order to highlight the effects of deep seated and shallow origin geologic sources. The compiled Bouguer gravity anomaly map and its derivatives (regional, residual maps) and gravity profiles constructed along selected lines reveal minimum anomalies over the south east and south west plateaus, superimposed with relatively high values over the major volcanic centers and high density rift floor. Correspondingly, the compiled magnetic anomaly map including its derivatives (regional and residual maps) and magnetic profiles constructed along selected lines reveal that the volcanic centers residing the rift floor are associated with relatively high magnetic anomalies as compared to the relatively low magnetic anomalies associated with the sediment dominate rift lakes and parts of the highlands. Close examination of the regional and residual gravity and magnetic anomaly maps and enhancement techniques reveal that the Quaternary volcano-tectonically active zones of the Wonji Fault Belt (WFB) and Silti DebreZeit Fault Zone (SDZFZ) with a general NNE - SSW to N - S trending anomaly zones are interpreted to underlie by shallow magmatic intrusions and/or magmatic chambers. In addition, our result confirms the presence of deep and regional E-W trending anomaly zone in the south west of the study area which is assumed to be coincident with the Goba-Bonga transverse tectonic lineament and associated Wagebeta caldera complexes. Based on the evidences derived from 2-dimensional gravity modeling and seismic data, the crustal thickness (Moho depth) in the study area varies from 35 – 40 km beneath SW plateau, 38 - 39 km under the rift floor and ranges from 42 - 43 km beneath the SE plateau. Our investigation results generally support the idea which suggests that rift extension and crustal deformation in the central Main Ethiopian Rift are currently concentrated in the Quaternary volcano-tectonically active zones of the Wonji Fault Belt, Silti DebreZeit Fault Zone and the Goba-Bonga tectonic lineaments.



***Keywords:*** Central Main Ethiopian Rift; Bouguer gravity anomaly; magnetic anomaly; receiver function; crustal thickness.

# ACKNOWLEDGEMENTS

This MSc thesis work was funded by the School of Earth Sciences of Addis Ababa University and Geo-power Africa.

I would like to express my feeling of gratitude to my advisors, Dr. Abera Alemu and Dr. Ameha Atnafu, for their excellent supervision, guidance, reviewing the thesis and providing all the relevant literatures and information for the success of this MSc thesis work.

Special thanks go to Prof. Tilahun Mammo, Ato Ayele (senior geophysicist) and Prof. Tigistu Haile for their fruitful and supportive discussions on various aspects of the thesis and geophysical software manipulations.

I would like to thank Dr. Balemwal Atnafu, head of the School of Earth Sciences of Addis Ababa University for his invaluable support and field arrangement.

My special thanks go to Ato. Wondwosen Sisay for his incredible support and assistance in the magnetic data collection.

I would like to thank the PhD candidates of the geophysics stream at the School of Earth Sciences of Addis Ababa University, especially Mr. Addis and Mr. Haileyesus for assisting me in processing gravity and magnetic data using Geosoft Oasis Montaj software.

I am also thankful to Ato. Samuel Getachew and Ato. Abate Assen for their excellent guidance and assistance in Arc GIS software manipulation.

Finally I would like to express my deepest gratitude to all graduate students of the geophysics stream for their discussion and encouragement for the success of this MSc thesis work.

# TABLE OF CONTENTS

## LIST OF FIGURES

## LIST OF ACRONYMS

| | |
|---|---|
| 2D | Two dimensional |
| 3D | Three dimensional |
| CMER | Central Main Ethiopian Rift |
| ER | Ethiopian Rift |
| EARS | East African Rift System |
| FFT | Fast Fourier Transform |
| GPS | Geographic positioning system |
| GSE | Geological survey of Ethiopia |
| IGRF | International Geomagnetic Reference Field |
| IGSN | International Gravity Standardization Network |
| MER | Main Ethiopian Rift |
| msl | Mean sea level |
| nT | Nano Tesla |
| NE | North East |
| NE –SW | North East – South West |
| N - E | North – East |
| NMER | Northern Main Ethiopian Rift |
| NNE | North North East |
| NW | North West |
| NW- SE | North West – South East |
| NNE – SSW | North North East – South South West |
| NNW | North – North –West |
| N – S | North – South |
| SDZFZ | Siliti Debre Zeit Fault Zone |

| | |
|---|---|
| SE | South East |
| SI | Structural Index |
| SMER | Southern Main Ethiopian Rift |
| SSW | South South West |
| S –W | South – West |
| SW | South West |
| WFB | Wonji Fault Belt |

# CHAPTER ONE

# INTRODUCTION

## 1.1 General background

The Main Ethiopian Rift (MER) is the northern terminus of the East African Rift system and forms a major graben from about $6^0$ N in southern Ethiopia to about $9^0$ N where it starts to funnel out into the Afar Depression (Tadiwos Chernet et al., 1998). According to Ebinger (2005) the Main Ethiopian Rift is a magmatic rift that records all the different stages of rift evolution from rift initiation to break up and incipient oceanic spreading. Thus the Main Ethiopian Rift is considered to be an ideal place to analyze the evolution of continental extension, the rupture of lithospheric plates and the dynamics by which distributed continental deformation progressively focuses at oceanic spreading centers (e.g., Corti, 2009).

The most voluminous eruptive stage in Ethiopia was during the late Oligocene-Early Miocene (32-21 Ma) with most of the volcanic activity occurring between 30 and 29.5 Ma, followed by a central Ethiopian volcanic episode from 13 to 9 Ma and a period of volcanism in central Afar from 4.5 to 1.5 Ma (Ukstins et al., 2002 and references therein). Significantly older volcanic rocks have been dated at 45 Ma in southern Ethiopia. As a result most of the geologic sections exposed along the rift margins are dominated by Tertiary volcanic rocks except for a few locations where crystalline basement is unconformably overlain by Mesozoic sedimentary and/or Tertiary volcanic rocks (Gidey WoldeGabriel et al., 1990). These tertiary volcanic rocks was followed by the Quaternary (<1.6–1.8 Ma), bimodal volcanic rocks (lava, pyroclastics and volcanoclastic strata) which were generally closely associated with Wonji Fault Belt (WFB) affecting the rift floor [e.g., Gidey WoldeGabriel et al., 1990].

The rift floor is typically down thrown 500–1000 m below the bounding plateau. The structural margins of the MER, where not obscured by trachytic and rhyolitic centers, are normal step faults and antithetic normal faults (Tadiwos Cherenet et al., 1998). These fault systems shows a general trending structure of NE-SW (Boccaletti et al., 1998). A more recent structural feature of the MER is the Wonji Fault Belt (WFB); a 5–12-km-wide belt of intense normal faulting and volcanism related to the Quaternary episodes of extension (Tadiwos Cherenet et al., 1998).

As suggested by Boccaletti et al. (1998) the WFB is characterized by active NNE–SSW trending extension fractures and normal faults.

Geophysical observations in the MER can be used to map lithospheric properties and spatial variations in extension and magmatism, and provide a critical third dimension to constrain models of rift evolution (Keranen and Klemperer, 2008). These observations provide insight not only into the inherited structures which control rift evolution, but also into spatial variations in extension and magmatism which result from irregularities in rift evolution and therefore serve as markers of the extensional process. Accordingly, different geophysical studies have been conducted in the Main Ethiopian Rift. For example, a controlled source seismic experiment was undertaken in the central and northern sectors of the Main Ethiopian Rift for the aim of investigating the transition from continental rifting to oceanic spreading and how continental rifts develop into oceanic ridges (Maguire et al., 2003; 2006). Along the rift axis the crustal depth increases from 30 km in the southern Afar to 40 km in the central Main Ethiopian Rift region (Keller et al., 2004; Mickus et al., 2007). Despite many geophysical studies which were conducted within the Afar depression and MER, detailed understanding of the structure of the rift has not yet been achieved (Abera Tessema and Antoine, 2004). This is largely because of the limitation of geophysical and geological data. This indicates that to improve our understanding about the nature of crustal structure and Moho depth additional geophysical and geological data is required.

In the present study, gravity, magnetic and seismic data have been compiled, processed and interpreted to examine the crustal structure and depth to the Moho beneath the central MER and adjacent plateaus. Further, based on the results of Bouguer gravity and magnetic anomaly maps and profiles, this paper attempts to describe the tectonic and geologic implications of the study area.

## 1.2 Description of the study area

### 1.2.1 Location and accessibility

The study area is located in the central part of Main Ethiopian Rift which is about 240 km south of Addis Ababa (Fig 1.1).

Geographically, it is bounded between$7^0$ $00^{'}$ $00^{''}$ – $8^0$ 02’00’’ N latitude and $37^0 30^{'} 00^{''}$ - $39^0$ 02’$00^{''}$ E longitude. The study area can be accessed through the Addis Ababa - Shashemene - Awasa asphalt road.

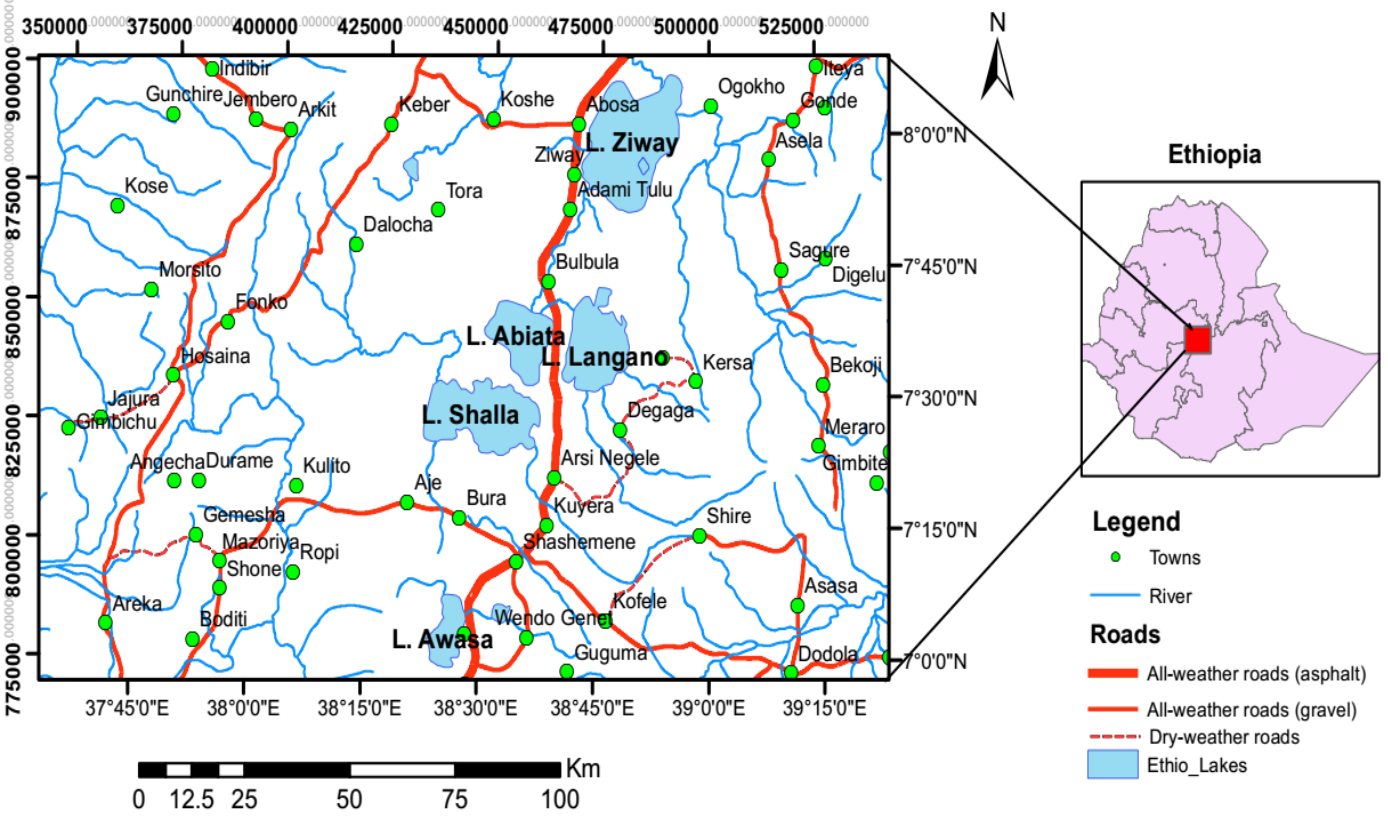


**Figure 1.1** Location map of the study area

### 1.2.2 Physiography

The Ethiopian sector of the East African Rift system extends for more than 1000 km in a NE-SW to N-S direction from the Afar depression, at Red Sea-Gulf of Aden junction, southwards to the Turkana depression. The MER which estimated to be about 80 Km wide, separates the uplifted Somalian and Ethiopian plateau and these plateaus rises more than 2000m above mean sea level. The rift floor increases in elevation from the Turkana depression up to the main watershed between the Meki and Awash rivers north of Lake Ziway. To the north direction the elevation of rift floor decreases as we move to the Afar depression, and obtains a value below mean sea level in the Dallol area. Hence, the rift valley in general and the study area in particular shows a local increase and/or decrease in elevation due to the volcanic centers/edifices and fault scarps.

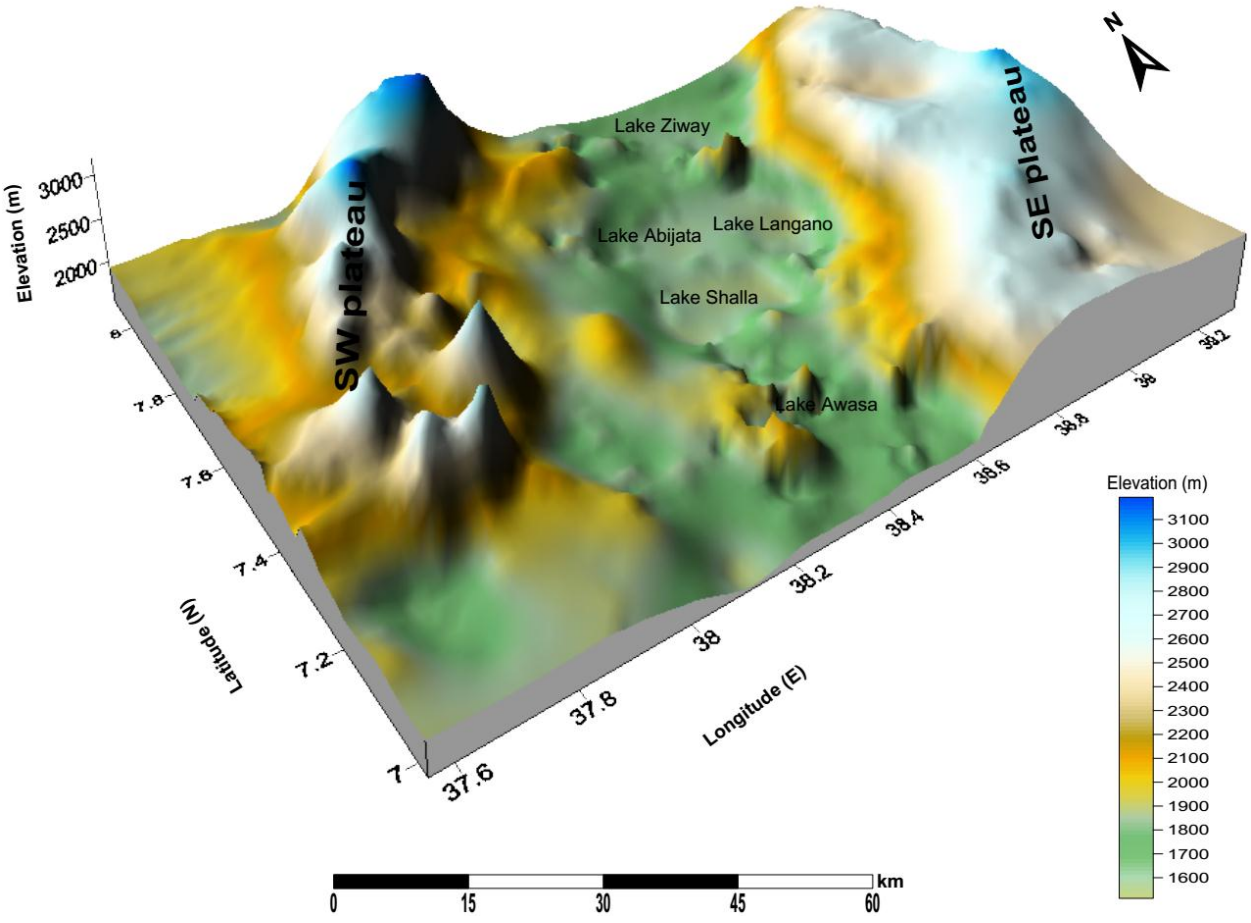


**Figure 1.2** 3D physiographic map of the CMER and adjacent plateaus

## 1.3 Climate, drainage and vegetation

The study area lying in the subtropical climate is characterized as humid (high land, "Dega to Weina Dega") to arid (low land, "Kola") climatic zones (EIGS, 2012). The western and eastern rift escarpments are relatively cold. The annual average temperature varies approximately from $27^0$C in the rift floor to $13^0$C at the adjacent plateaus. Generally the area gains an annual rainfall of less than 750mm on the rift floor and about 1250mm on the highlands.

The main river of the study area is the Bilate River which is located on the western part. In addition, there are several minor and major tributaries that drains to the main river system and/or lakes. The rift floor is dominated by five major lakes: Lake Ziway, langano, Abijata, Shalla and Awassa from north to south respectively. All the tributaries around these lake regions flow to the lake.

The nature of vegetation growing on the highlands and rift floor are different. Generally the highland is dominated by Junipers, Hagenia, Abyssinica, Podacarpus Grcilior (Zigiba), and Vernonia. Whereas the low lands and rift floor are dominated by Prosopis Juliflora, Acacia (Girar), Shrubs, bushes.

## 1.4 Population and settlement

The study area is located partly in the Oromia regional state and partly in the Southern nations nationalities and peoples regional state of Ethiopia. The western part and southern extremities of the study area are inhabited by southern nations nationalities and peoples of Ethiopia, whereas the central and northern part of the study area is inhabited by Oromo peoples. Population settlement is dense in towns and villages. Of course, the towns are inhabited by multiethnic peoples. However, there are also peoples sparsely inhabited in the whole study area. Generally, the peoples in the study area are Christian and Muslim religion followers.

The livelihood of the peoples can be characterized by mixed farming which exercises ploughing and cultivating of crops and animal production. There are also peoples working in irrigation activities following the lakes and major rivers found in the rift floor.

## 1.5 Statement of the problem

The East African Rift System where the Main Ethiopian Rift takes northern part, is a magmatic rift that records all the different stages of rift evolution from rift initiation to break-up and incipient oceanic spreading and hence it is an interesting place to study the evolution of continental extension, the rupture of lithospheric plates and its dynamics (e.g. Ebinger, 2005; Corti, 2009).

As a result, different geological, structural and geophysical investigations were carried out in the northern, central and southern Main Ethiopian Rift, though there is still a debate regarding its evolution. Due to the presence of a relatively large volumes geological and geophysical data, the northern MER is fairly known in terms of its crustal structure and volcano-tectonic deformation. In contrast, the crustal structure and Moho depth beneath the central MER and adjacent plateaus has not been investigated in detail as that of the northern MER. In addition, there is no sufficient magnetic data collected in the central Main Ethiopian Rift in particular and the MER as a whole.

Therefore, to improve our knowledge about the nature of the crustal structure and depth to Moho of the central MER and adjacent plateaus, a synthesis of a newly acquired magnetic data and the existing gravity, magnetic and seismic data has been carried out. This study also compares the present reprocessed Bouguer gravity and magnetic anomaly and seismic investigations results with those of the previous geophysical investigation results carried out in the study area and the MER as a whole. Furthermore, the present MSc thesis research attempts to correlate findings of the integrated geophysical surveys considered with geological and tectonic features of the central MER and adjacent plateaus in relation to the evolution of the Main Ethiopian Rift.

## 1.6 Research questions

The research questions that necessitated us to identify the research problem are formulated as follows:

- What does the crustal structure in the CMER and the adjacent plateaus look like?
- How do the distribution of the Bouguer gravity anomalies and magnetic anomalies correlate in the study area?
- How does the Moho depth vary over the rift floor and the adjacent plateaus?

In order to answer the above formulated research questions the general and specific objectives of the present MSc thesis work is designed as follows.

## 1.7 Objectives of the study

### 1.7.1 General objective

The main objective of this thesis is to examine the nature of the crustal structure and depth to Moho underlying the central MER and adjacent plateaus using new magnetic and existing gravity, magnetic and seismic data.

### 1.7.2 Specific objectives

The specific objectives of this research are:

- To compile Bouguer gravity and magnetic anomaly maps of the study area
- To determine the crustal structure model of the central MER and the adjacent plateaus
- To determine depth to the Moho in the study area using the integrated geophysical data considered for this MSc research work

- To identify the prominent geologic and tectonic features of the central MER and the adjacent plateaus by correlating the results of the integrated geophysical surveys and previous works of other researchers

## 1.8 Expected outcome and Significance/contribution of the study

The possible outcomes of this MSc research work can be summarized as follows;

- This research work attempts to determine the spatial variations of the crustal structure and depth to Moho underlying the central Main Ethiopian Rift and adjacent plateaus.
- It presents a complete gravity and magnetic anomaly map of the study area using new and existing gravity and magnetic data.
- This study identifies areas associated with positive and negative Bouguer anomaly and its relationship with geologic and tectonic features
- It describes the relationship between the magnetic anomaly maps and profiles with their probable geologic and tectonic implications of the study area.
- Generally, this paper attempts to synthesize and integrate the current geophysical and geological investigations with previous geophysical, structural and geological works which contribute to the understanding and modeling of rifting process in the study area and MER as a whole.

The present research work will play its own role for the betterment of scientific work and community services. Hence some of the most important contribution of the study can be presented as follows;

- It provides a more reliable and recent geophysical data that can be used to determine the nature of crustal structure and depth to Moho and its implication for rift extension.
- Since the study area is located in the central Main Ethiopian Rift where the WFB is part of it, integrated geophysical, structural and geological study helps to understand the nature of rift development and associated natural resources.
- Identifying areas associated with positive and negative Bouguer gravity anomaly will be very important for understanding the density distribution within the crust and gives an insight to magma assisted rift extension

- ❖ Findings obtained from this study and geodynamic interpretations in the region together with the results of other geophysical and geological investigations produce a probable crustal model of the study area.
- ❖ The new magnetic data collected in this survey can be used by later researchers for further investigations of the rift.

## 1.9 Previous geophysical works and present study

The East African Rift System has long been recognized as a continental extension of the World Rift System (Fairhead, 1976 and references therein). Accordingly, different geophysical works have been conducted in the Ethiopian Rift and Afar depression and some of them will be discussed as follows.

According to Gouin (1970) reconnaissance gravity surveys carried out in Ethiopia by the Geophysical Observatory have revealed a broad negative Bouguer anomaly over the entire Ethiopian – Somalian swell. This anomaly has a minimum near the central part of Ethiopian Rift valley and thought to be caused by low density upper mantle (possibly asthenosphere) underlying the Ethiopian highlands (Searle and Gouin, 1972). The Main Ethiopian Rift, as compared to Ethiopian – Somalian swell, shows relative positive Bouguer anomalies and locally superimposed much narrower positive anomalies which have been interpreted as being due to intrusions associated with the Wonji Fault belt (Gouin and Mohr, 1964 in Gouin, 1972).

Thus the intensity of gravity field is closely connected to the morphological features. On the high plateaus the gravity minima are located in areas of maximum elevation (Makris et al., 1975). Descending from the highlands to Afar the gravity intensity changes to less negative values, and hence the gravity level in Afar increases with decreasing elevation and reaches zero – gravity level at the coast of Red sea (Makris et al., 1975).

The PhD work of Abera Alemu (1992) on the MER has tried to correlate the gravity trends with prevailing structural features and accordingly, the rift floor and belts of synclinal structures have been correlated with the axes of the positive anomalies while the negative axes have been correlated to the uplifted regions and belts of anticlinal structures.

Further regional gravity data have been collected for example by the Ethiopian Geological Survey and by Ebinger (1991) and have produced 3D density models beneath the MER (Rezene Mahatsente et al. 1999; Tiberi et al., 2005). A thinned crust beneath the rift axis (≤ 30km) with segmented high density upper and lower crustal intrusion beneath the surface magmatic segments which was attributed to melt resulting from partial melting of the lithospheric mantle was inferred (Rezene Mahatsente et al., 1999).

Shallow Moho exists beneath the rift (32 to 33 km) that thins to (C. 24 km) north wards to Afar with a C. 40 km thick crust being present beneath the broad uplifted Oligocene flood basalt province (Tiberi et al., 2005).

The present study relates to previous geophysical works in examining the temporal and spatial variations of crustal structures and probable depth to Moho across the rift floor, along the rift and adjacent plateaus. All the previous works are based on compilation and interpretation of gravity and seismic data. However, the current study introduces a new interpretational approach using new and existing gravity and magnetic data. Therefore, the aim of this work is to interpret the Bouguer gravity and magnetic anomaly maps and profiles to determine the crustal thickness, depth to Moho and the overall density distribution within the crust of central MER and adjacent plateaus.

## 1.10 Materials and methodology

### 1.10.1 Materials and software

The first step in every research is to identify the available materials and data needed to solve the problem formulated/identified. Therefore, for the present study the following materials and software have been utilized.

- Topographic map with a scale of 1:50,000 and Brunton compass were used during field survey
- Several geological map have been reviewed to know the surficial distribution of lithological and structural features
- Google earth online to help assessment of the area before going to the field
- Proton precession magnetometer (MP-2) for magnetic data collection

- Global positioning system (GPS) to record the exact data location point and digital camera for photographing
- Arc GIS 10.3 for the preparation of location and base map and other GIS analysis
- Global mapper 12 and surfer 10 to post, extrapolate and analyse gravity and magnetic data
- Geo-soft for processing, presenting and interpreting of geophysical data (i.e. gravity and magnetic data)

## . 1.10.2 Methodology

Any research project requires an appropriate and feasible methodology. Hence to achieve the general and specific objectives mentioned earlier the methodology involves three steps. These steps are classified as pre-field work, field work and post-field work.

### 1.10.2.1 Pre-field work

Identifying and reviewing of previous works relevant to the present work are very important and it was the first step in this study. Therefore the activities carried out in this step include;

- Identification and interpretation of topographic maps, aerial photographs and geological maps
- Literature review on geological and tectonic setting of the study area and the MER in general
- Identifying and reviewing of relevant previous geophysical works (gravity, seismic and magnetic) has been made.
- Obtain the available secondary data (gravity, magnetic and seismic) in the area for re-processing using the latest processing techniques available.

### 1.10.2.2 Field work

Field work was one of the most important parts of this study. Under this step all the necessary primary geological and geophysical data have been collected as follows;

- Acquisition of magnetic data using a proton precision magnetometer MP-2 have been carried out to fill the existing gaps in magnetic data coverage over the central MER and the adjacent plateaus.
- The magnetic data were collected randomly with average station spacing of 2-4 Km depending on the objectives, accessibility and field geological conditions.
- The magnetic data were collected by establishing a base station and at each station magnetometer reading, time and elevation were recorded. Each base station was recovered (revisited) every 2 or 3 hours depending on the survey design.
- Using all the measurements the magnetic data were corrected for diurnal and dipole variations
- Field observations on selected geological and structural features have been made

**1.10.2.3 Post field work**

The primary data collected during field work and available secondary data have been processed and re-processed using different software packages. This software's include Geo-Soft, Arc GIS, surfer, and global mapper. Then the results present in the form of geophysical anomaly maps and profiles. Finally, the result has been qualitatively and quantitatively interpreted and correlated with previous works to produce a probable crustal thickness and depth to Moho model in the study area.

Generally the general frame work of the study can be summarized by the following flowchart (Fig.1.3).

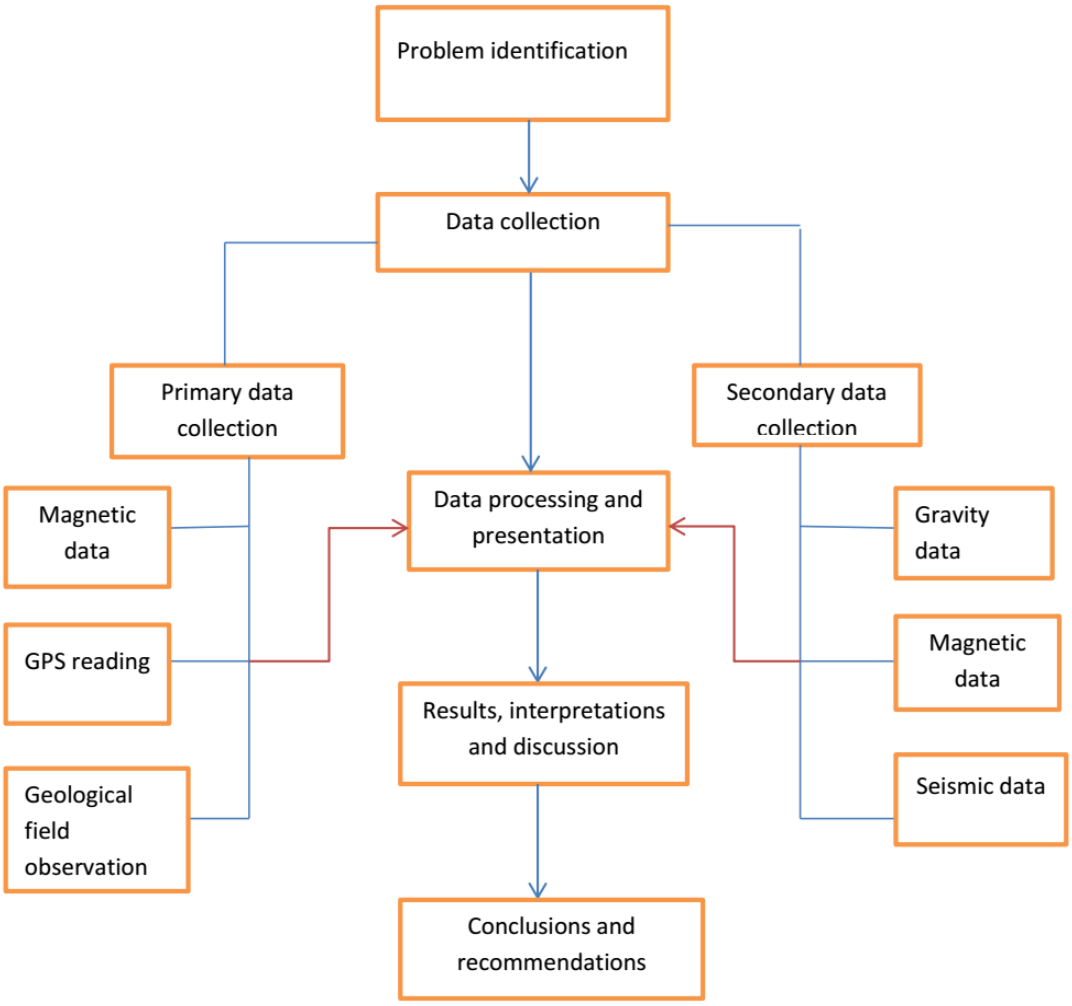


**Figure 1.3** Flow chart showing the general frame work of the study

## 1.11 Limitations of the present study

The integrated interpretation of Bouguer gravity anomaly and magnetic anomaly is relatively good in the rift floor. However, due to limited magnetic data coverage in the adjacent plateaus, it is almost solely interpreted using only gravity data. The Moho depth was determined using limited set of seismic data.

## 1.12 Structure of the thesis

This thesis work is organized into eight chapters. The first chapter deals with the general background of the study area. It briefly introduces the general frame work of the Main Ethiopian Rift (MER) in relation to the great East African Rift System (EARS). Specifically, it introduces the location and physiography of the study area, the nature of climate, drainage system and population density and settlement of the study area. It explains the problem of statement of the study and the associated research questions formulated to solve the problem. This chapter also includes the general and specific objective of the study, its contribution to the scientific world and the methodology adopted to solve the problem and the materials utilized. Further, it briefly justifies the previous geophysical works conducted in the study area and MER as a whole and its relationship with the present study. Finally, it indicates the limitations encountered and the overall structure of the thesis.

The second chapter deals with the geologic and tectonic setting of the study area. It discusses separately the regional geology and tectonic frame work of the CMER in particular and MER in general. The general stratigraphy and outcrop distribution of the study area have been also summarized. For detail discussion different available and new geologic and tectonic maps has been used.

Chapter three discusses the theoretical background of the geophysical methods of investigation compiled from different sources. This chapter explains briefly the principles, instrumentations, data reduction processes and interpretations followed in both gravity and magnetic methods of prospecting.

The fourth chapter deals with the instrumentation, data acquisition and surveying procedures, data distribution and processing techniques of both gravity and magnetic methods employed in this thesis work. In addition, it explains the different filtering and data enhancement techniques used in this work.

Chapter five presents the results obtained and its interpretations. It presents the different Bouguer gravity anomaly and magnetic anomaly/intensity maps. Here the results have been tried to interpret from regional and local perspectives of the CMER and adjacent plateaus.

The sixth chapter deals with Moho depth investigations using seismic data (data obtained from receiver function and surface wave dispersion) and 2D gravity modeling.

Chapter seven, deals with discussions and implications of the present study. It discusses the overall findings of the study by integrating the Bouguer gravity and magnetic anomaly/intensity maps and its geological and tectonic implications. Here, we have tried to correlate the present findings with previous geological and geophysical works and discussed accordingly.

Chapter eight, deals with conclusions and recommendations of the present investigations. This chapter concludes the major findings of the study and forwarded some recommendations for further research works.

# CHAPTER TWO

# GEOLOGIC AND TECTONIC SETTING

## 2.1 Regional geology

The Ethiopian Rift (ER) is part of the East African Rift System (EARS) and comprises a series of rift zones extending over a distance of about 1000 Km from the Afar Triple Junction at Red Sea – Gulf of Aden intersection to the Kenya Rift (Fig.2.1) (e.g., Boccaletti et al., 1999). The seismically and volcanically active Main Ethiopian rift is one of few places worldwide where rift evolution from broadly distributed to focused strain can be followed (Ebinger and Casey, 2001).

The MER is divided geographically into three sectors: northern, central, and southern MER (Gidey WoldeGabriel et al., 1990; Bonini et al., 2005 and references therein). The MER divides the 1,000-km-wide uplifted Ethiopian volcanic province asymmetrically into the northwest and southeast plateaus (Gidey WoldeGabriel et al., 1990). Volcanic sequences that cover an area several hundred kilometers across are more voluminous and widespread on the northwest plateau than on the opposite side.

The Northern MER is considered to extend from the true Afar depression up to the Lake Koka region following the middle course of the Awash River valley (Bonini et al., 2005). As indicated by Tadiwos Chernet et al. (1998); Wolfenden et al. (2004) early synrift volcanism in the area has been started at about 10–11 Ma. The Central MER encompasses most of the Lakes Region, up to the Lake Awasa area (Bonini et al., 2005). Gidey WoldeGabriel et al. (1990) suggested that the age of the earliest synrift volcanic deposits in this sector is estimated to be ~8 Ma. The Southern MER extends south of Lake Awasa into the ~300-km-wide system of basins and ranges that characterizes the overlapping area between the Ethiopian and Kenya Rifts (Bonini et al., 2005 and references therein). In this rift sector volcanism started in the early Miocene around 18–21 Ma.

These three segments as represents different stages of extensional process, from early rifting in the Southern MER to more evolutes stages in the Central and Northern MER preceding the incipient seafloor spreading in Afar (Hayward and Ebinger, 1996). However, the age of onset of faulting and volcanism outlined above for the three rift segments point to a heterogeneous time-space evolution and progression of the continental rifting process along the MER.

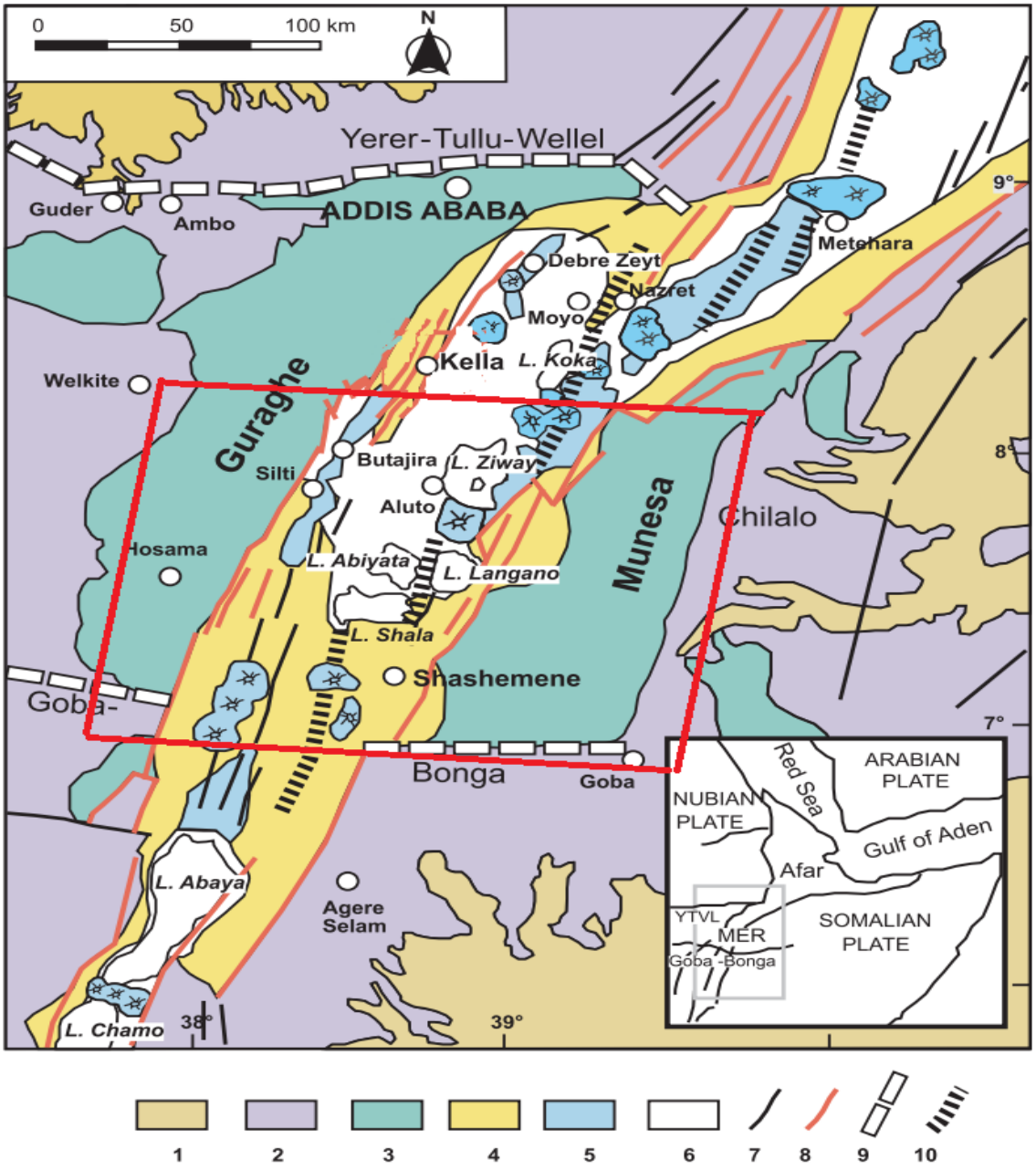


**Figure 2.1** Simplified geological map of central Ethiopia (after Tsegaye Abebe et al., 2010). (1) Pre-Tertiary sediments and crystalline basement, (2) Oligocene (32–29 Ma) and lower Miocene (12–8 Ma) plateau volcanics, (3) Miocene–Pliocene rift-shoulder trachytic–rhyolitic volcanics and pyroclastic layers, (4) Plio-Pleistocene rift floor, (5) Quaternary central volcanics and basaltic lava flows, associated scoria cones and phreato-magmatic deposits, (6) Quaternary lacustrine sediments and interbedded pyroclastics, (7) faults, (8) major rift border faults, (9) major transversal tectonic lineaments in the basement, (10) Wonji Fault Belt segments. In the inset: YTVL, Yerer-Tullu-Wellel volcano-tectonic lineament. The study area is indicated by red rectangle.

Apart from some fluvio-lacustrine sediment, which was deposited on the rift floor, the Main Ethiopian Rift is dominated by Tertiary and Quaternary volcanic (Tsegaye Abebe et al., 2010). However, there is one exception outcrop of Precambrian crystalline rocks overlaid by Mesozoic sediments at the base of Guraghe escarpment near Kella village. Apart from Kella, basement rocks in the Main Ethiopian Rift are exposed in the extreme south and in the Northern Afar (Tsegaye Abebe et al., 2010).

The volcanic products of the whole Ethiopian Rift has been subdivided into six main tectono-magmatic chronozones since the Eocene – Oligocene and among these the WFB-related volcanism represents the most recent volcano-tectonic activity in the MER (Gidey WoldeGabriel et al., 1990).

According to Gidey WoldeGabriel et al. (1990); Ebinger et al. (1993) the tectonic development of the MER is matched by intense volcanic activity ranging in age from the late Eocene up to historical times. Volcanism started during the Eocene-late Oligocene with the eruption of flood basalts that have generally been related to either one or two mantle plumes impinging the base of the lithosphere under Afar or Afar-Northern Kenya rifts (e.g., Ebinger and Sleep, 1998; George et al., 1998; Rogers et al., 2000). The oldest flood basalts crop out in the broadly rifted zone of Southern Ethiopia and are of Eocene in age (~ 45 Ma (Ebinger et al., 1993; George et al., 1998). According to Hofmann et al. (1997) and Ukstins et al. (2002) flood basalts forming the Ethiopian Plateau instead apparently erupted in a rather short time interval (<5 Ma) with the greatest eruption rates occurring from 31 to 28 Ma. Starting from these early episodes of volcanism, magmatic activity in the MER was episodic rather than continuous (Gidey WoldeGabriel et al., 1990). As suggested by (Ebinger et al., 1993) a second episode of flood basalt volcanism has been described in the southern Ethiopia at 18–11 Ma and in the MER-Afar transition zone at about 10–11 Ma (Tadiwos Chernet et al., 1998; Wolfenden et al., 2004). In the Central MER, early eruption of flood basalts was locally followed by undersaturated intermediate and acidic rocks (at ~17–12 Ma (Bonini et al., 2005 and references therein) and by eruption of late Miocene (~11–8 Ma) basalts and subordinate silicic flows (e.g., Gidey WoldeGabriel et al., 1990; Tsegaye Abebe et al., 1998; Tadiwos Chernet et al., 1998). After these episodes of prerift activity (with widespread flood basalts and subordinate felsic products), rifting in the various MER sectors was characterized by volcanism with fundamentally bimodal character (Bonini et al., 2005).

Widespread late Miocene-Pliocene rhyolitic ignimbrites (~7–3 Ma) with intercalated minor mafic lavas occur throughout the Northern and Central MER (e.g., Gidey WoldeGabriel et al., 1990; Tadiwos Chernet et al., 1998). In the Quaternary (<1.6–1.8 Ma), bimodal volcanic rocks (lava, pyroclastics and volcanoclastic strata) were generally closely associated with Wonji Fault Belt affecting the rift floor (Gidey WoldeGabriel et al., 1990). Further the beginning of the Quaternary within MER is characterized by the eruption of more than 10 alternating flows of aphyric basalts and basaltic agglomerates overlain by silicic pyroclastics; this sequence is typically exposed by the Asela border fault (Bekele Abebe et al., 2007). Ebinger et al. (1993) suggested that in the Southern MER, volcanic activity was resumed in the early Pleistocene with eruption of ignimbrites and basalts.

## 2.2 Tectonic settings

The East African Rift System is a Miocene-Quaternary intracontinental extensional system composed of several interacting rift segments, from Mozambique to Afar (Bekele Abebe et al., 2007 and references therein). As a result different ideas have been suggested regarding the evolution and propagation of the Main Ethiopian Rift. Wolfenden et al. (2004) stated that the rift propagation in the Main Ethiopian Rift progressed northwards in contrary to the idea of Buck (2006) which suggested southward propagation. The Main Ethiopian Rift is bounded by discontinuous boundary faults that give rise to major fault escarpments separating the rift depression from the Somalian and Ethiopian plateaus (Fig.2.2). These faults are widely spaced and characterized by large vertical offsets (greater than 1 Km, Boccaletti et al., 1998). Their orientation varies in the different of the Main Ethiopian Rift segments.

The Northern Main Ethiopian Rift shows two well-developed fault systems, which the border faults and set of faults affecting the rift floor referred to as Wonji Fault Belt (WFB) (Boccaletti et al., 1998). According to Hayward and Ebinger (1996) and Boccaletti et al. (1998) the border faults are normally long, widely spaced and characterized by large vertical offset and are interpreted to have accommodated the tectonic deformation during the initial stages of rifting. Whereas the WFB is a tectonovolcanic system characterized by short closely spaced, active faults that exhibit minor vertical throw, which develops in the last 2 My (Boccaletti et al., 1999; Ebinger and Casey, 2001).

The WFB structures form clearly defined right stepping en- echelon segments obliquely cutting the rift floor that are believed to accommodate the majority of current deformation as indented by GPS measurements (Agostini et al., 2011).

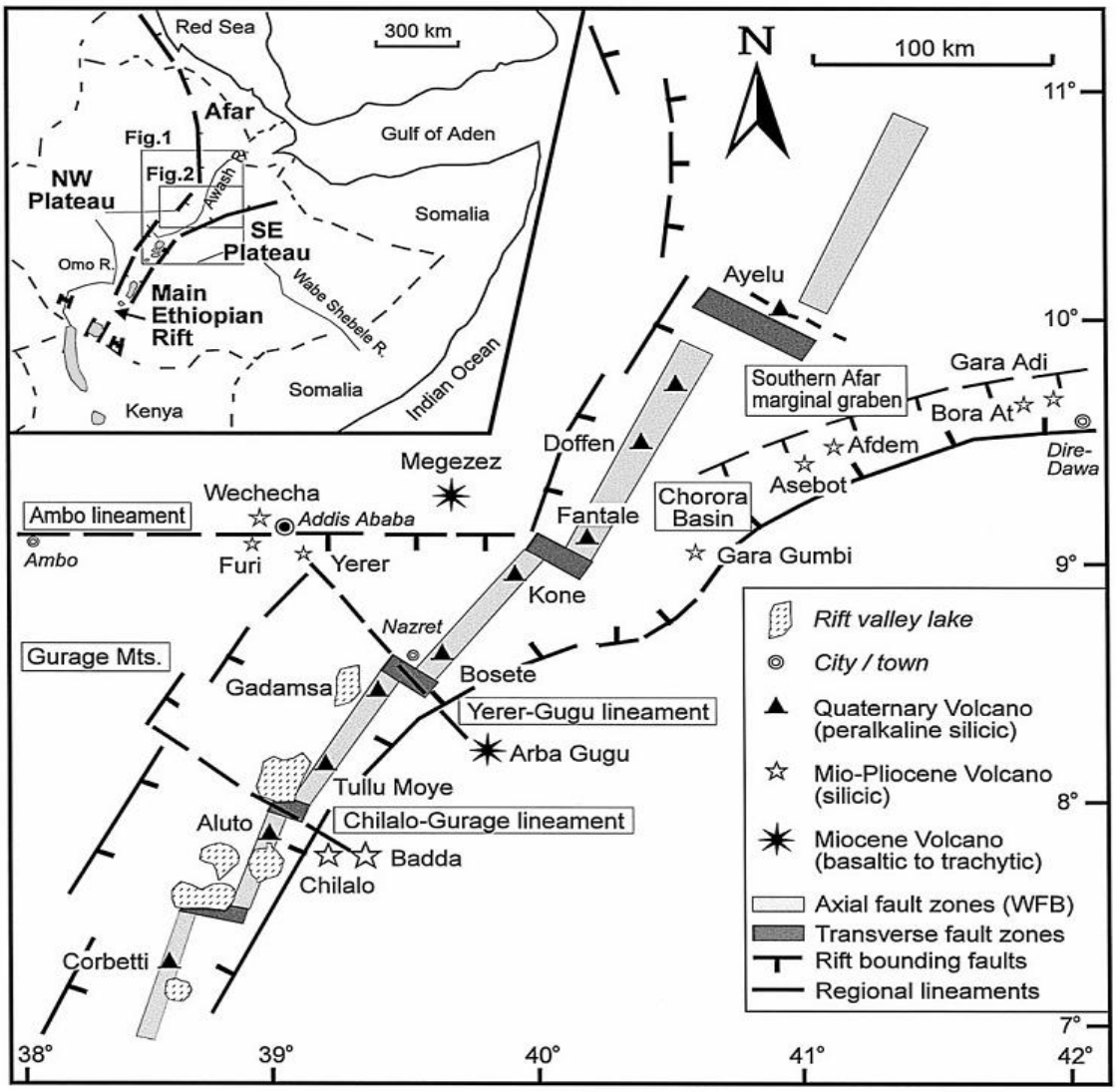


**Figure 2.2** Structural outline of the Main Ethiopian Rift–southern Afar transition region. Important features shown include the axial Wonji Fault Belt, regional lineaments, and the location of major volcanic centers. The inset map illustrates the regional context and the locations of the enlarged portion of this figure (adopted from Tadiwos Cherenet et al., 1998).

In the Central MER, the rift valley orients between N25° and N45° and is characterized by major rift escarpments on both western and eastern margins; boundary faults show an average trend around N30°E (Corti, 2009).

The rift floor is affected by dense NNE – SSW trending fault swarms, with relatively small throws (less than 100m) which comprises the Wonji Fault Belt (WFB) (Corti, 2009). The WFB started to develop at the beginning of the Quaternary (1.8 – 1.6 Ma). As stated by Corti (2009) the southern Main Ethiopian Rift is characterized by a rotation of the rift valley from N20 – $35^0$ to N5 – $20^0$ and hence accordingly the orientation of the boundary faults is N$0^0$E to N$20^0$E in this Main Ethiopian Rift sector.

In addition, there are also E-W striking fault zones that have affected propagation of the rift margin faults (i.e. the Ambo Fault Zone). These well-developed Ambo Fault Zone with vertical scarps of about 150m downthrown to the south was active during Oligocene (Tesfaye Korme et al., 2004 and references therein).

## 2.3 Geology and stratigraphy of the study area

The central part of the Main Ethiopian Rift is bounded by the Goba-Bonga lineament to the south and the Yerer-Tullu –Wellel volcano tectonic lineament to the north (Tsegaye Abebe et al., 2010). In addition, it is bounded to the east by Munesa fault escarpments and to the west by Guraghe fault escarpments (Fig.2.1). The major rock units exposed in the study area are given in Figure 2.3 and briefly discussed below.

### 2.3.1 Pre – rift volcanics

Volcanism in the central sector of the MER and the adjacent plateaus started as early as mid-Oligocene time or earlier, considering that the bases of some of these basalts are not exposed (Gidey WoldeGabriel et al., 1990).

**Alaji group:** Alaji group is one of the pre-rift (mid-Tertiary) volcanic rocks of the area and comprises of basalt, trachy-basalt, trachyt and ryholit (EIGS, 2012). It covers all parts of the Gibe gorge at the North-Western side of the study area.

**Anchar basalts:** This unit is exposed at the north-western extremities of the study area. According to Tsegaye et al. (2005) it comprises of aphyric to plagioclase and pyroxene phyric basalts and trachy-basalts intercalated with rhyolitic tuffs with radiometric ages range between 11.5 and 8.3 Ma.

## 2.3.2 Late Tertiary volcanics

**Nazreth group:** This unit is exposed at the eastern rift margin near Munesa town and at the rift floor unconformably overlapped by younger volcanic of Dino formation. It consists of stratoid silicics, ignimbrites, unwelded tuffs, ash flows, rhyolites and trachytes with ages range between 9.5 and 3 Ma years (EIGS, 2012 and references there in). Further this unit includes the alkaline and per alkaline silicics and ignimbrite forming the escarp of Awassa caldera.

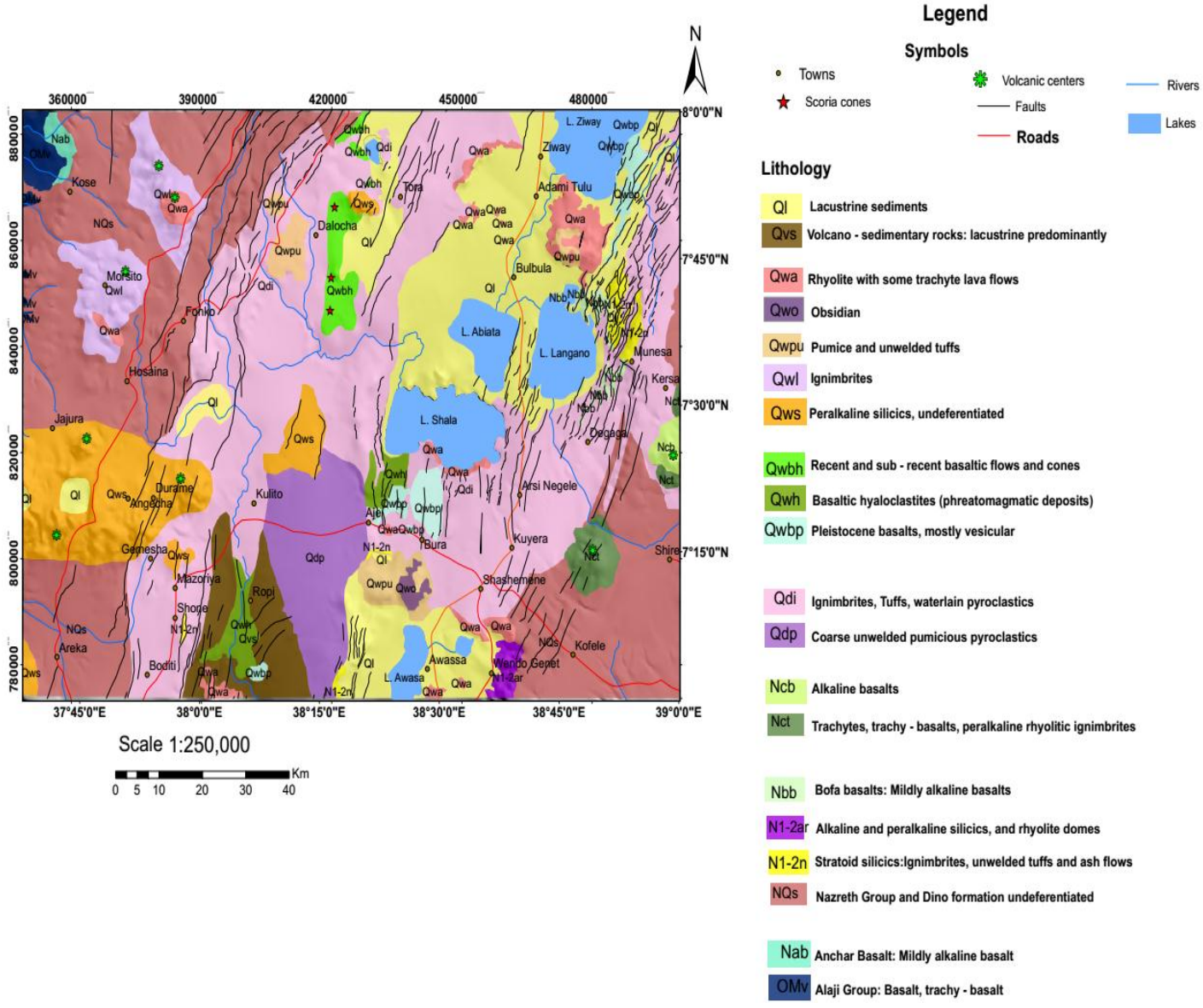


**Figure 2.3** Geological map of the central MER and adjacent plateaus (modified after EIGS, 2012)

**Bofa basalts:** The Nazret group mentioned before are overlain by a unit of fissural flood basalts. The Bofa Basalts form a wedge between the Nazret and Dino silicics and occur as separate exposures north and east of lake Langano where they are known as 'old Rift Basalts' (EIGS, 2012 and references there in), and where they finally wedge out. The ages of this unit ranges between 2.5 and 2.8 Ma.

**Chilalo volcanics:** This middle to upper Pliocene stratigraphic unit comprises the products of the Pliocene centers of the eastern and western shoulder of the rift and compositionally correlative units from the Awasa caldera (Gidey WoldeGabriel et al., 1990). This unit includes trachyte, silicic rocks, and basalt that overlie units of either the Shebele Trachyte or the Butajira Ignimbrite.

### 2.3.3 Quaternary volcanics / Wonji groups (<1.6 Ma)

The general Quaternary volcano-tectonic setting of the MER is controlled by the en-echelon arrangement of the Wonji Fault Belt (Bekele Abebe et al., 2007 and references there in). These NNE–NE Quaternary rift zones of the WFB form areas of active deformation obliquely cutting the rift floor in the MER (Bekele Abebe et al., 2007). This group consists of diverse Quaternary lava, pyroclastic rocks, and volcaniclastic strata (<1.6 Ma) that are generally confined to the Wonji fault belt in the study area and along the entire MER (Gidey Woldegabriel et al., 1990 and references therein). Generally the following units are part of the WFB in the study area.

**Dino Formation:** According to EIGS (2012) this formation covers a considerable portion of the rift floor and it comprises a number of flows of compacted fiamme ignimbrites in place intercalated with aphyric basalt and unwelded pyroclastics. Specifically it covers North West of lake Awassa which is probably related to the formation of Awassa and Shalla caldera.

**Basalts of the rift floor:** These basalts are exposed at East of lake Ziway, south of Lake Shalla and far north east of Lake Abiata- near Mito town (EIGS, 2012). The basalts are clearly controlled by extensional fractures and generally display fresh aa surfaces with chains of scoriaceous cones.

**Central volcanic complexes:** Most of the central volcanoes of the Wonji group are disposed along the axial zone of the rift, the WFB. The main volcanic centers with in the rift include Bora, Aluto, Shalla and Corbetti from north to south respectively.

This volcanic complexes generally comprises of rhyolitic and tracytic lava flows, ignimbrites, pumice, unwelded tuffs, obidians and pitchstones. Of course the composition of the volcanics varies from center to center.

### 2.3.4 Quaternary sediments

Quaternary sediments are the youngest units in the study area and constitute volcano sedimentary rocks and lacustrine sediments. As explained by Kazmin et al. (1980) lacustrine sediments intercalated with volcanics mainly ashes and tuffs, which in places are extensively developed and the sequence is shown as volcano-sedimentary which covers large are at the east of Shone town.

Numerous large lakes occupy the present day floor of the central Main Ethiopian Rift. A flat floor of red, yellow and white sands, tuffs, clays and diatomite are the common sediments in the lakes of Ziway, Langano, Abijata and Shalla and indicates these lakes were all joined as one huge lake during the pluvials (Mohr, 1971). Hence, Pleistocene-Holocene lacustrine sediments cover a significant tract of ground and were deposited in a huge lake whose level before 3500 to 2100 years used to be 100m higher than its current level (Kazmin et al., 1980). The lacustrine sediments which are dominated by sand and silt are intercalated with re-deposited volcanic ash and tuffs (EIGS, 2012). The main components of the derived sediments are volcanic origin, such as pumice and volcanic ash, obsidian, rhyolite and basaltic rock fragments. The thickness of sediments on the floor of lakes basin is not accurately known, however, sediments are probably thick in tectonic troughs, which correspond in part to the topographic lows occupied by lakes.

# CHAPTER THREE

# PRINCIPLES AND THEORETICAL FOUNDATIONS OF METHODS OF INVESTIGATION

## 3.1 Gravity methods

### 3.1.1 Introduction

Gravity and magnetic prospecting involves using passive potential fields of the Earth, and the fieldwork is thus fairly simple. In gravity surveying, subsurface geology is investigated on the basis of variations in the Earth's gravitational field arising from differences of density between subsurface rocks (Kearey et al., 2002).

### 3.1.2 Principles of gravity

The basis of the gravity survey method is Newton's Law of Gravitation, which states that the force of attraction $F$ between two masses $m_1$ and $m_2$, whose dimensions are small with respect to the distance $r$ between them (Kearey et al., 2002), is given by

$$F = \frac{Gm_1m_2}{r^2} \tag{3.1}$$

Where $G$ is the Gravitational constant ($6.67\times10^{-11} m^3 kg^{-1} s^{-1}$). Consider the gravitational attraction of a spherical, non-rotating, homogeneous Earth of mass $M$ and radius $R$ on a small mass $m$ on its surface. It is relatively simple to show that the mass of a sphere acts as though it were concentrated at the centre of the sphere and by substitution in equation (3.1)

$$F = \frac{GM}{R^2} m = mg \tag{3.2}$$

Force is related to mass by an acceleration and the term $g = GM/R^2$ is known as the gravitational acceleration or, simply, gravity. The weight of the mass is given by $mg$. On such an Earth, gravity would be constant. However, the Earth's ellipsoidal shape, rotation, irregular surface relief and internal mass distribution cause gravity to vary over its surface. The gravitational field is most usefully defined in terms of the gravitational potential $U$:

$$U = \frac{Gm}{r} \tag{3.3}$$

whereas the gravitational acceleration *g* is a vector quantity, having both magnitude and direction (vertically downwards), the gravitational potential *U* is a scalar, having magnitude only. The first derivative of *U* in any direction gives the component of gravity in that direction. Consequently, a potential field approach provides computational flexibility. Equipotential surfaces can be defined on which *U* is constant. The sea-level surface, or geoid, is the most easily recognized equipotential surface, which is everywhere horizontal, that is, at right angles to the direction of gravity.

### 3.1.3 Gravity field and figure of the Earth

Since the Earth is not a perfect homogeneous sphere, the gravitational acceleration is not constant over the surface of the Earth (Telford et al., 1990). Hence the magnitude of gravity field varies due to latitude, topography, elevation, Earth tides and density variations in the subsurface.

**The reference spheroid:** Geodetic measurements and satellite tracking shows that the shape of the Earth is nearly spheroidal, bulging at the equator and flattened at the poles (Telford et al., 1990). Hence the polar flattening is given by

$$\frac{(R_{eq} - R_p)}{R_{eq}} = \frac{1}{298.25} \tag{3.4}$$

Where $R_{eq}$ and $R_p$ are the Earth's equatorial and polar radii, respectively. The reference spheroid then approximates the mean sea level surface with the land above it removed. In 1930 the International Union of Geophysics and Geodesy (IUGG) adopted a formula for the theoretical value of gravity $g_t$ and later revised by the Geodetic Reference System in 1967 and is given by

$$g_t = 978031.846(1 + 0.005278895 \sin^2\phi + 0.000023462 \sin^4\phi) \text{ mGals} \tag{3.5}$$

where $\phi$ is latitude.

**The geoid:** Sea level is influenced by the variation of continental elevations and ocean depressions as well as lateral changes in density.

Hence to account for these variations it is necessary to define the geoid, as the average sea level over the oceans and over the surface of sea water that would lie in canals if they were cut through the land masses (Telford et al., 1990). Due to lateral variations the geoid and reference spheroid do not coincide. As indicated in (Fig.3.1b) local mass anomalies warp the geoid. Therefore, the geoid warped upward under continents because of attracting material above and downward over the ocean basins due to the low density of water (Fig.3.1a). However, deviations from the spheroid do not correlate with the continents or with the lithospheric plates, suggesting that density differences exist below the lithosphere (Telford et al., 1990).

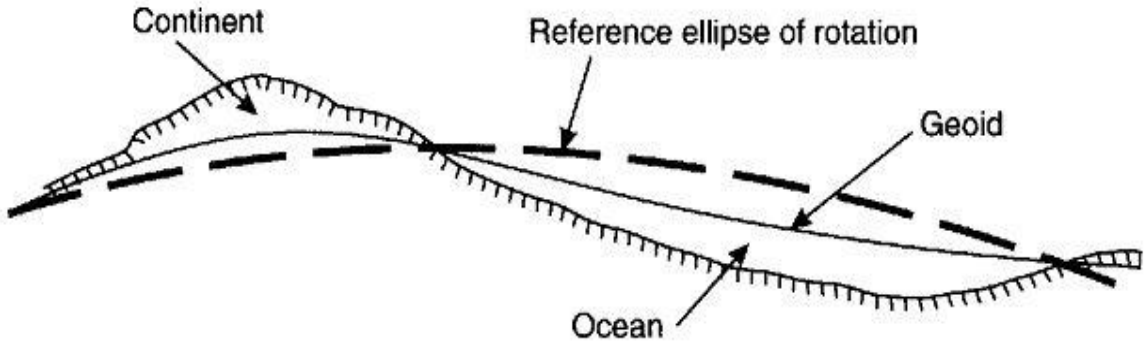


**(a)**

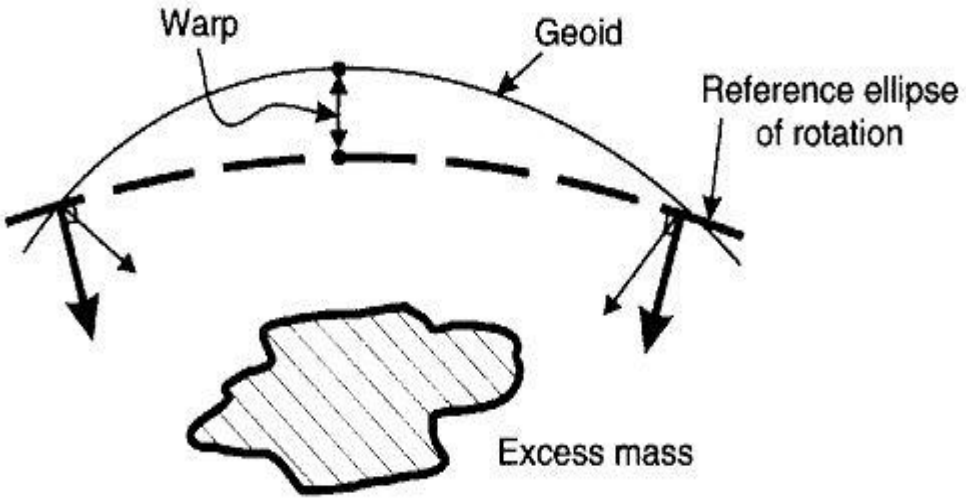


**(b)**

**Figure 3.1** Comparison of reference spheroid and geoid. **a)** Warping of the geoid due to regional-scale effect **b)** warping of the geoid by local mass (after Reynolds, 1997)

### 3.1.4 Gravity Reductions

In gravity work large and (in principle) calculable effects are produced by sources which are not of direct geological interest. Hence, we must make corrections to reduce gravity to the values they would have a datum on equipotential surface such as the geoid (or a surface everywhere parallel to it) (Telford et al., 1990)**.** The various corrections to be made are discussed as follows.

#### 3.1.4.1 Drift correction

Correction for instrumental drift is based on repeated readings at a base station at recorded times throughout the day. The meter reading is plotted against time and drift is assumed to be linear between consecutive base readings. The drift correction at time *t* is *d*, which is subtracted from the observed value. After drift correction the difference in gravity between an observation point and the base is found by multiplication of the difference in meter reading by the calibration factor of the gravimeter. Knowing this difference in gravity, the absolute gravity at the observation point *g*obs can be computed from the known value of gravity at the base. Alternatively, readings can be related to an arbitrary datum, but this practice is not desirable as the results from different surveys cannot then be tied together (Kearey et al., 2002).

#### 3.1.4.2 Latitude correction

Both the rotation of the Earth and its equatorial bulge produce an increase of gravity with latitude. The centrifugal acceleration due the rotating Earth is maximum at the equator and zero at the poles; it opposes the gravitational acceleration, while the polar flattening increases gravity at the poles by making the geoid closer to the Earth's center of mass (Telford et al., 1990). A latitude correction $\Delta g_l$ is given by

$$\Delta g_l = 0.812 \sin 2\varphi \text{ mGal/km} \qquad (3.6)$$

#### 3.1.4.3 Free-air correction (FAC)

The basis of this correction is that it makes allowance for the reduction in magnitude of gravity with height above the geoid irrespective of the nature of the rock below (Reynolds, 1997).

The free-air correction is the difference between gravity measured at sea level and at an elevation of *h* metres with no rock in between. An increase in height implies an increase in distance from the Earth's centre of mass and the effect is negative for stations above sea level. The free-air correction is thus positive, and for all practical purposes it is given by

$$FAC = 0.3086h \; mGal \tag{3.7}$$

### 3.1.4.4 Bouguer correction (BC)

The free-air correction accounts solely for variation in the distance of the observation point from the centre of the Earth; no account is taken of the gravitational effect of the rock present between the observation point and datum (Kearey et al., 2002). The Bouguer correction (BC) removes this effect by approximating the rock layer beneath the observation point to an infinite horizontal slab with a thickness equal to the elevation of the observation above datum. If ρ is the density of the rock, then the Bouguer correction is given by

$BC = 2\pi G\rho h = 0.4191\rho h$ gu ( whre *h* is the plate thickness in metres, and ρ is the density in Kg $m^{-3}$). The Bouguer effect is positive and the correction is therefore negative.

### 3.1.4.5 Terrain correction (TC)

As explained by Telford et al. (1990) terrain correction allows for surface irregularities in the vicinity of the station. Hills above the elevation of the gravity station exert an upward pull on the gravimeter, whereas valleys (lack of material) below it fail to pull downward on it. Thus both types of topographic undulations affect gravity measurements in the same sense and the terrain correction is added to the station reading.

### 3.1.4.6 Tidal correction

Gravity measured at a fixed location varies with time because of periodic variation in the gravitational effects of the Sun and Moon associated with their orbital motions, and correction must be made for this variation in a high precision survey (Kearey et al., 2002). The correction can be calculated from knowledge of the location of the Sun and Moon. However, because the variation is smooth and relatively slow, usually it is included in the instrument drift correction.

### 3.1.4.7 Isostatic correction (IC)

The worldwide average of Bouguer anomalies on land near sea level is approximately zero. In regions of large elevation they are generally negative, while in oceanic regions mainly positive (Telford et al., 1990). These large-scale effects are due to density variations in the crust, indicating denser material beneath oceans and less dense material in elevated areas.

As a result two hypotheses were formulated in the 1850's to account for this large scale variation in density. The first hypotheses given by Airy proposed a crust of uniform density but variable thickness floating on a liquid substratum of higher density, whereas Pratt suggested a crust where the density varies with topography, being lower in mountain regions and higher beneath oceans (Telford et al., 1990). Hence an isostatic correction occasionally is necessary in large scale surveys to compensate for crustal variations.

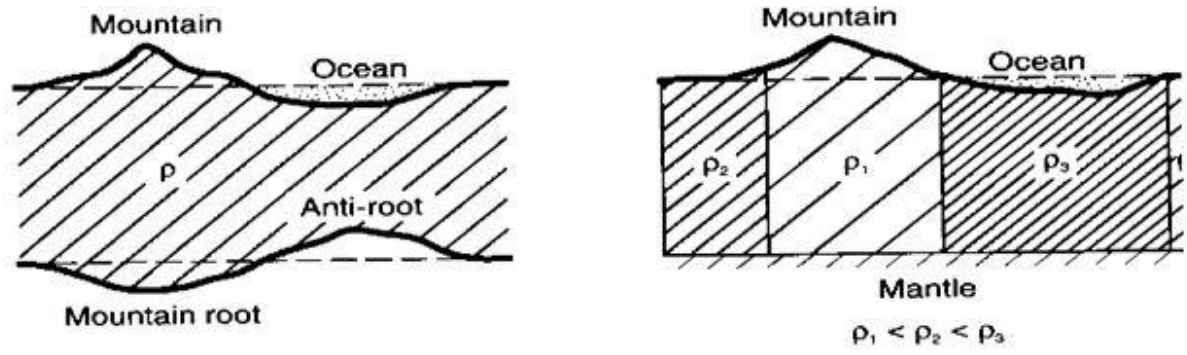


(**a**) (**b**)

**Figure 3.2 a)** Airy and **b)** Pratt's models for isostasy (after Reynolds, 1997).

### 3.1.5 Free-air and Bouguer anomalies

After the appropriate corrections made the free-air anomaly (FAA) and Bouguer anomaly (BA) can be determined by the following equations.

The equation for Free-Air anomaly (FAA) is given by

$$FAA = g_{obs} - g_{\phi} + FAC \tag{3.8}$$

The FAA may be thought of as squashing up all the mass above sea level into an infinitesimally thin layer at sea level, and measuring gravity there. The FAA is mostly used for marine surveys and for investigating deep mass distribution (e.g., testing theories of isostasy) (Foulger and Peirce,__ ).

And the equation for Bouguer anomaly (BA) is:

$$BA = g_{obs} - g_{\phi} + FAC \pm BC + TC \tag{3.9}$$

The BA is equivalent to removing away everything above sea level. The Bouguer anomaly forms the basis for the interpretation of gravity data on land.

### 3.1.6 Isostatic anomaly (IA)

Isostatic anomalies (IA) correspond to gravity anomalies resulting from a homogeneous crust having a flat surface, a standard reference density and constant thickness for the isostatic model (Airy-Heiskanen or Pratt-Heyford model). Thus it is given by the following equations

Isostatic anomaly (IA) = Bouguer anomaly (BA) + Isostatic correction (IC)

$$IA = g_{o} - g_{\phi} + FAC \pm BC + Tc + IC \tag{3.10}$$

### 3.1.7 Interpretation of gravity data

There are two approaches to the interpretation of Bouguer anomaly data. The first one is direct where the original data are analysed to produce an interpretation. The other is indirect, where models are constructed to compute synthetic gravity anomalies which are compared in turn with the observed Bouguer anomaly (Reynolds, 1997). Due to the ambiguity of gravity anomaly, different geological and geophysical methods are used together to constrain the geologic model.

#### 3.1.7.1 Regional fields and residual anomalies

Bouguer anomaly fields are often characterized by a broad, gently varying, regional anomaly on which may be superimposed shorter wavelength local anomalies. Therefore, in order to interpret separately isolation of residual from regional or vice versa is very important. Extraction of residual from regional can be done by graphical and computational methods.

In regional studies, it may be desirable to remove anomalies from features of small lateral extent so as to bring out large-scale structures more clearly (Dobrin and Savit, 1988).

### 3.1.7.2 Depth estimation

One of the major importance's in the interpretation of gravity data is the determination of depth to the top of the causative body and/or to the center of mass (Reynolds, 1997). As a result there are different techniques and models employed to determine the possible depth to a given causative body. Here we prefer to discuss forward and inverse modeling.

**Forward modeling:** The most commonly used technique for quantitative interpretation of gravity data involves the direct calculation of the gravity effect of an assumed density distribution, and the comparison of the calculated values with those that were observed (Dobrin and Savit, 1988). The assumed density distribution is then modified by trial and error with the help of constraints from geological and other geophysical data until a good fit is obtained between the observed and calculated values. This can be achieved by two and three dimensional forward modeling.

**Inverse modeling:** Iterating upon the forward calculation process can modify the shape or density distribution of the sources until the calculated anomaly closely approximates the observed anomaly and all other available constraints are reasonably satisfied (Dobrin and Savit, 1988). Therefore, through inverse modeling it is possible to infer directly and automatically from the observed gravity data certain information about the source.

## 3.2 Magnetic methods

### 3.2.1 Introduction

Magnetic and gravity methods have much in common, but magnetics is generally more complex and variations in the magnetic field are more erratic and localized (Telford et al., 1990). This is partly due to the difference between the dipolar magnetic field and the monopolar gravity field, partly due to the variable direction of the magnetic field, whereas the gravity field is always in the vertical direction. In addition, magnetic field varies with time whereas gravity field is time invariant (ignoring small tidal variations).

Hence, the aim of a magnetic survey is to investigate subsurface geology on the basis of anomalies in the Earth's magnetic field resulting from the magnetic properties of the underlying rocks (Kearey et al., 2002).

### 3.2.2 Principles and elementary theory

If two magnetic poles of strength $p_1$ and $p_2$ are separated by a distance r, a force exists between them is given by

$$F = \frac{p_1 p_2}{4\pi\mu r^2} \tag{3.11}$$

Where $\mu$ is the magnetic permeability of the medium separating the poles; $p_1$ and $p_2$ are pole strengths and *r* the distance between them. The force is attractive if the poles are of different sign and repulsive if they are of like sign.

The *magnetic field B* due to a pole of strength *p* at a distance *r* from the pole is defined as the force exerted on a unit positive pole at that point

$$B = \frac{p}{4\pi\mu r^2} \tag{3.12}$$

### 3.2.3 The Earth's magnetic field

The geomagnetic field at or near the surface of the Earth originates largely from within and around the Earth's core. Magnetic anomalies caused by rocks are localized effects superimposed on the normal magnetic field of the Earth (geomagnetic field) (Kearey et al., 2002). Consequently, knowledge of the behavior of the geomagnetic field is necessary both in the reduction of magnetic data to a suitable datum and in the interpretation of the resulting anomalies. The geomagnetic field is geometrically more complex than the gravity field of the Earth and exhibits irregular variation in both orientation and magnitude with latitude, longitude and time (e.g., Kearey et al., 2002). Generally there are three components of the Earth's magnetic field.

### 3.2.3.1 The Earth's main field

This field represents the main components of the geomagnetic field and is believed to be originated in the Earth's outer core. This field varies relatively slowly and its magnitude on the earth's surface is given in terms of the geomagnetic field elements (Fig. 3.3). The total field vector *B* has a vertical component *Z* and a horizontal component *H* in the direction of magnetic north. The dip of *B* is the inclination *I* of the field and the horizontal angle between geographic and magnetic north is the declination *D*. *B* varies in strength from about 25000nT in equatorial regions to about 70000nT at the poles (e.g., Kearey et al., 2002).

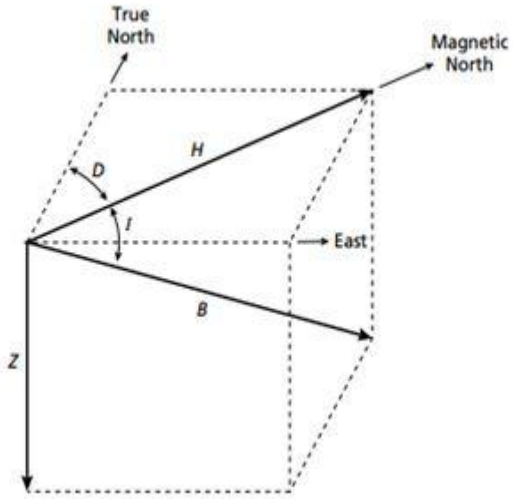


B = Total magnetic field vector

H = Horizontal component of the total field vector

Z = vertical component of the field vector

*D* = Declination

*I* = Inclination

Where, $B^2 = H^2 + Z^2$

$I = \tan^{-1}(Z/H)$

$D = \tan^{-1}(H_E/H)$, $H_E$ = East component of horizontal field vector

**Figure 3.3** The geomagnetic elements

### 3.2.3.2 The external magnetic field

Most of the remaining small portion of the geomagnetic field appears to be associated with electric currents in the ionized layers of the atmosphere (e.g., Telford et al., 1990). The time variations of this field portion are much more rapid than for the main field and is caused by external activities.

### 3.2.3.3 Crustal (anomalous) magnetic field

Local changes in the main field result from variations in the magnetic mineral content of near surface rocks. The sources of local magnetic anomalies cannot be very deep because of the Curie temperature. Thus local anomalies must be associated with features in the upper crust (e.g., Telford et al., 1990). Generally the total magnetic field can be expressed by

$$B_T = Bext + B\text{int} = Bext + B_D + Brm \quad (3.13)$$

Where $B_T$ is the total magnetic field, Bext is external magnetic field, $B_D$ is dipole field, which is mainly generated by the fluid outer core and Brm is the field of rock magnetism.

## 3.2.4 Temporal variations of the Earth's magnetic field

The magnetic field of the Earth varies with time. As a result the temporal variation of the Earth's magnetic field can be explained in terms of three temporal variations.

**Secular variations:** These are very long period changes that result from convective changes in the core. They are monitored by measuring changes in I, D and B at observatories. Because these variations occur slowly with respect to the time of completion of a typical exploration magnetic survey, these variations will not complicate data reduction efforts.

**Diurnal variations:** Magnetic effects of external origin cause the geomagnetic field to vary on a daily basis to produce diurnal variations. Under normal conditions (quiet days) the diurnal variation is smooth and regular and has an amplitude of about 20–80nT, being at a maximum in polar regions (Kearey et al., 2002). This variation should be accounted for when conducting exploration magnetic surveys.

**Magnetic storms:** Occasionally, magnetic activity in the ionosphere will abruptly increase. The occurrence of such storms correlates with enhanced sunspot activity. The magnetic field observed during such times is highly irregular and unpredictable, having amplitudes as large as 1000 nT. Exploration magnetic surveys should not be conducted during magnetic storms. This is because the variations in the field that they can produce are large, rapid, and spatially varying. Therefore, it is difficult to correct for them in acquired data (Kearey et al., 2002).

### 3.2.5 Magnetic instruments

Magnetic instruments basically used in geophysical exploration can be classified in to three groups: the torsion (and balance), fluxgate and resonance type's magnetometers. Magnetometers measure horizontal and/or vertical components of the magnetic field or the total field.

**Magnetic balance:** A magnet pivots about a point that is not the centre of gravity. The torque of the Earth's magnetic field balances with the gravity effect at the centre of gravity. The angle of pivot is a function of the magnetic field, and is measured by a light beam that is projected onto a scale. This changes between measuring stations and thus the magnetic balance is a relative instrument (Foulger and Peirce,_ ).

**Flux-gate magnetometer:** The construction of this instrument involves two coils wound in opposition. A current is passed through to induce magnetisation. A secondary winding measures the voltage induced by the induced magnetization. In the absence of the Earth's field these two cancel out. An AC current is applied that saturates the cores in opposition in the absence of the Earth's field. The Earth's field reinforces one core and opposes the other. This causes the voltages induced in the secondary coils to get out of step. The result is a series of pips whose height is proportional to the ambient field (Foulger and Peirce,__ ).

**Proton precession magnetometer:** The most commonly used magnetometer for both survey work and observatory monitoring is currently the nuclear precession or proton magnetometer. The sensing device of the proton magnetometer is a container filled with a liquid rich in hydrogen atoms, such as kerosene or water, surrounded by a coil (Kearey et al., 2002). Field instruments provide absolute readings of the total magnetic field.

### 3.2.6 Magnetic surveying

Magnetic exploration can be carried out on land, at sea, and in the air. As a result magnetic surveys either directly seek magnetic bodies or they seek magnetic material associated with an interesting target. Land surveys are usually done with portable proton precession magnetometers. Profiles or networks of points are measured in the same way as for gravity. It is important to survey perpendicular to the strike of an elongate body or two-dimensional modeling may be very difficult.

It is necessary to tie back to the base station at 2-3 hour intervals, or to set up a continually-reading base magnetometer. This will give diurnal drift and detect magnetic storms (Foulger and Peirce,__). In magnetic surveying the operator must: record the time at which readings were taken for drift correction, stay away from interfering objects (e.g., wire fences, railway lines, roads), not carry metal objects (e.g., mobile phones), and take multiple readings at each station to check for repeatability.

### 3.2.7 Magnetic data reduction

To remove all causes of magnetic variation from the observations other than those arising from subsurface geology it is necessary to make correction of magnetic data.

#### 3.2.7.1 Diurnal variation correction

The effects of diurnal variation may be removed in several ways. On land the magnetometer is read at a fixed base station periodically throughout the day. The differences observed in base readings are then distributed among the readings at stations occupied during the day according to the time of observation. Magnetometers do not drift and base readings are taken solely to correct for temporal variation in the measured field (Kearey et al., 2002).

#### 3.2.7.2 Geomagnetic correction

In order to produce a magnetic anomaly map of a region, the data have to be corrected to take in to account the effect of latitude and to a lesser extent longitude (Reynolds, 1997). Survey data at any given location can be corrected by subtracting the theoretical field value $B_{th}$, obtained from the International Geomagnetic Reference Field (IGRF) from the measured value, $B_{ob}$. Therefore, the magnetic anomaly ($\Delta B$), obtained by subtracting the diurnal correction ($\delta B_D$) and geomagnetic correction ($B_{th}$) is given by

$$\Delta B = B_T - \delta B_D - B_{th} \tag{3.14}$$

# CHAPTER FOUR

# DATA ACQUISITION, PROCESSING AND PRESENTATION

## 4.1 Gravity data acquisition and distribution

A total of about 2260 gravity data with an average spacing of 2 to 4Km between consecutive stations has been obtained and used for this study. These points are randomly distributed along seasonal roads, dry weather roads (gravel and asphalt) and off road transect (Fig. 4.1).

As can be seen from (Fig. 4.1) there is good gravity data coverage throughout the study area. The gravity data obtained for this thesis work were collected by individual researchers (Abera Alemu, 1983, 1992) and the Geological Survey of Ethiopia (EGS).

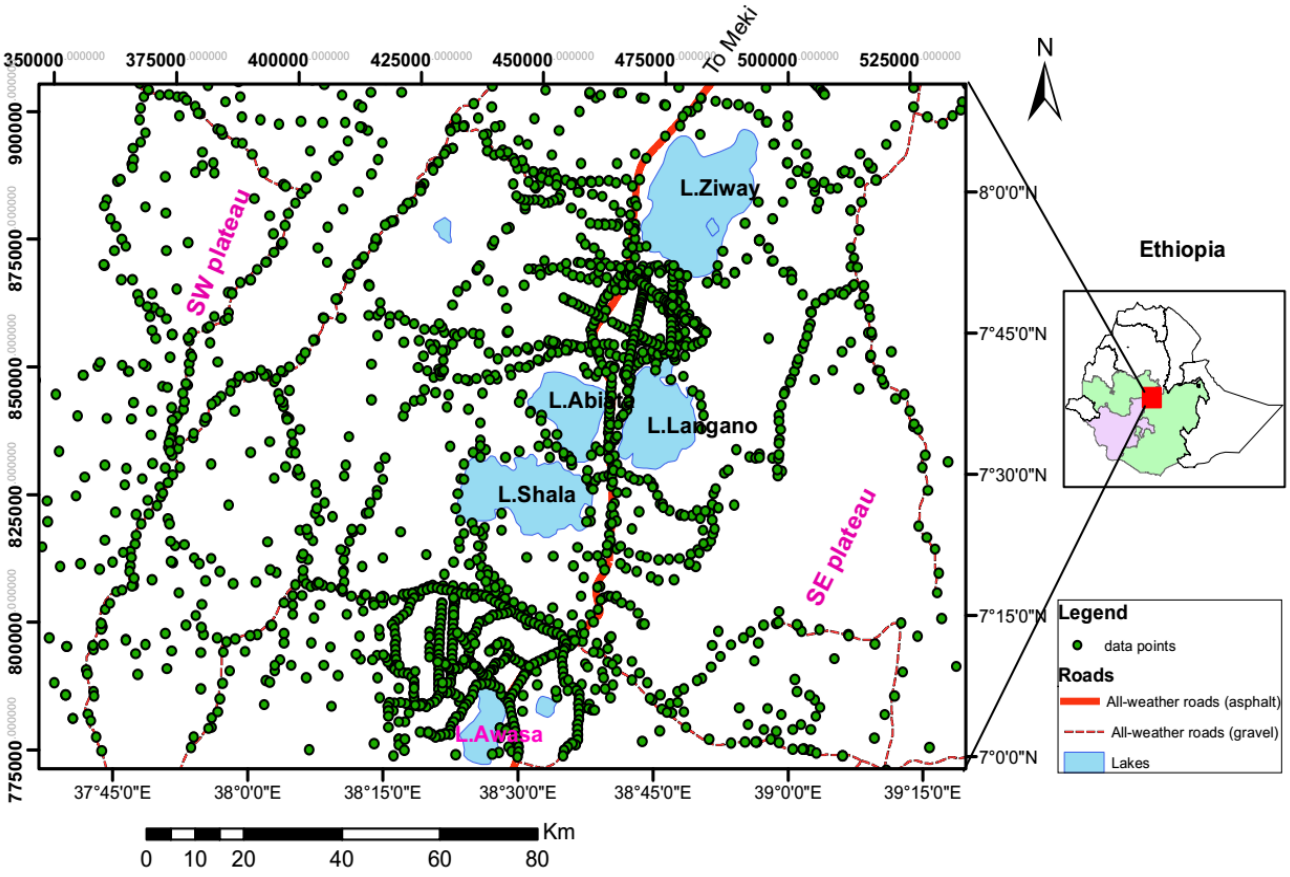


**Figure 4.1** Gravity data distribution of the study area, the rift lakes (left) and inset map (right).

The secondary data acquired and reprocessed from the work of Abera Alemu (1983; 1992), were collected using the Canadian sharp Gravimeter No. 128 (Worden type gravimeter) and the Lacoste and Romberg, model G Gravimeter with reading precession of 0.1 and 0.05 mGal respectively. On the other hand, the secondary gravity data obtained from GSE as cited in their reports were collected using the Lacoste and Romberg Model 304 gravimeter which also has a precision of 0.05 mGal. The survey reports of the secondary data indicate that locations (Latitude, Longitude and elevations) of the gravity stations were determined using classical surveying instruments (altimeters, theodolits, and hand held global positioning system (GPS). All the secondary data obtained are randomly distributed throughout the study area. All the data were tied and adjusted to the International Gravity Standardization Network 1971 (IGSN71). The theoretical gravity value at each observation station is computed using the Geodetic Reference System 1967 (GRS67) gravity formula.

## 4.2 Gravity data processing

### 4.2.1 Gravity data reduction

Gravimeters do not give direct measurement of gravity for interpretation. Therefore, before interpreting the survey in terms of geological and geophysical features, the raw gravity data have to be reduced to the mean sea level in order to remove the effects that result from indirect geological interest.

All the secondary gravity data have been reprocessed by applying all the standard gravity corrections (drift correction, free air correction, simple and complete Bouguer correction and terrain correction) using average crustal density of 2.67g/cm3. The end results of the survey data such as the free-air anomaly values and the complete Bouguer anomaly values of all the stations considered in the study area have been determined as part of the processing sequence using the Geosoft OasisMontaj (version 6.4.2) gravity and magnetic data processing and mapping software.

### 4.2.2 Gravity data gridding and contouring

The final reduced gravity data was compiled in spread sheet excel format with different file extension for the respective software and imported in to Global mapper 12, Arc GIS 10.3,

Surfer10 and Geosoft OasisMontaj (Version 6.4.2) for further processing. All the reduced gravity values and their corresponding elevation values were then gridded using the minimum curvature gridding option of the Geosoft OasisMontaj software. Following the gridding techniques employed, the topographic map (Fig. 5.1), the free-air anomaly map (Fig. 5.2) and the complete Bouguer anomaly map (Fig. 5.4) were produced.

The topographic map was constructed with a contour interval of 100 m, whereas the free-air and Bouguer anomaly map was produced with contour interval of 10 mGals.

### 4.2.3 Regional – residual gravity anomaly separation and data enhancement

The compete Bouguer gravity anomaly represents the total effect of gravity variations caused by deep seated geologic sources that give rise to regional (long wavelength) gravity anomalies and shallow (subsurface) geologic sources that give rise to residual (short wavelength) gravity anomalies. Therefore, it is necessary to separate the complete Bouguer anomaly into its regional and residual components so that we can interpret them independently. This requires estimating the regional anomaly using an appropriate standard technique to estimate the regional so that the estimated regional component can be subtracted from the complete Bouguer anomaly in order to determine the residual component. There are different techniques (wavelength filtering, upward and downward continuation technique, graphical method, and polynomial trend surfaces filtering technique, etc.) that are applied to separate the complete Bouguer anomaly into its regional and residual components. In this thesis work the 2D FFT Gaussian regional/residual filter was used to estimate the regional component using the Geosoft OasisMontaj software. This technique suppresses all the short wavelength (residual) components arising from shallow sources and enhances the long wave length (regional) components arising from deep seated sources.

## 4.3 Magnetic data acquisition and distribution

Ground magnetic survey was conducted by using the Scintrex made MP-2 model Proton Precision Magnetometer which measures the total magnetic field intensity. Establishing and positioning of magnetic stations including base stations were done using hand held global positioning system (GPS, GARMIN-12).

For this study a single proton precession magnetometer was used in the survey and hence a base station was chosen at the beginning of a day's work and reoccupied after about every two or three hours. Accordingly, diurnal corrections and International Geomagnetic Reference Field (IGRF) corrections have been carried out for the collected magnetic data. Generally, the magnetic data were collected randomly throughout the survey area depending upon the accessibility and field conditions. In this study a total of about 170 magnetic data has been collected and this stands as one of the major contributions of this MSc thesis research. In addition about 425 secondary magnetic data has obtained from previous MSC research works of Tsegaye (2015). Both the new and existing magnetic data were collected along cross-country roads, all weather and seasonal roads at average spacing between 2 to 4Km. All the primary and secondary data are plotted in (Fig. 4.2). As we can observe from the magnetic data point distribution map, the data density is generally variable throughout the study area being denser around the Aluto and Corbetti volcanic complexes. In contrast to gravity data distribution map (Fig. 4.1), which has a good coverage, the magnetic data coverage is limited to the rift floor and some part of the highlands.

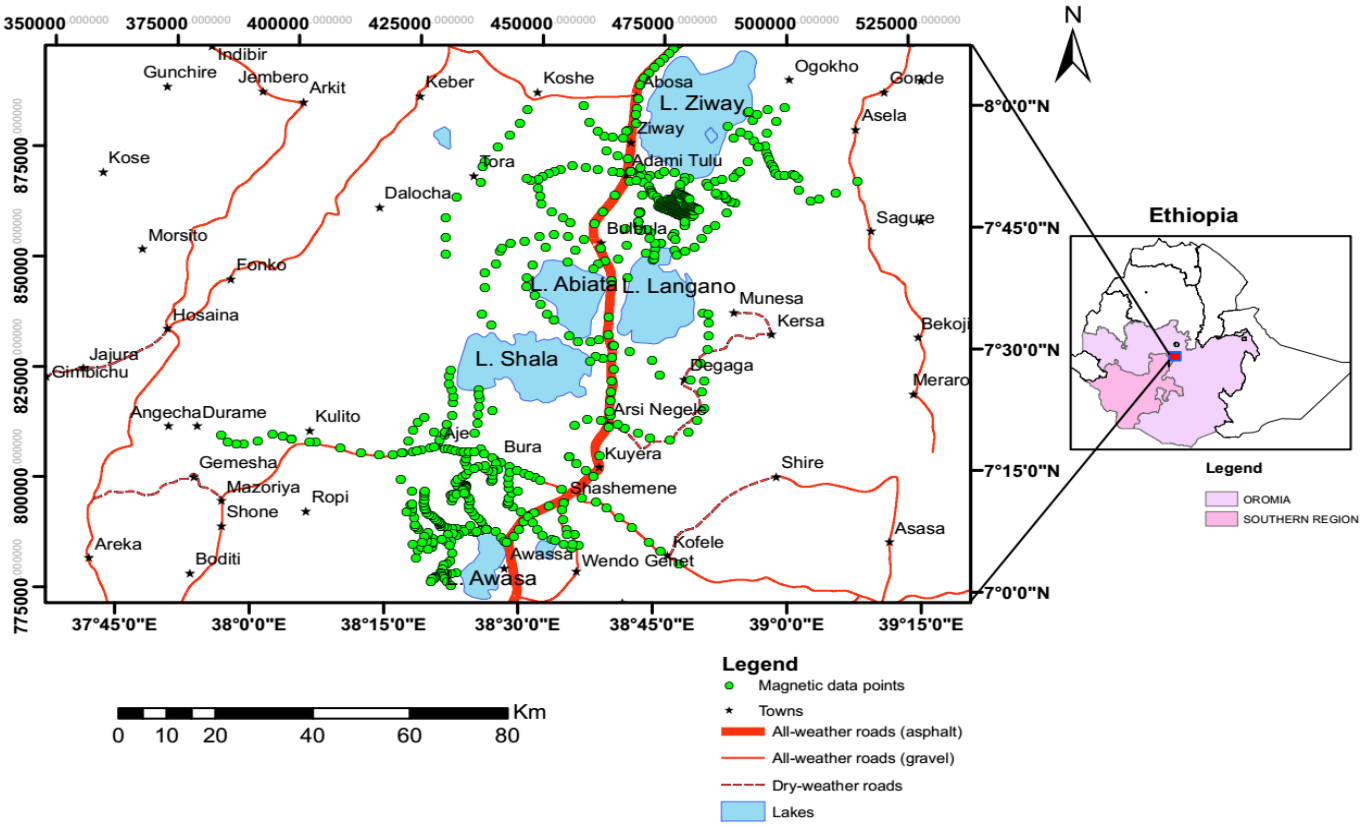


**Figure 4.2** Magnetic data distribution of the study area, the rift lakes (left) and inset map (right).

## 4.4 Magnetic data processing

### 4.4.1 Magnetic data reduction

To remove all causes of magnetic variation from the observations other than those arising from subsurface geology it is necessary to make a correction to magnetic raw data. Therefore, all the primary magnetic data collected and the secondary data obtained were corrected for diurnal effects and for the variations caused by dipole field. Diurnal correction for each magnetic data was computed by using the formula:

$$\delta B_D = \gamma i \pm (\Delta\gamma/\Delta T)(\Delta Ti) \quad (4.1)$$

Where, $\delta B_D$ = diurnal corrected data measured at time ti, γi = magnetic field measured at time ti. Δγ = γ2- γ1, γ1 = base station magnetic reading at the beginning of the survey, γ2 = base station magnetic reading at the end of the survey. ΔT = T2 – T1, $T_1$ = base station time reading at the beginning of the survey, T2 = base station time reading at the end of the survey, (ΔTi ) = ti - T1.

The diurnally corrected magnetic data represents the total magnetic field intensity value at each station. The diurnally corrected magnetic data was further reduced using the value obtained from IGRF to determine the total magnetic field anomaly for each station using the following formula;

$$\gamma_{IGRF\_Corrected} = \gamma\,corr - IGRF \quad (4.2)$$

Where, $\gamma_{IGRF\_Corrected}$ = IGRF corrected total magnetic intensity value at a given observation point, γ corr = diurnally corrected magnetic intensity value at a given observation point, IGRF = the International Geomagnetic Reference Field value at the given point defined by its latitude.

### 4.4.2 Magnetic data gridding and contouring

Since both gravity and magnetic methods are potential field methods, the gridding and contouring of gravity and magnetic data are more or less the same. Therefore, the final reduced magnetic data was compiled in spread sheet excel format with different file extensions corresponding to the respective softwares used.

The files with the different file extensions are imported to the Global mapper 12, Arc GIS 10.3, Surfer 10 and Geosoft Oasis Montaj (Version 6.4.2) for further processing of the primary data and re-processing of the secondary data. The resulting compiled magnetic data were then gridded using minimum curvature gridding system. Following the gridding techniques, the total magnetic intensity map (Fig. 5.12) and total magnetic anomaly map (Fig. 5.13) were produced.

### 4.3.3 Regional-residual magnetic data separation

Like the complete Bouguer gravity anomaly, the total magnetic field anomaly map is the total effect of shallow (short wavelength) and regional (long wavelength) anomaly sources. Therefore, with the objective of suppressing the response from shallow sources and enhances the response of the deeper sources or vice versa different enhancement techniques are used. In this thesis work the 2D FFT Gaussian regional/residual filter was used to estimate the regional component using the Geosoft OasisMontaj software.

## 4.5 Data presentation

The end results of the gravity survey (free-air anomaly values and complete Bouguer anomaly values) computed at all the stations considered in the study area are plotted at their specific locations to compile the free-air anomaly map (Fig. 5.2) and the complete Bouguer anomaly map (Fig. 5.4) of the study area using the Geosoft OasisMontaj mapping software.

The complete Bouguer anomaly map has been used to compile the regional gravity anomaly map (Fig. 5.6) and the residual gravity anomaly map (Fig. 5.7) in accord with the procedures outlined in section 4.2.3 for a further enhancement and interpretation interms of geology of the gravity data.

Similarly, the end results of the magnetic survey (total magnetic field intensity values and total magnetic field anomaly values) computed at all the stations considered in the study area are plotted at their locations to compile the total magnetic field intensity map (Fig. 5.12 ) and the total magnetic field anomaly map (Fig. 5.13 ) of the study area. The total magnetic field anomaly map has been used to compile the regional magnetic anomaly map (Fig. 5.15) and the residual magnetic anomaly map (Fig. 5.16) for a further enhancement and interpretation interms of geology of the magnetic data.

## 4.6 Data enhancement

Data enhancement techniques of potential field data (mostly, the residual gravity or residual magnetic anomaly field data) are analytical methods that are employed for highlighting the contrast of gravity or magnetic anomalies generated by deep-seated and shallow origin anomalous geologic bodies. The commonly used data enhancement techniques including the analytical signal method, Euler depth method and tilt derivative method are employed here. As a result, the analytical signal gravity map (Fig. 5.9), the tilt derivative gravity map (Fig. 5.10), the Euler depth gravity map (Fig. 5.11), the analytical signal magnetic map (Fig. 5.17), the tilt derivative magnetic map (Fig. 5.17) and the Euler depth magnetic map (Fig. 5.19) are produced from values of the residual gravity anomaly map (Fig. 5.7) and the residual magnetic anomaly map (Fig. 5.16) compiled for the study area.

## 4.7 Data interpretation

Interpretation of the gravity data or the magnetic data in terms of geology involves the art of translating the compiled gravity anomaly maps or magnetic anomaly maps of the survey area in terms of geology in order to obtain information about nature of the major geologic units and structures that give rise to the major anomalies revealed by both the gravity and magnetic anomaly maps of the study area.

Knowledge of the surface geology, the tectonic setting and dimensions of the survey area, are important constraints for making reliable interpretations of the compiled gravity and magnetic anomaly maps interms of the prominent volcanological, lithological and structural units of the study area. Therefore, the volcano-tectonic map (Fig. 5.8) and the simplified geologic map (Fig. 2.3) of the central MER and adjacent areas have been used for the interpretation of the various gravity and magnetic anomaly maps compiled for the study area

# CHAPTER FIVE

# RESULTS AND INTERPRETATION

## 5.1 Gravity data results and interpretation

### 5.1.1 Topographic and free-air anomaly maps

The free air correction compensates the observed gravity for the fact that it was measured at a given height above (or below) the mean sea level. It assumes, however, that there is nothing but air between the sea level and the observation point. In this thesis work, the free air anomaly at each observation point is computed by applying the free air correction. The air anomaly map (Fig. 5.2) compiled from the computed point free air anomalies and the topographic map (Fig. 5.1) compiled from elevations of the observation points are produced using the Geosoft OasisMontaj software.

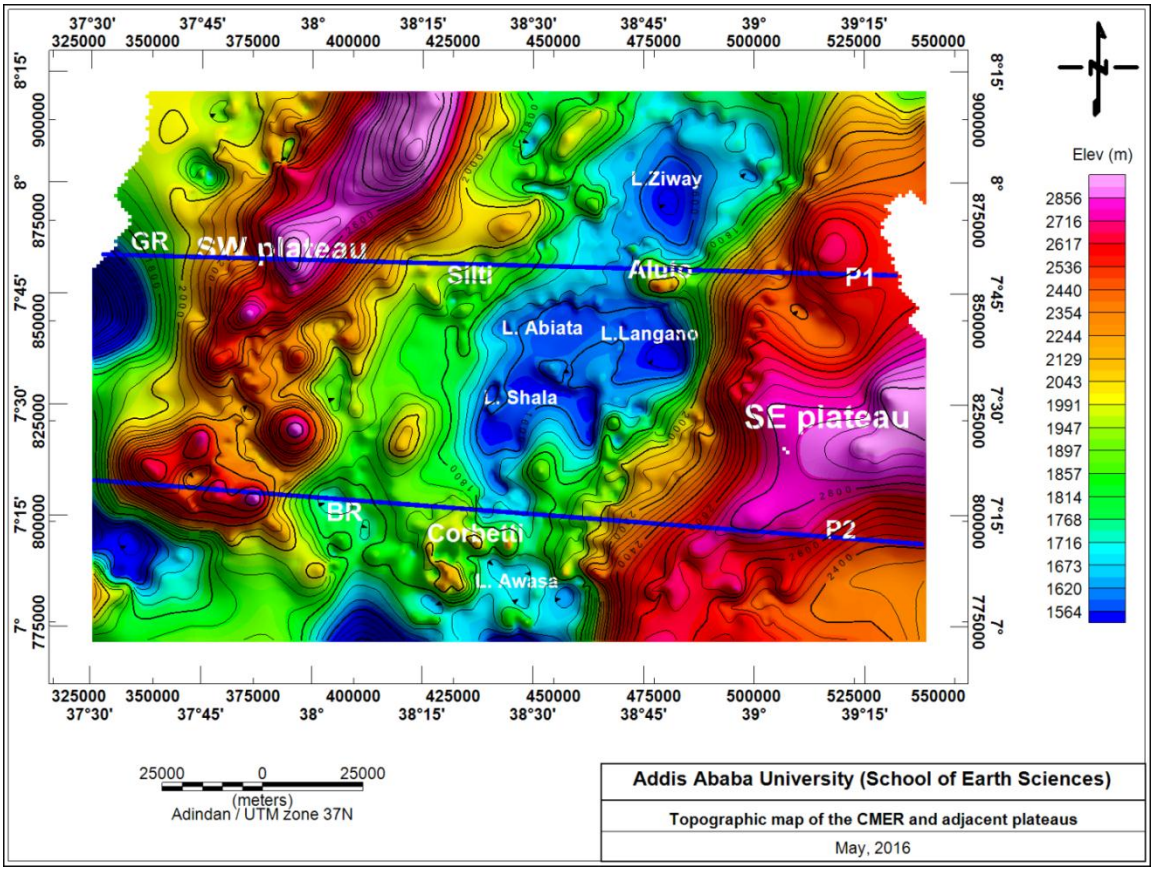


**Figure 5.1** Topographic map of the study area

As can be observed from the compiled topographic map (Fig. 5.1) of the study area, the south eastern and south western plateaus are characterized by highly elevated topography. In contrast, the central part of the study area is dominated by topographically low areas which basically constitute the rift floor. In fact, there are several volcanic complexes/centers (e.g. Aluto and Corbrtti) with relatively high and circular topography within the rift floor. Specifically, the topographic map (Fig. 5.1) reveals a minimum value of about 1400m above mean sea level (msl) at about the location of Lake Shalla and values greater than 2800 m above msl on both the eastern and western plateaus flanking the rift floor in the study area. The free-air anomaly map (Fig. 5.2) reveals a minimum value of about -20 mGal at the locations of Lake Langano, Lake Abiata and Lake Ziway and values greater than 120 mGal on the shoulders the eastern and western plateaus.

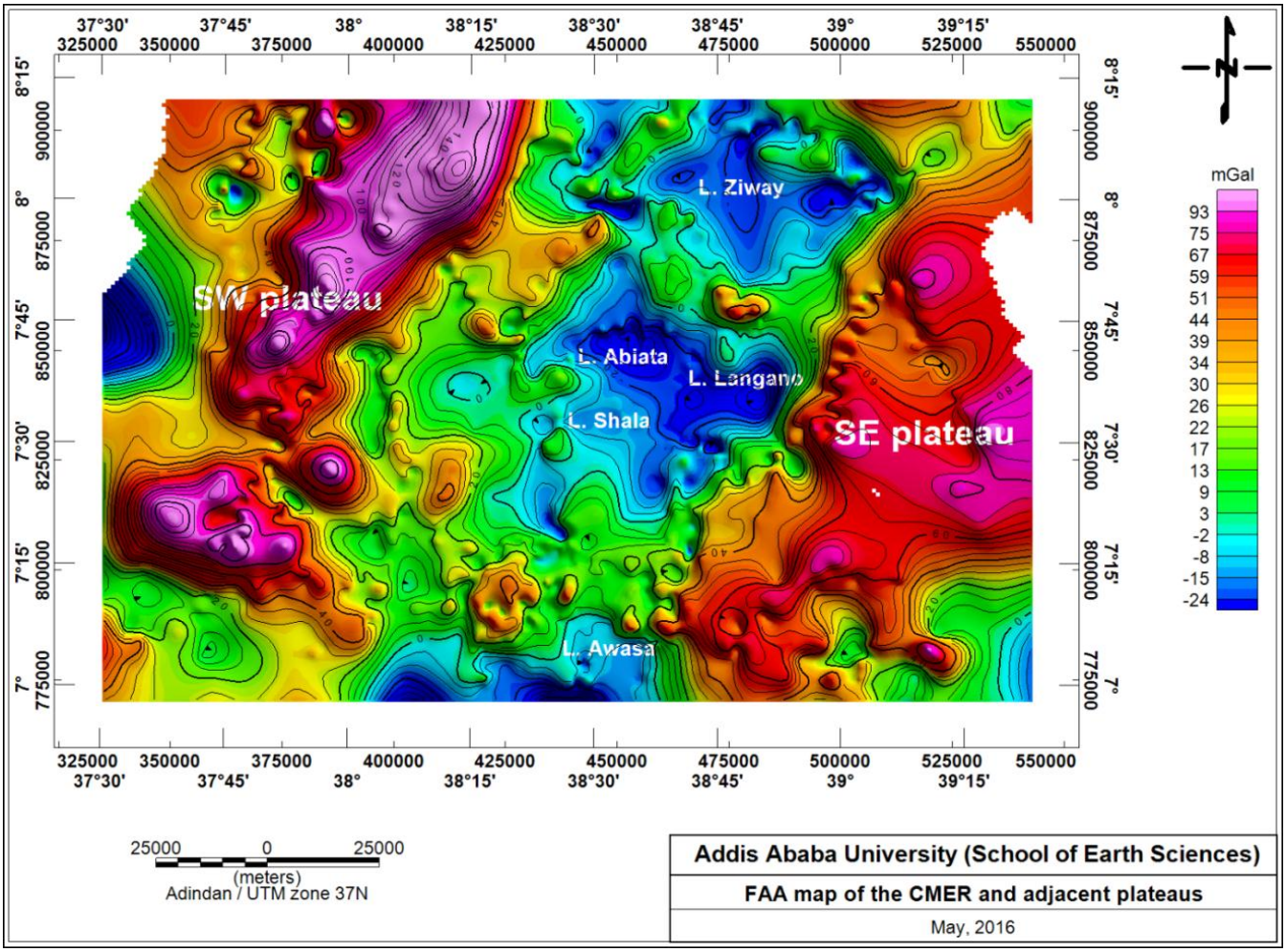


**Figure 5.2** Free air anomaly map of the study area

Generally, the pattern of the major high and low elevation values revealed by the topographic map and the corresponding high and low free air anomaly values revealed by the free-air anomaly map exhibit positive correlations (i. e. as elevation increases the corresponding free air anomaly also increases and vice versa). The rift components (the SE plateau, the rift floor and the SW plateau) are clearly demarcated on both maps and mark the major structural units (the SE plateau, the rift floor and the SW plateau) of the study area.

### 5.1.2 Topographic trend along two selected profiles

Two topographic profiles (Fig. 5.3a and b) are constructed from elevation values extracted from the topographic map along two lines (P1 and P2) drawn in an W-E direction and crossing the major structural units (the rift floor and the adjacent plateaus). The purpose of constructing these profiles is primarily to show how the topography varies over the study area. The maximum elevation of the profile lines coincides with the SW and SE plateaus and crosses the rift floor with minimum elevation. Of course, in the rift floor there are different volcanic centers and ridges that show a higher elevation than the surrounding depressions. In addition, the profile lines are characterized by steep gradient over the transition zones between the rift floor and the two adjacent plateaus indicating a significant physiographic variation.

Generally, the topographic map, free-air anomaly map and the topographic profiles show similar elevation patterns.

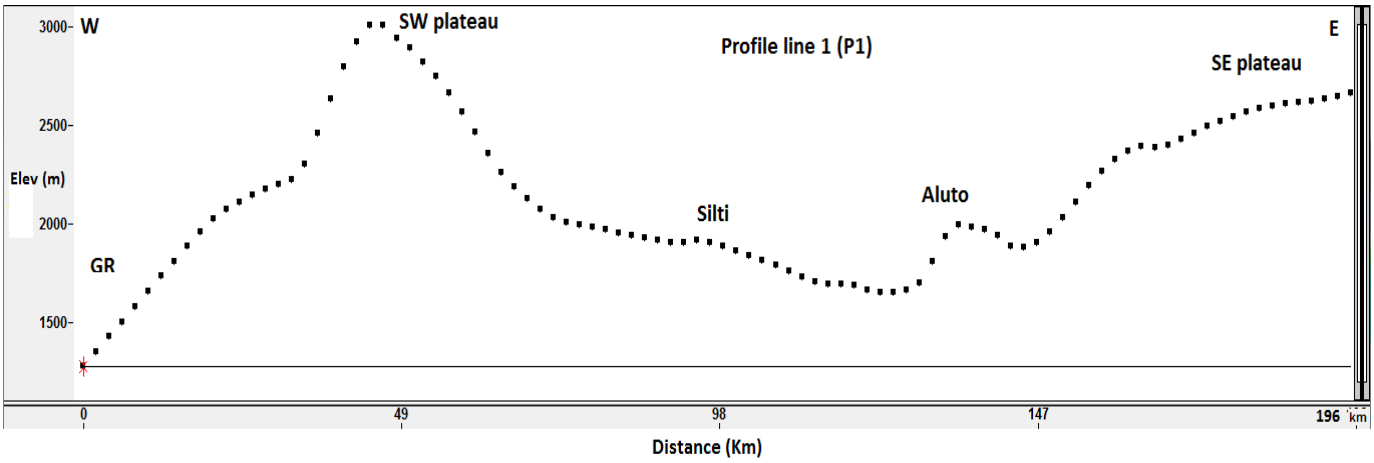


**Figure 5.3a** Trend of topography along profile P1

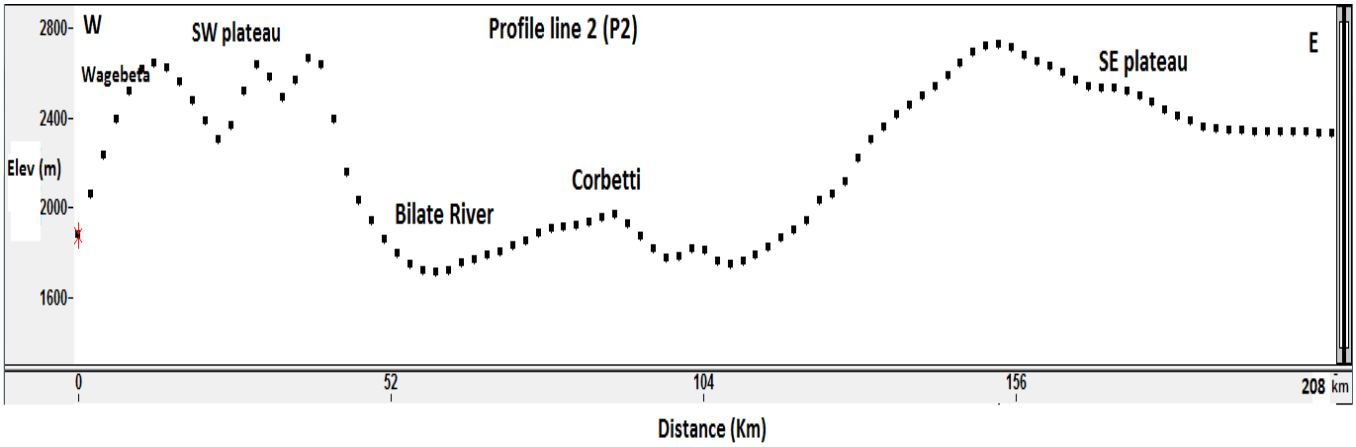


**Figure 5.3b** Trend of topography along profile P2

## 5.1.3 Complete Bouguer gravity anomaly map

Gravity data in the form of Bouguer anomaly map can be considered as one of the most important sources of information regarding the internal structure of the earth's crust and probable density distributions. Hence, in order to interpret the crustal structure of the central MER and adjacent plateaus a complete Bouguer anomaly map has been produced (Fig.5.4). The complete Bouguer anomaly map shows a strong negative gravity field value on both the SW and SE plateaus. The map also reveals a steep gravity gradient along the SE escarpment of the rift floor and a relatively low gradient along the SW escarpment. The SE plateau is characterized by a minimum value of about -260 mGal at a location NE and SW of Kofele town, whereas, the SW plateau shows a minimum value of about -240 mGal at a location east of Kose village. The SE plateau is extensively characterized by strong negative value than the SW plateau in the study area. These minimum values corresponding to the elevated platforms are superimposed by strong positive Bouguer anomalies of two linear zones within the rift floor with a general trending structure of NNE-SSW. The first linear zone traced by a smooth blue line that runs parallel and close to the eastern rift escarpment is interpreted to be due to the volcano-tectonically active zones of the WFB. The WFB passes through the lakes region and connects all the silicic volcanic centers (Fig. 5.4). Specifically, the strong positive values running along the WFB are coincident with the Aluto, Shala and Corbetti volcanic compexes/calderas. Around the Shala and Corbetti areas the complete Bouguer gravity anomaly shows an N-S to NNE-SSW trending structure. Towards the northern end of Lake Ziway the general trend of the Bouguer anomaly is changed to NE-SW.

This change in the Bouguer gravity anomaly trend coincides with the change in the geologic structure from NNE-SSW to NE-SW at the locations of Lake Ziway and Asela region noticed by Meyer et al. (1975). From the map one can easily notice that there is no gravity data coverage for the Lakes Ziway, Abiata, Langano and Awasa. Thus, the observed anomaly over each lake is a result obtained through interpolation of gravity data collected from the surrounding areas.

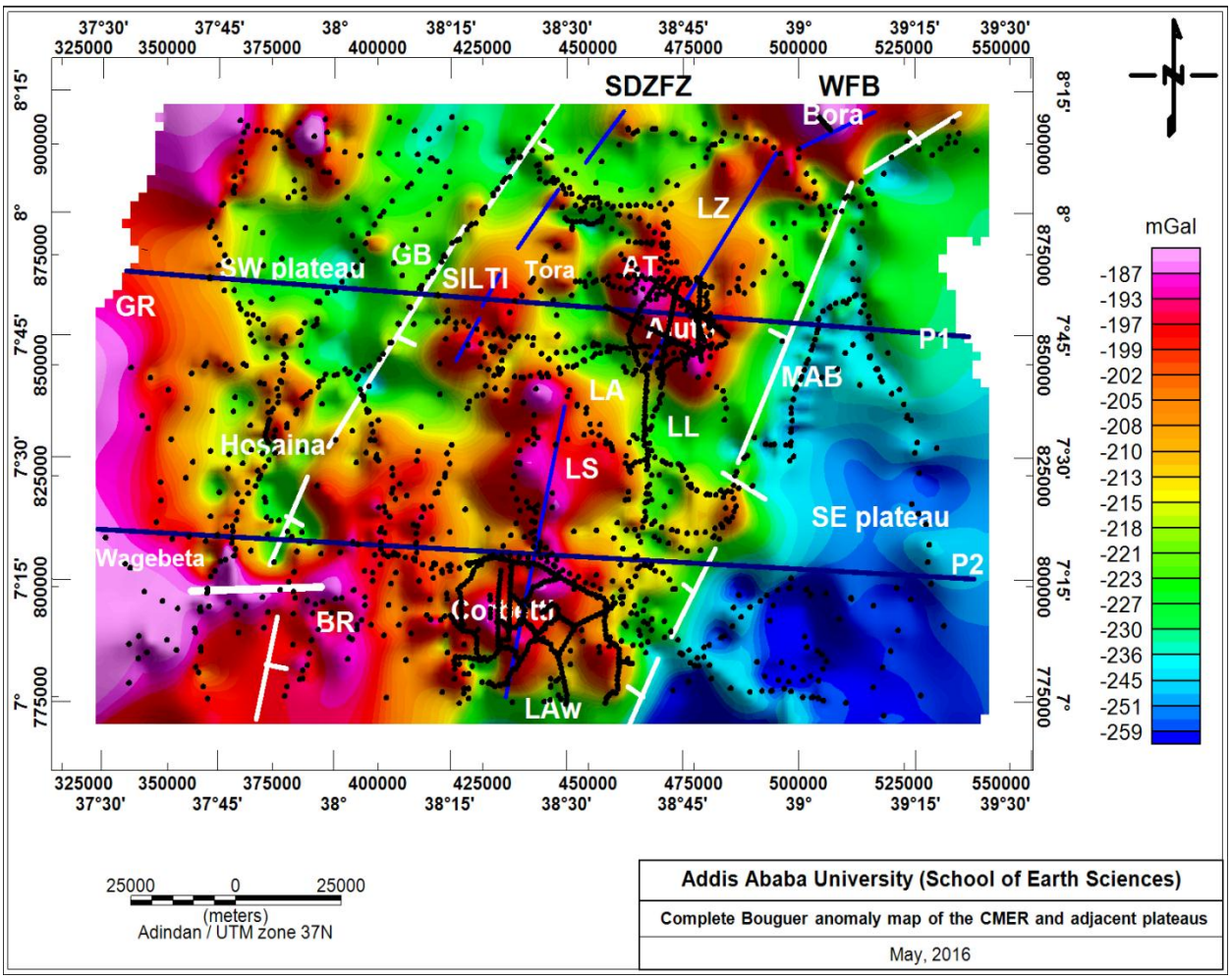


**Figure 5.4** Complete Bouguer gravity anomaly map of the study area. Where LZ (Lake Ziway), AT (Adami Tulu), LA (Lake Abiata), LL (Lake Langano), LS (Lake Shala), Law (Lake Awasa), BR (Bilate River), GR (Gibe River), MAB (Munesa-Asela border fault), GB (Guraghe border Fault). White smooth line represents fault escarpment with ticks on the down thrown side and black dots represent gravity data distribution of the study area.

The second positive Bouguer gravity anomaly zone indicated by a smooth blue line (Fig.5.4), which runs parallel and close to the western escarpment seem to follow the active Silti DebreZeit Fault Zone (SDZFZ) trend. In the study area this active zone is associated with high density geologic units of basaltic origin (e.g. scoria cones, cinder cones etc.,) as shown on the geological map of the study area (Fig. 2.3) and also confirmed during field observations.

The rift floor west of Lake Awasa and Corbetti caldera complex is characterized by a strong Bouguer gravity maximum with a general orientation of N-S and coincident with the rift-controlled basin of the Bilate River. Immediately west of the Bilate River basin and at the southern end of the Guraghe border fault (GB) escarpment, the positive Bouguer gravity anomaly has an E-W trend. This E-W anomaly trend coincides with an offset of the NNE-SSW trending western rift margin. Further to the west of the E-W trending positive Bouguer anomaly zone there exists another NW-SE trending high Bouguer gravity anomaly zone. This high anomaly zone is coincident with the location of the huge Wagebeta caldera complexes (Fig. 5.4 and. 5.8). The Wagebeta calderas and associated domes are arranged linearly transverse to the NNE-SSW trending rift margin along the cross-rift Bonga lineaments (Gidey Woldegabriel et al., 1990 and references therein) (Fig. 5.8). The mismatch in alignment of the rift margin and the Wagebeta caldera complexes have been witnessed by several previous geological and geophysical works (e.g., Rezene Mahatsente et al., 1999). This zone is also considered as a transition zone of the southern termination of the CMER and the northern termination of the SMER.

There is also a high anomaly zone in the NW extremities ($8^0$ $10^{'}$ N) of the study area. This high anomaly zone is associated with the Gibe River basin where the western plateau is decreasing in elevation when going westwards and an increase in the Bouguer gravity anomalies is expected.

The strong positive Bouguer gravity anomaly zones of the WFB, SDZFZ, Goba-Bonga transverse lineament and the Wagebeta caldera complexes are possibly attributed to the intrusion of relatively higher density material from the upper mantle to the low density crust though their degree of intrusion varies. That is, the high density upper mantle material intruding in to the low density crustal material gives rise to a positive density contrast resulting in the observed positive Bouguer gravity anomalies over the rift floor.

The areas occupied by Lakes Abiata, Langano, and east and west of Lake Ziway are characterized by low gravity anomaly values which are possibly due to the accumulation of thick sediments.

### 5.1.4 Complete Bouguer gravity anomaly trend along two selected profiles

Two complete Bouguer gravity anomaly profile (Fig. 5.5a and b) are constructed from complete Bouguer gravity anomaly values extracted along line P1 and P2 shown on the complete Bouguer anomaly map (Fig. 5.4). The profiles are intended to show variation of the Bouguer gravity field over the two plateaus and the rift floor. Profile (P1) is characterized by maximum Bouguer gravity anomaly over the Gibe River, Silti and Aluto volcanic center whose locations are limited to the rift floor. Profile (P2) shows a maximum Bouguer gravity field over the Wagebeta caldera complexes, Bilate River basin and the Corbetti volcanic centers whose locations are limited to the rift floor. The maximum values observed over the rift floor occur at the location of Silti which is part of the SDZFZ, and over the locations of the Aluto and Corbetti volcanic centers which are coincident with the WFB. The high values observed over the rift floor decrease rapidly when going towards the shoulders of the adjacent plateaus. There appears to be a steep Bouguer gravity gradient over the SE rift escarpment as compared to the SW rift escarpment. Comparison of the Bouguer gravity along the two profile lines generally show similar patterns consisting alternating bands of negative anomalies over the shoulders of both the SE and SW plateaus and positive anomaly over the rift floor.

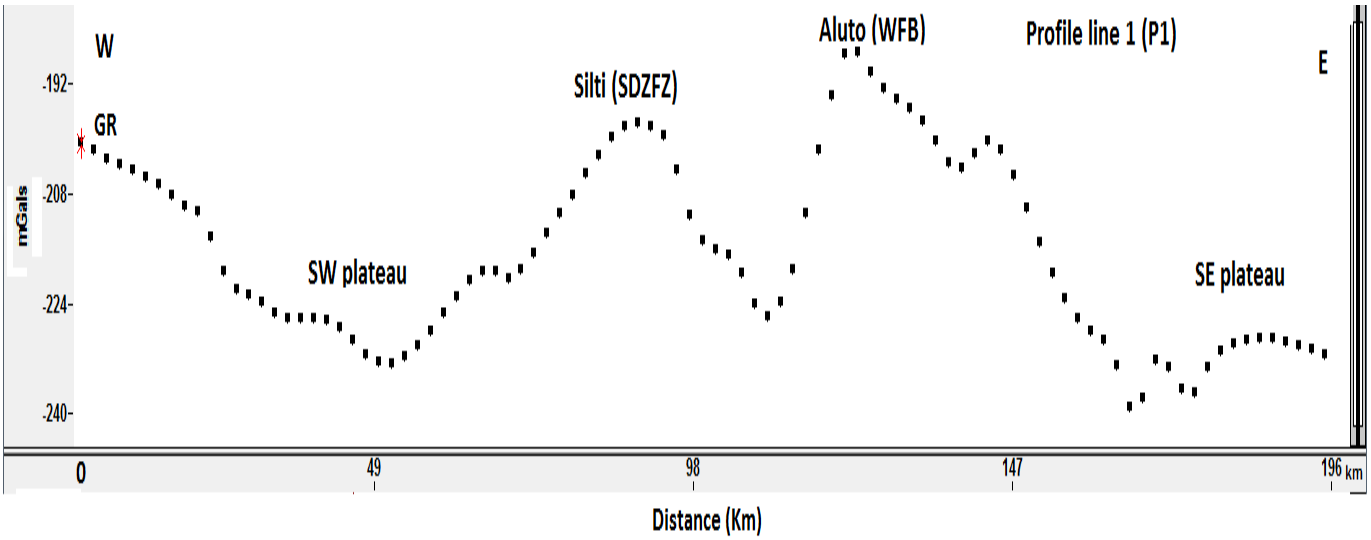


**Figure 5.5a** Trend of complete Bouguer gravity anomaly along profile P1.

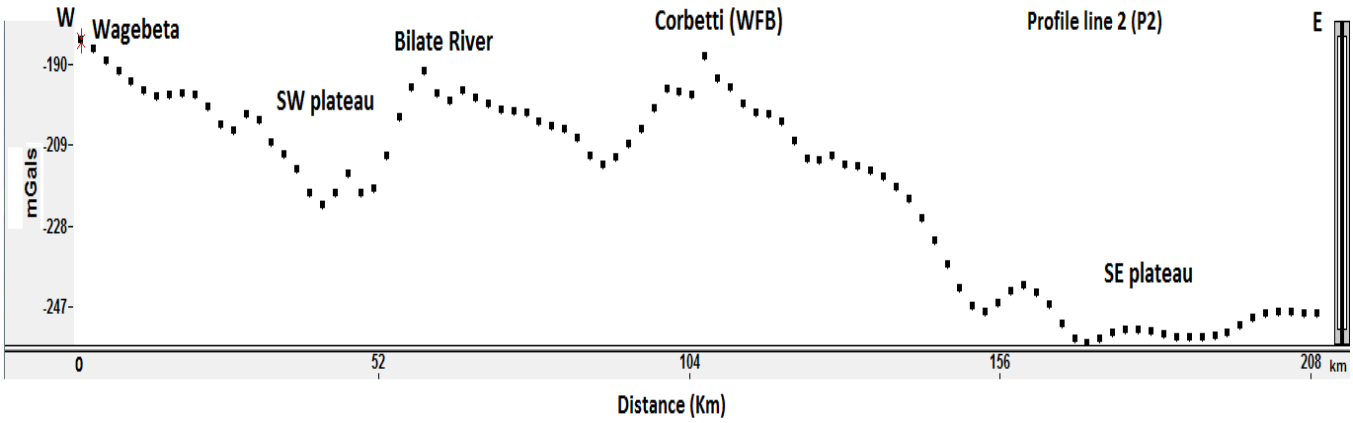


**Figure 5.5b** Trend of complete Bouguer gravity anomaly along profile P2.

## 5.1.5 Regional gravity anomaly map

The estimated regional gravity values of all the gravity stations considered that are determined following the procedure outlined in section 4.2.3 are plotted to produce the regional gravity anomaly map (Fig. 5.6) of the study area, which is basically attributed to variations in the deep-seated crustal structure.

The regional anomaly map reveals lineated anomalies corresponding to four distinct broad zones over the study area. These zones are identified interms of orientation and relative intensity of the regional gravity anomaly they are associated with. The first zone which corresponds to the shoulder of the SE plateau is characterized by a minimum regional gravity anomaly ranging from -260 mGal to -215 mGal. The second zone which corresponds to the shoulder of the SW plateau is characterized by a minimum regional gravity anomaly ranging from -230 mGal to -215 mGal indicating that the SW plateau is associated with a relatively higher regional gravity anomaly as compared to the SE plateau. This anomaly difference over the SE and SW plateaus is attributed to either low density asthenospheric material at the base of the lithosphere or in the upper mantle beneath the SE plateau as isostatic compensation (i.e. the SE plateau is compensated at depth by mass deficiencies) (Oluma 1986 and references therein).

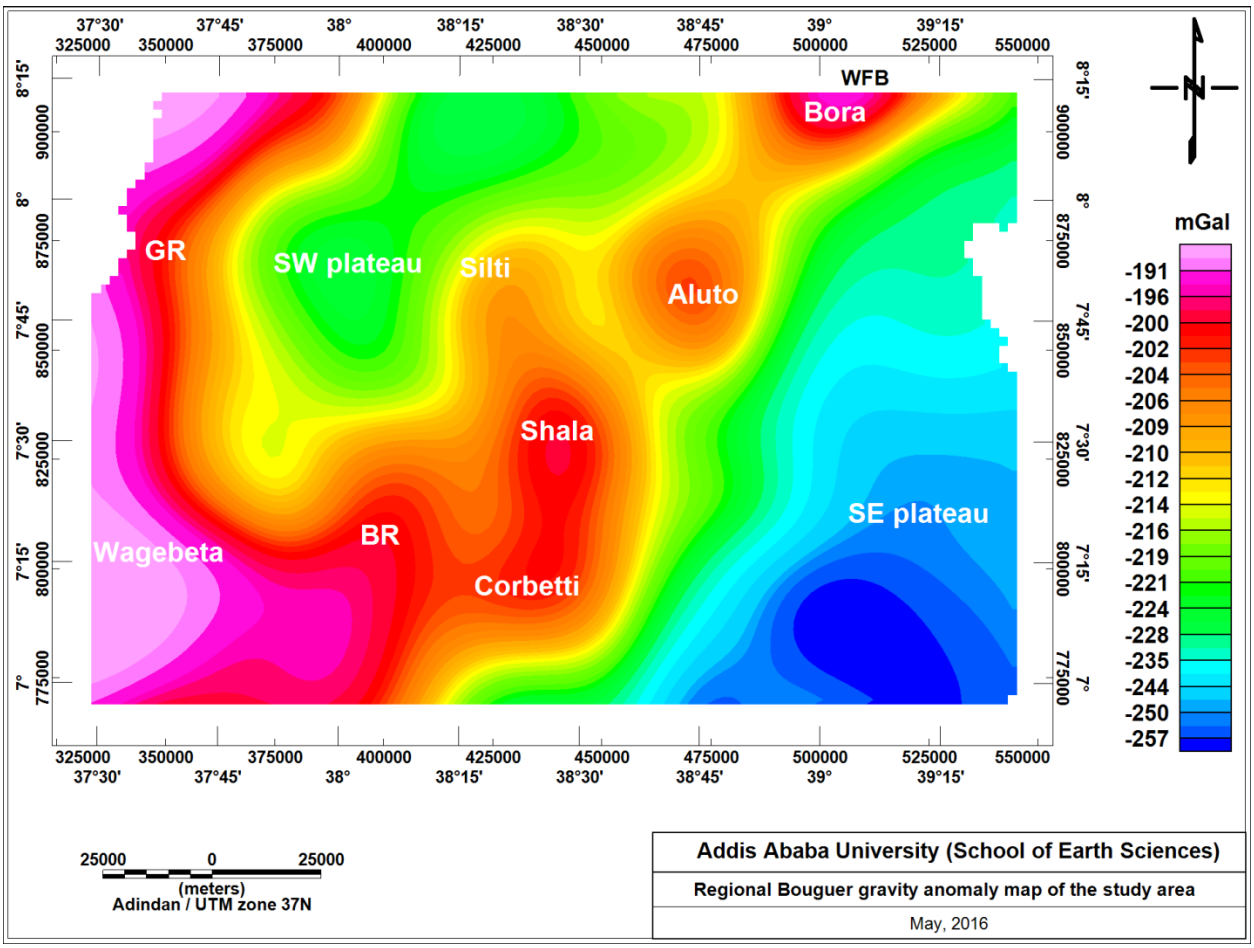


**Figure 5.6** Regional gravity anomaly map of the study area. Where, BR (Bilate River), GR (Gibe River).

The third zone corresponds to the rift floor extending in a NNE-SSW direction from Bora to Corbetti volcanic centers is characterized by a relatively higher regional gravity anomaly ranging from -210 mGal to -190 mGal. This zone consists of distinct positive regional anomalies corresponding to the locations of the Bora, Aluto, Shala and Corbetti volcanic complexes. In particular the positive regional anomaly extending from Aluto to Bora is oriented NNE-SSW following orientation of the WFB. South of the Aluto volcanic center, the regional gravity anomaly trend over the Shala and Corbetti volcanic complexes changes to N-S direction and seems to be connected with the location of Silti which marks the southern termination of the SDZFZ (Fig. 5.8). The localized patches of positive gravity anomalies corresponding to the location of the SDZFZ observed on the complete Bouguer anomaly map (Fig. 5.4) are not clearly delineated on the regional gravity anomaly map. The absence of these patches of positive anomalies on the regional anomaly map indicates that the effect of the deep source is dominant.

The fourth zone which generally covers the western and SW parts of the study area is characterized by a relatively much higher regional anomaly (> -195 mGal) extending in a N-S direction from the Wagebeta caldera complexes towards the Gibe River (GR). Moreover, west of Corbetti volcanic center, there is a N-S oriented regional gravity high coincident with the rift controlled Bilate River basin.

The width of the positive anomaly zone corresponding to the rift floor increases southwards and eventually shifts to the west towards the E-W trending positive anomaly zone coincident with the Goba-Bonga tectonic lineament and the Wagebeta volcanic complexes (Fig. 5.8). This regional gravity high zone with an E-W trend is clearly evident on the regional gravity anomaly map as compared to the complete Bouguer anomaly map (Fig. 5.4). This E-W trending regional gravity high occurs at the latitude where the negative gravity anomaly zone of the SW plateau is attenuated and the NNE-SSW trending positive gravity anomaly zone of the rift floor axis is shifted westwards.

The distribution of the major regional gravity (positive and negative) anomalies over the study area appears to demarcate the major volcano tectonic features of the CMER and adjacent plateaus. The site of intense gravity maxima with in the study area correspond to the sites of deep origin magmatic intrusions which are generally accepted to play a significant role in rift extensions.

### 5.1.6 Residual gravity anomaly map

In this section interpretation of the residual gravity anomaly map (Fig. 5.7) in terms of geology has been made using the volcano-tectonic map (Fig. 5.8), the simplified geologic map (Fig. 2.3) and superimposed faults affecting the central MER and adjacent areas. The compiled map reveals distribution of the major residual (positive and negative) anomalies (< -12 to > 10 mGal). which are supposed to arise from subsurface (shallow) anomalous geologic sources occurring over the rift floor and the adjacent plateaus.

The rift floor is dominated by several localized relatively positive residual anomalies (> 5 mGal) that are coincident with the prominent volcanic centers and relatively negative anomalies (< -4 mGal) over the location of the rift lakes and intermediate anomalies ranging from -4 to 2 mGal.

The adjacent plateaus are associated with dominantly low (< -4 mGal), intermediate (-4 to 2 mGal) and high (> 5 mGal) residual anomalies at specific locations.

Specifically, the peralkaline silicic volcanic centers of Bora, Aluto, Shala, Corbetti and Awasa caldera are characterized by strong gravity highs (> 10 mGal) (Fig. 5.7). These local residual gravity highs observed over the volcanic centers are attributed to the higher density materials supposed to exist beneath intrusions. The positive residual gravity high observed at the location of the southern termination of the SDZFZ is thought to arise from a high density material (possibly high density intrusion). This high density material is clearly evident on the geologic map (Fig. 2.3) marked as to consist of high density basaltic and scoriacious materials aligned in NNE-SSW direction.

The superimposed active faults on the residual gravity anomaly map (Fig. 5.7) indicate the active volcanic centers (Bora, Aluto, Shala, Corbetti and Awasa caldera) that lie within the WFB and the SDZFZ are not dissected by recent faults. This indicates that these volcanic centers are filled by hot magmatic intrusions that are possibly found at shallow depth, so that the faults are unable to propagate through these magmatic intrusions. Rather, the faults start to shift their propagation direction away from these magmatic intrusions to accommodate their extension. The occurrence of the superimposed faults (e.g. MAB) is generally associated with intermediate residual gravity anomaly over the study area.

The Munesa-Asela major border faults (MAB) are characterized by intermediate to low residual gravity anomalies that results due to the low density rocks exposed in the area. Geological maps and field observations indicate that these areas are dominated by ignimbrite, welded and unwelded tuff units (Fig. 2.3).

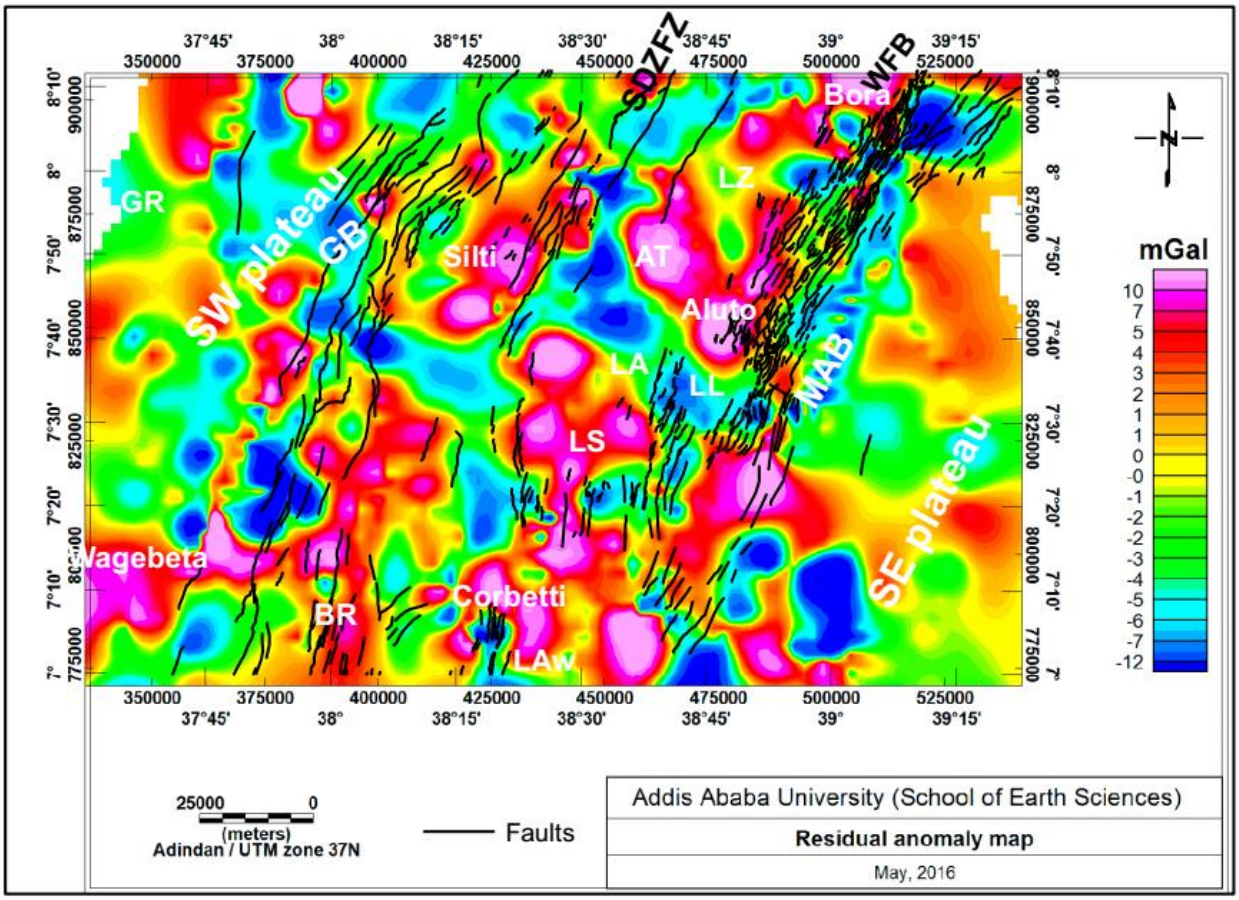


**Figure 5.7** Residual gravity anomaly map of the study area. LZ (Lake Ziway), AT (Adami Tulu), LA (Lake Abiata), LL (Lake Langano), LS (Lake Shala), Law (Lake Awasa), BR (Bilate River), GR (Gibe River), GB (Guraghe border fault) and MAB (Munesa-Asela border fault).

The high residual gravity anomalies found in the south western part of the study area is associated with an E-W trending anomalous zone at the location of Wagebeta volcanic complexes is associated with the major transfer faults and cuts the southward continuation of the Guraghe fault escarpment (GB). This major offset is in agreement with the volcano tectonic map (Fig. 5.8). According to Lakemariam Asfaw (1992), this zone is characterized by strong seismicity. West of Corbetti and Lake Awasa there is an elongated intermediate residual gravity anomaly aligned in N-S direction which is coincident with the rift controlled Bilate River basin.

If we compare the regional gravity anomaly with the residual one the two active zones (WFB and SDZFZ), their effect is more pronounced on the residual anomaly map. This indicates that these volcano-tectonically active zones are probably located at a shallower depth.

In conclusion, when we compare the different rift magmatic centers with one another, the Shala caldera which lies within the WFB is dissected to some extent by N-S oriented normal faults. Further, the magmatic segment around Silti area, which lies within the SDZFZ, is affected by NNE-SSW oriented normal faults at least in the study area. All these issues are very important to establish the relationship between tectonic and magmatic evolutions of the study area in relation to the evolution of the MER.

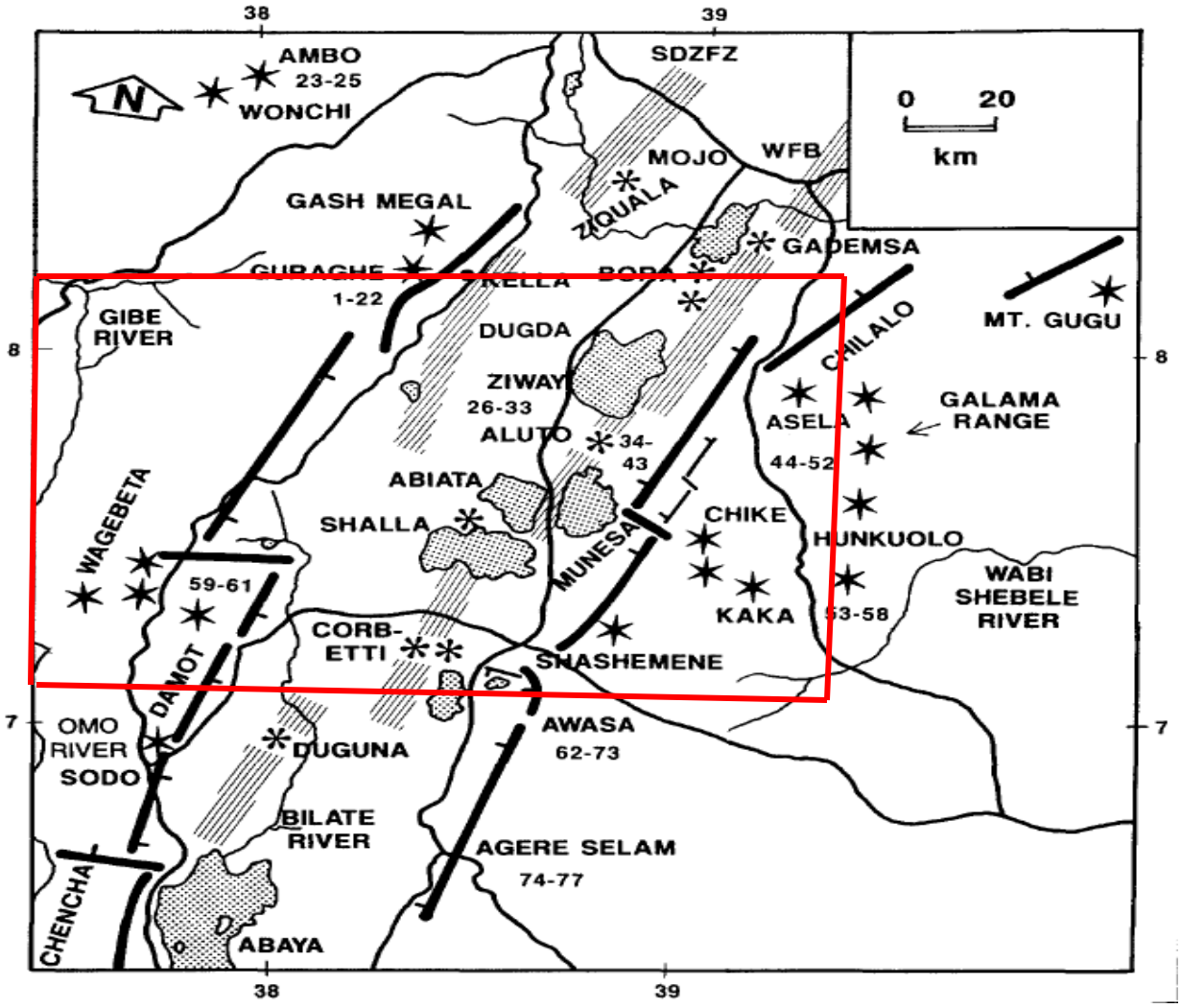


**Figure 5.8** Simplified volcano-tectonic map of the central sector of the MER and adjacent areas. Thick line segments represent rift margin faults with ticks on the downthrown side. Pointed stars represent rift-shoulder central volcanoes, and asterisks are Quaternary peralkaline rhyolite centers of the rift axis. The dual marginal Quaternary rift axes on the rift floor of the northern part of the central sector of the MER are expressed by tightly defined lines (after Gidey WoldeGabriel et al., 1990). The study area is indicated by red rectangle.

### 5.1.7 Gravity analytic signal map

According to Dentith and Mudges (2014) the analytical signal map of a potential field like gravity field, is produced by compiling the 3-directional gradient values of the gravity field (residual gravity anomaly field) computed at several locations in the survey area given by:

$$As(x, y, z) = \sqrt{(\frac{\partial f}{\partial x})^2 + (\frac{\partial f}{\partial y})^2 + (\frac{\partial f}{\partial z})^2} \quad (3.15)$$

Where, *f* is the gravity field (the residual gravity anomaly field) considered in the computation.

The analytic signal map (Fig. 5.9) of the study area is constructed from the residual gravity anomaly map of the study area. This map is supposed to reveal patterns of positive maximum values over geologic units that are in vertical contact.

On the analytic signal map faults affecting the CMER are superimposed to facilitate its interpretation. As can be revealed from the map, the maximum values of the analytic signal map are generally coincident with the gravity anomaly peaks observed in the residual magnetic anomaly and with known structural and geological features/contacts. This is evident in the case of Munesa-Asela and Guraghe border faults which are characterized by strong analytic signal peaks and traces very well all the faults with a general trend of NNE-SSW, N-S, and NE-SW (Fig. 5.9). The two major tectono-magmatic zones of the WFB and SDZFZ and the rift controlled Bilate River basin are also clearly highlighted on the analytical signal map. In fact, the peaks of the map are not only due to the faults and volcanic centers, but also due to lithological contacts.

As one can notice easily from the map, the SE and SW plateaus are characterized by low analytic signal map. The analytical signal map which high lights all the different parts of rift proper and adjacent plateaus are in a good agreement with the geologic map produced by Gidey WoldeGabriel et al. (1990) (Fig. 5.8) and Tsegaye Abebe et al. (2010) (Fig. 2.1) and simplified geologic map of the study area (Fig. 2.3).

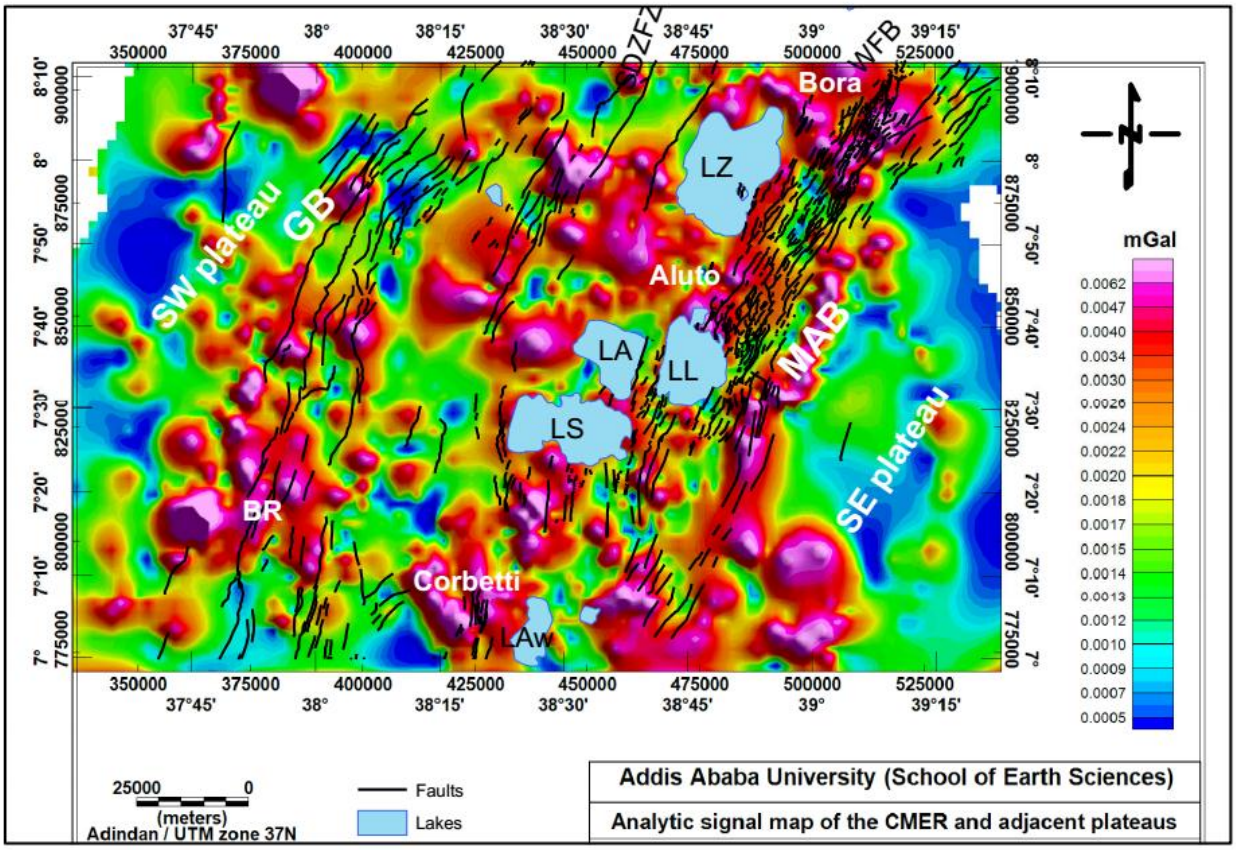


**Figure 5.9** Gravity analytic signal map of the study area. The faults traced on the map were obtained (from Corti, 2016). LZ (Lake Ziway), LL (Lake Langano), LA (Lake Abiata), Law (Lake Awasa), BR (Bilate River), GB (Guraghe border fault), MAB (Munesa-Asela border fault).

## 5.1.8 Gravity Tilt derivative map

The tilt derivative map (Fig. 5.10) of the study area is compiled by applying a tilt derivative filter to the gravity analytical signal map using Geosoft OasisMontaj software. The map is supposed to easily identify the location of faults, contacts inorder to locate edges and geological boundaries in the study area. The tilt derivative map (Fig. 5.10) shows more detailed structural contacts/boundaries than the analytic signal map. It shows positive values over magnetic sources, cross through zero at or near the fault/contact locations and negative outside source zones.

Accordingly the study area is characterized by a set of numerous faults in the N-S, NE-SW and NW-SE directions. These directions are correlated with the general tectonic history of the study area with abundant N-S and NNE-SSW trending structures.

In addition, the tilt derivative map reveals the presence of abundant E-W trending anomaly zones which are possibly coincident with fault offsets. Also there are some other trends in the study area with NW-SE orientation. Generally, the possible structural contacts are indicated by smooth white line, while the possible lithological contacts are shown by the smooth black line.

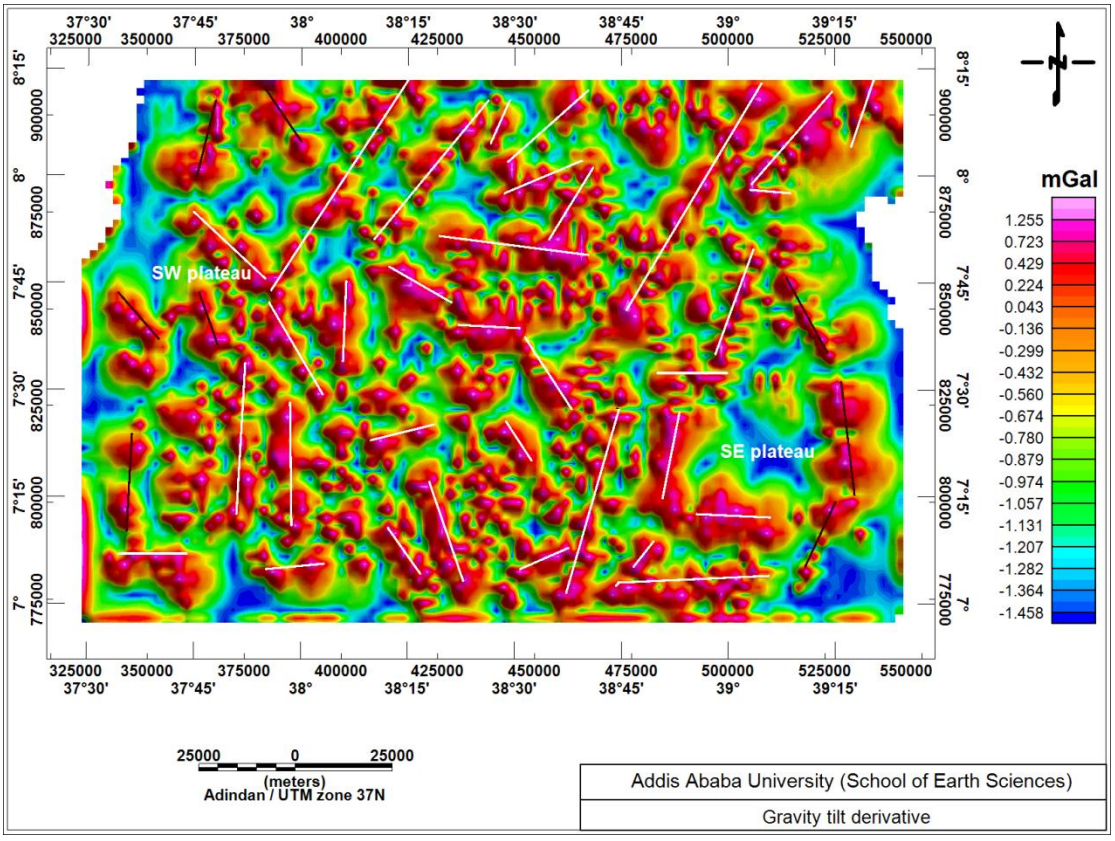


**Figure 5.10** Gravity tilt derivative map of the study area

## 5.1.9 Euler deconvolution gravity map

Euler deconvolution technique is applied in order to estimate the depth and location of the gravity source. In standard Euler deconvolution process, each model contains solutions of a particular structural type defined by the structural parameter. From the principle of Euler deconvolution (GETECH manual), structural index of a value 0, 1, 2 represents geological features of sill/dike, vertical pipe/horizontal cylinder and sphere respectively.

The Euler deconvolution gravity map (Fig.5.11) of the study area is compiled by applying a standard 3D Euler deconvolution filter using the Geosoft OasisMontaj software.

The optimal structural index is selected by a visual inspection of maps which compiled using various structural indices until the best clustering of solutions is obtained. Based on this procedure, a structural index of 2 was determined and applied to the residual magnetic anomaly map to derive the Euler deconvolution map. The map reveals gravity anomaly sources of different depths marked by different colored symbols plotted on the map. These include; a yellow circle indicating gravity sources with depth less than 2 K. The red boxes indicate gravity sources that range from 2 to 3 Km depth. The green triangles represent sources that range from 3 to 5 Km depth. The dark blue inverted triangles represent sources that range from 5 to 7 Km depth. The light blue circles represent sources that range from 7 to 8 Km depth. The letter 'x' represents sources that are greater than 8 Km.

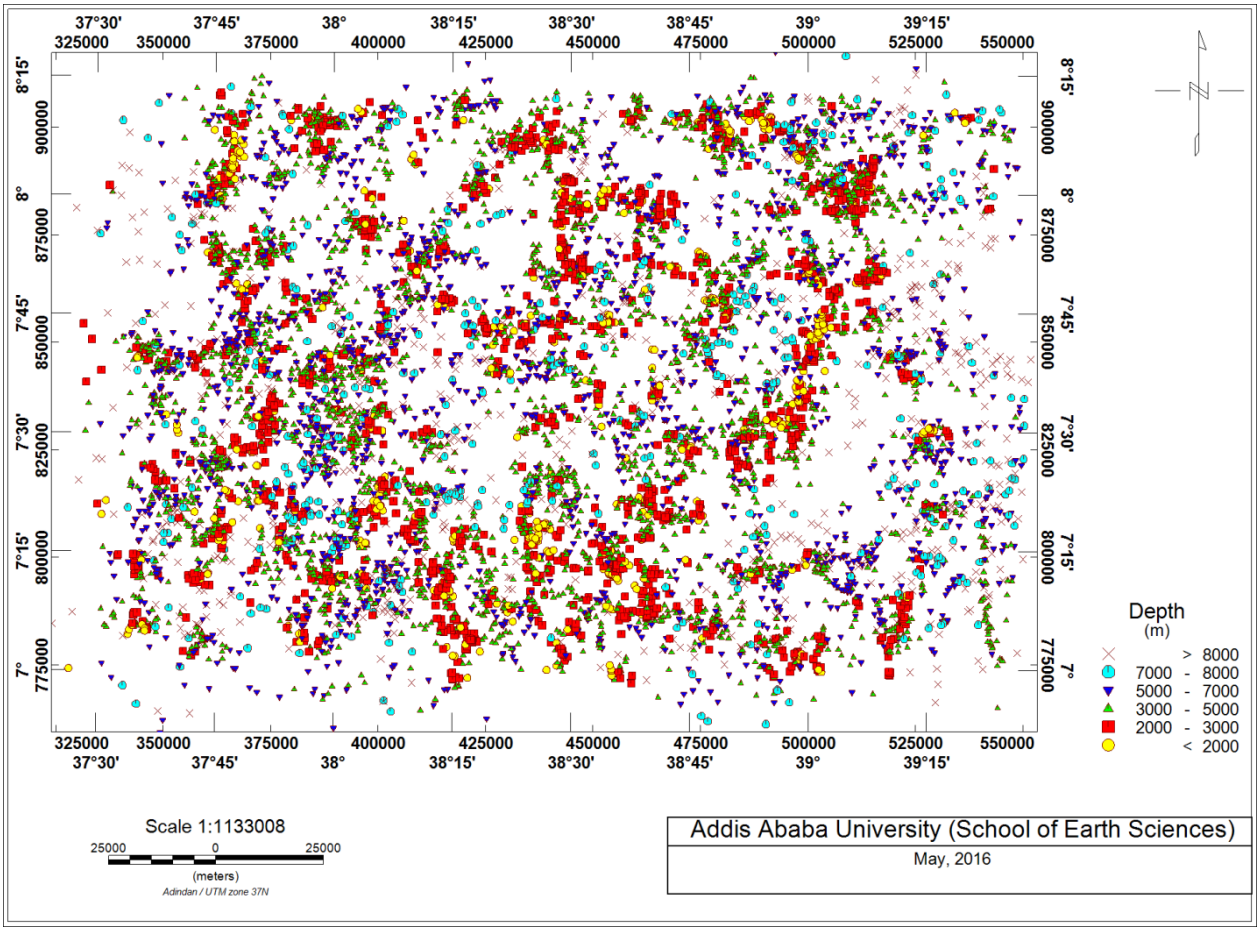


**Figure 5.11** Euler deconvolution gravity map for SI = 2

The yellow circles and red boxes represent relatively shallow sources that are distributed along the WFB. The letter ‘x’ which represents relatively deeper (> 8 Km) is mostly distributed over the shoulders of the SW and SE plateaus indicating the gravity sources below the shoulders of the plateaus are relatively deeper.

The green triangles, dark blue inverted triangles and light blue circles representing relatively intermediate depth (3 to 8 Km) gravity sources are sparsely distributed over the study area.

The distribution of the sources (shallow, intermediate and depth sources) over the study area revealed by the Euler deconvolution map appear to be consistent with the distribution of the sources revealed by the regional gravity anomaly map (Fig. 5.6) and the residual gravity anomaly map (Fig.5.7).

## 5.2 Magnetic data results and interpretation

The aim of magnetic surveying is to identify and characterize the Earth’s crust that is associated with anomalous regions. As a result different magnetic intensity/anomaly maps that are assumed to be relevant for this thesis work were produced following the appropriate reduction procedures. All the magnetic anomaly maps were generated using Geosoft Oasis Montaj (Version 6.4.2) software.

### 5.2.1 Total magnetic field intensity map

The total magnetic field intensity map (Fig.5.12) of the study area is compiled by plotting all the magnetic data that are corrected for diurnal variation at their respective locations. The map is thought to show the variation in magnitude of the combined effect rock magnetization the dipole field over the survey area. The total field intensity values over the survey area vary from a minimum of 34905nT to a maximum of 35475nT. The uneven areal distribution of the major (relatively positive and negative) anomalies and the maximum difference (670 nT) between the maximum and minimum intensity values revealed by the map indicate the presence of prominent anomalous geologic features in the survey area.

Generally, the total magnetic field intensity map can be classified into three anomalous localities of different intensity values.

The first anomalous localities are characterized by high total magnetic intensity values ranging from 35245 nT to 35400 nT and associated with the locations of Aluto volcanic center, Lake Ziway, Adami Tulu (AT), Gademota caldera (GA) and the Corbetti volcanic center. The second anomalous localities are characterized by intermediate magnetic intensity values ranging from 35150 nT to 35180 nT and associated with the locations Shala caldera, Awasa caldera and Munesa boarder fault. The third anomalous localities are characterized by magnetic intensity values of less than 35150nT and associated with the locations of Lake Langano, Lake Abiata, the area between Corbetti and Lake Shala and north of Lake Awasa. Evidences derived from geologic map (Fig. 2.3) of the study area and field observations indicate that these localities are occupied by thick accumulation of sediments.

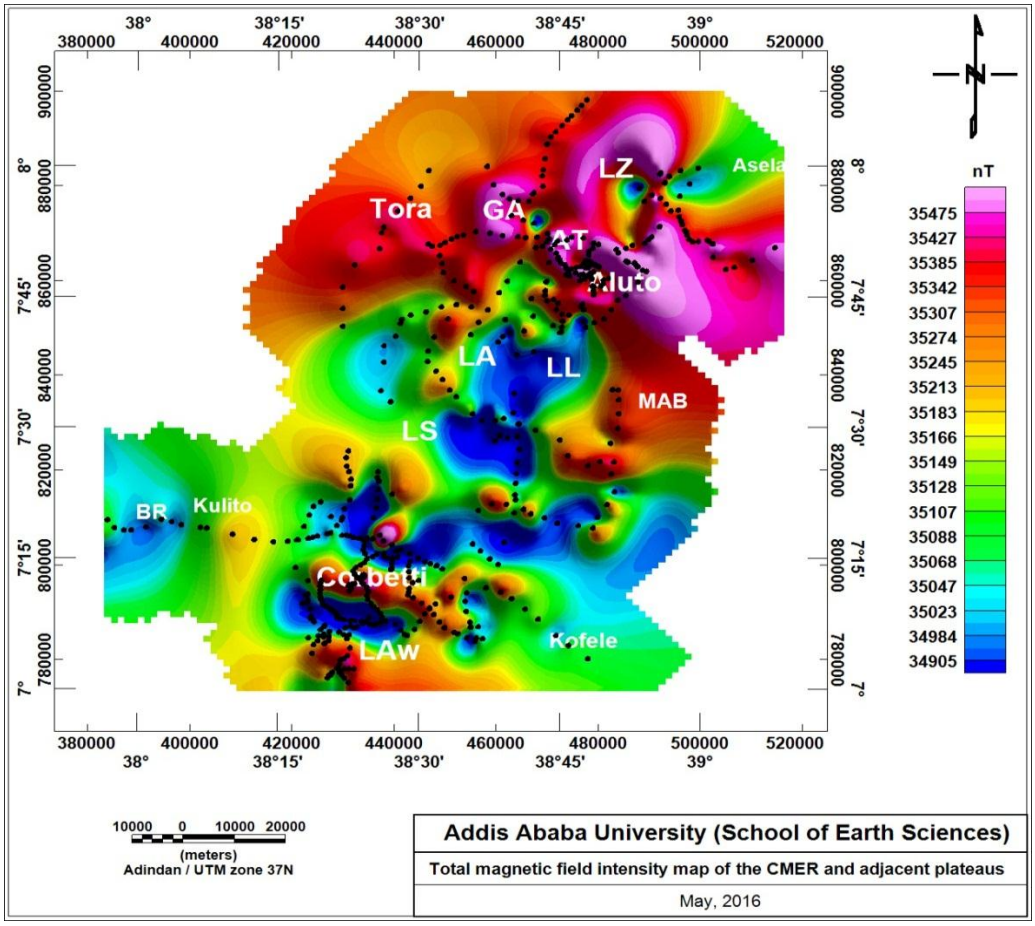


**Figure 5.12** Total magnetic field intensity map of the study area. Where LZ (Lake Ziway), AT (Adami Tulu), GA (Gademota caldera), LA (Lake Abiata), LL (Lake Langano), LS (Lake Shala), Law (Lake Awasa), BR (Bilate River), GR (Gibe River), MAB (Munesa-Asela border fault). The black dots represent magnetic data distribution.

In addition, the regions SW of the study area running towards Kulito town and Bilate river covering a substantial part of the SW plateau and the regions SE of the study area running towards Kofele town covering a substantial part the SE plateau are characterized by low to very low (35100 nT – 35900 nT) total magnetic field intensity values.

### 5.2.2 Total magnetic field anomaly map

The magnetic anomaly map (Fig. 5.13) produced is the difference between the diurnally corrected total magnetic field and the expected value of the IGRF. The map is supposed to give an insight into the overall subsurface structure and to some extent composition of the Earth's crust. The magnetic field recorded in the field using the proton precession magnetometer was due to the effect of the Earth's main magnetic field and the anomalous magnetic field. Magnetic data collected from low latitude is difficult to interpret due to the small magnetic field intensity and horizontal ambient field direction. At low magnetic latitudes, anomalies over magnetically susceptible bodies show negative values instead of positive and the anomalies largely depend on azimuthal direction (Beard et al., 2000).

As seen in (Fig. 5.13) the study area shows high to very high total magnetic anomaly over Aluto volcanic center, Adami Tulu, Gademota caldera, Tora, Munesa-Asela border fault, Corbetti volcanic complex, Lake Awasa and west of Corbetti. These high to very high total magnetic anomalies are attributed to either low magnetic susceptibility of magmatic intrusion below the volcanic center or due to the low magnetic susceptibility of rocks. In contrast, mafic volcanic rocks like basalt and scoria which are expected to show high remanent magnetization as compared to other felsic volcanic rocks, reveals high total magnetic anomaly. This is because remanent magnetization may complicate the interpretation of magnetic anomaly at low latitudes and may also enhance the total magnetic anomaly of a body by increasing its detectability. This is evident in the east and SE of Lake Ziway, south of Lake Langano and south of Lake Shala where the high anomalies are due to the basaltic lava flow and scoriaceous materials exposed in the area.

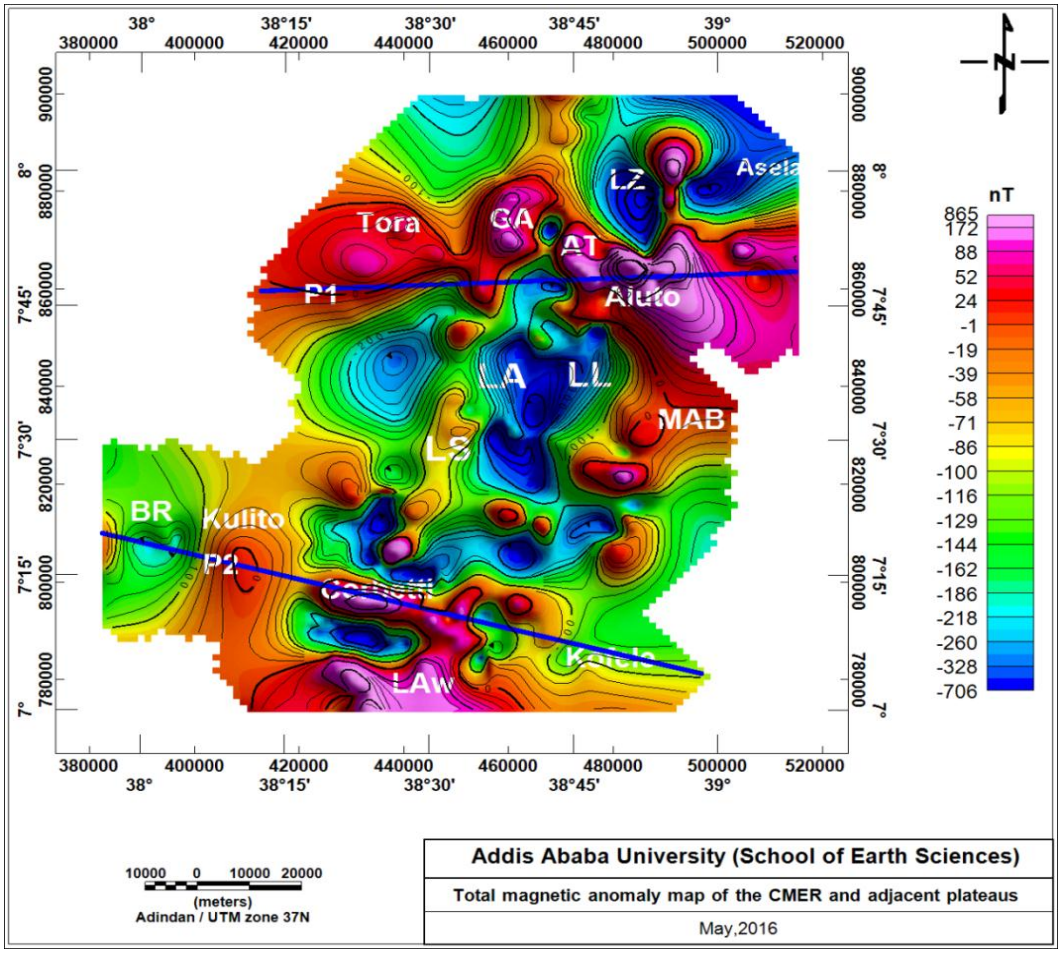


**Figure 5.13** Total magnetic field anomaly map of the study area. Where LZ (Lake Ziway), AT (Adami Tulu), GA (Gademota caldera), LA (Lake Abiata), LL (Lake Langano), LS (Lake Shala), Law (Lake Awasa), BR (Bilate River), GR (Gibe River), MAB (Munesa-Asela border fault).

The Lakes region occupied by Lake Abiata, Langano, Ziway and other parts of the study area in NE of Lake Ziway up to Asela region, NW of Lake Awasa and the areas between Lake Shala and Corbetti are characterized by low to very low magnetic anomalies, which may be attributed to the thick accumulation of sediments. Field observations and geological map (Fig.2.3) show these areas are entirely covered by sediments though the thickness of the sediment varies from place to place. As mentioned earlier these low to very low anomalies are possibly due to the high magnetically susceptible sediments which are possibly derived from the neighboring volcanic materials that have high magnetic contents. The high anomaly value over Corbetti shows an E-W trend which is unlikely in the study area as confirmed from independent gravity and geological studies; rather this is an inherent problem of magnetic anomaly interpretation at low latitude.

This is because equatorial anomalies tend to be stretched in an E-W direction (Beard et al., 2000).

The Shala caldera is characterized by N-S elongated intermediate magnetic anomaly on its western part and it shows low anomaly on its eastern part. There are also areas found in the far NW of the study area, west of Lake Abiata, Bilate River and north of Kofele which are dominated by intermediate to low magnetic anomalies.

Generally, there is no strong relationship as in the case of the complete Bouguer gravity anomaly map, between the volcano tectonically active zones of the WFB, major fault patterns and associated magnetic anomalies. This is because long N-S striking structural features, magmatic intrusions and/or dikes and contacts may not be visible and identifiable on the total magnetic anomaly map of the study area which belongs to low latitude.

### 5.2.3 Total magnetic anomaly trend along two selected profiles

Two total magnetic anomaly profiles (Fig. 5.14a and b) are constructed from the total magnetic anomaly values extracted along line P1 and P2 shown on the total magnetic anomaly map (Fig. 5.13). The profiles are intended to show variation of the total magnetic anomaly field over the rift floor and the SE and SW highlands along the latitudes the profiles are constructed. Profile (P1) is characterized by maximum total magnetic anomaly over the Aluto volcanic center whose location is limited to the rift floor. Along this profile (P1) the total magnetic anomaly trend shows an intermediate value over the locations of Tora and Munesa-Asela border fault (MAB). Profile (P2) shows a maximum total magnetic anomaly field over the Corbetti volcanic centers and is characterized by minimum total magnetic anomaly over the locations of Bilate River and Kofele town. The maximum values observed over the rift floor occur at the locations of the Aluto and Corbetti volcanic centers which are coincident with the WFB.

Comparison of the total magnetic field along the two profile lines generally show similar patterns consisting alternating bands of negative anomalies over parts of the highland and positive anomalies over the rift floor coincident with the major volcanic centers of the study area.

Since the study area is located in equatorial regions there exists an inverse relationship between magnetic susceptibility natures of the geologic bodies/sources and related magnetic responses.

Therefore, the high to very high magnetic anomalies depicted over the volcanic centers are attributed to low magnetic susceptibility (due to heat treatment) geologic materials beneath the silicic volcanic centers. There is also a possibility where the positive magnetic anomalies are associated with basaltic and scoriaceous rock units that are possibly resulted from high remanent magnetization.

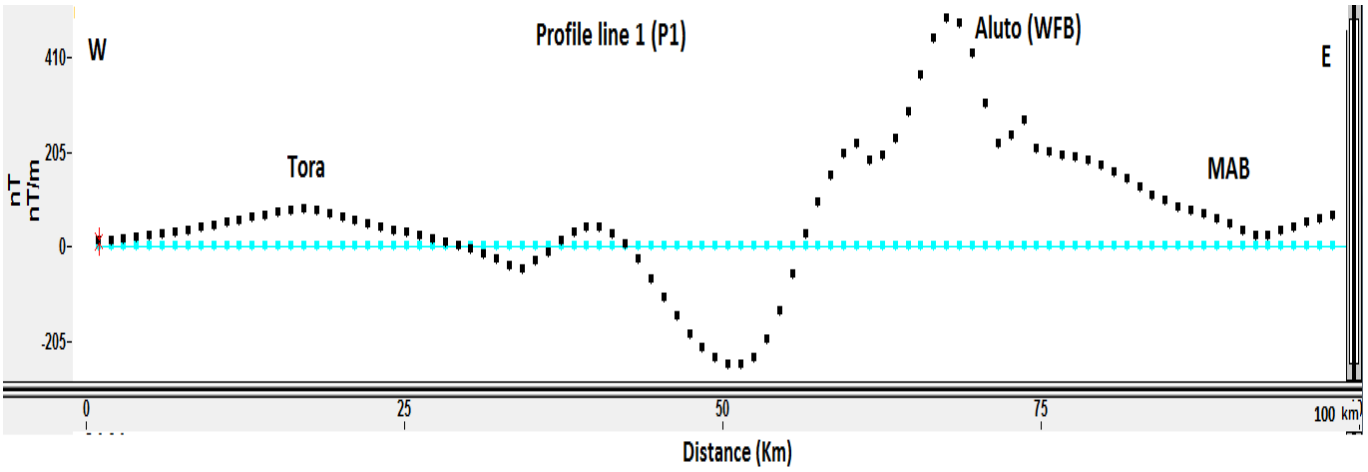


**Figure 5.14a** Trend of total magnetic anomaly along profile P1.

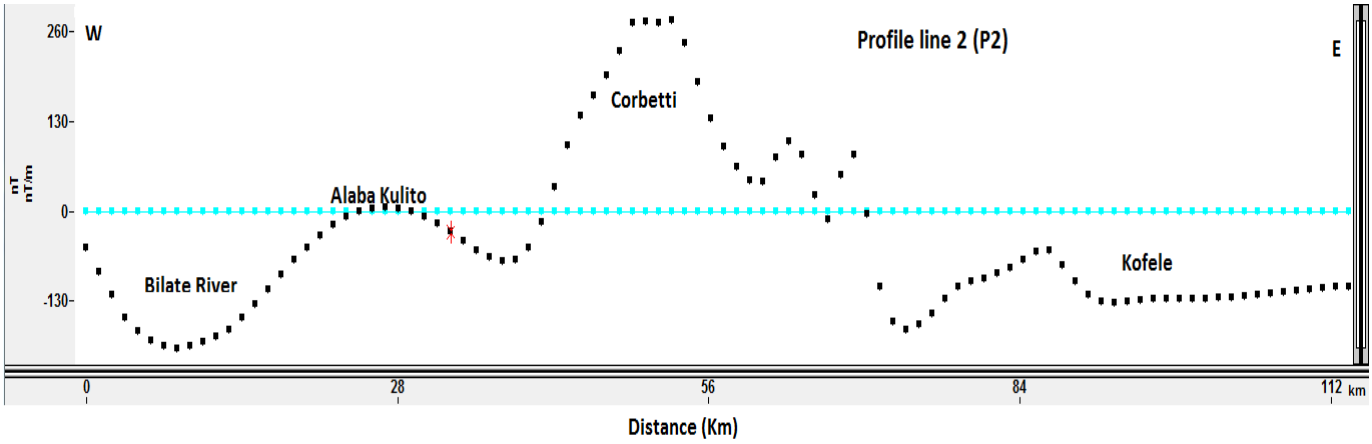


**Figure 5.14b** Trend of total magnetic anomaly along profile P2.

## 5.2.4 Regional magnetic field anomaly map

The regional magnetic anomaly map (Fig. 5.15) reveals four distinct zones with alternating bands of negative and positive magnetic anomalies over the study area from north to south.

The first zone which coincides with the location of Lake Ziway and its flanking areas is associated with a broad negative magnetic anomaly. The second zone which coincides with the locations of Tora, Gademota caldera (GA), Adami Tulu (AT), Aluto volcanic center and Munesa-Asela major border faults (MAB) is characterized by a relatively high to very high (-30 to 85 nT ) magnetic anomalies with the highest peak occurring east of the Aluto volcanic center. The third zone which coincides with the location of Lakes Abiata, Langano, Shala and the flanking areas is characterized by a broad negative magnetic anomaly. The fourth zone which coincides with the location of Corbetti, Lake Awasa and the flanking areas is associated with a broad zone of positive anomaly decreasing towards the west with a minimum over the location of the Bilate River.

The high magnetic anomaly zones observed over the study area are associated with the low susceptibility (heat treated volcanic materials) related to the associated volcanic centers. In particular the magnetic highs over Aluto and corbetti volcanic centers, Gademota and Awasa calderas are correlated with the low magnetic susceptibility geologic bodies beneath the volcanic centers or calderas. Moreover, the high magnetic anomalies over the locations of the Tora and surrounding areas and Munesa-Asela border faults are due to the low magnetic susceptibility rocks exposed in the area (Fig. 2.3).

The first and third low magnetic anomaly zones coinciding with the locations of Lake Ziway and its flanking areas including Lakes Abiata, Langano, Shala and the flanking areas is attributed to the thick accumulation of high magnetic susceptibility sediments that are derived from the surrounding volcanic units.

The northern and central part of the study area is characterized by low to very low regional magnetic anomalies. As explained earlier the regional gravity anomaly shows an N-S oriented magmatic intrusion beneath Shala caldera which is invisible in the regional magnetic anomaly. This is due to the inherent problem of magnetic anomaly interpretation at low latitude zones where an N-S oriented magmatic intrusion/dike injection is not clearly identifiable. Further, the areas west of Corbetti and west of Lake Ziway shows N-S oriented intermediate anomaly.

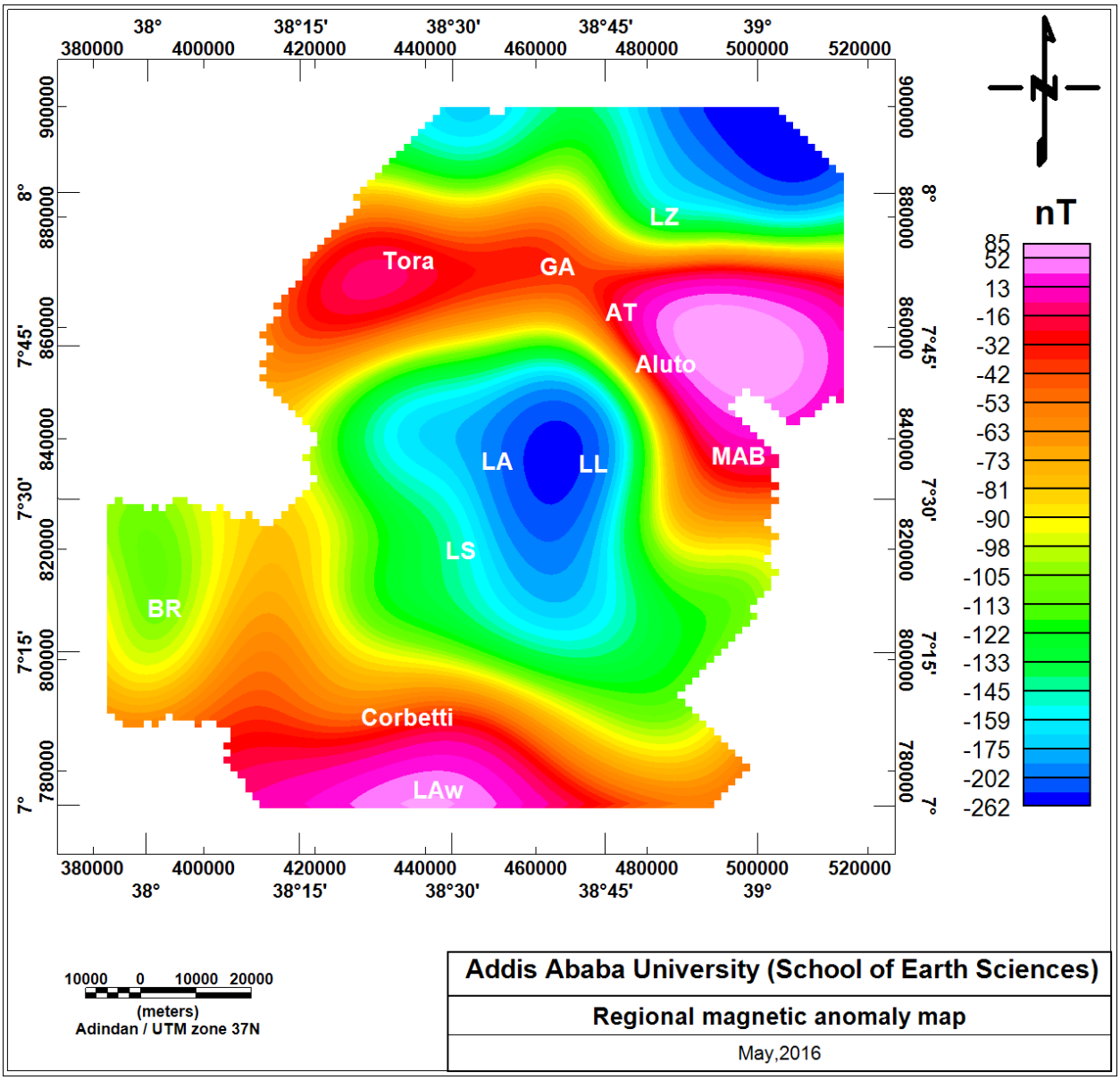


**Figure 5.15** Regional magnetic anomaly map of the study area. Where LZ (Lake Ziway), AT (Adami Tulu), GA (Gademota caldera), LA (Lake Abiata), LL (Lake Langano), LS (Lake Shala), Law (Lake Awasa), BR (Bilate River), MAB (Munesa-Asela border fault).

In contrary, the central part of Lake Ziway, NE of Lake Ziway, Lake Abiata, Lake Langano, west of Lake Abiata, the areas between Lake Shala and Corbetti, NW of Lake Awasa and Bilate River (BR) are characterized by low to very low magnetic anomalies. These low to very low values are associated with thick sediments which are expected to show high magnetic susceptibilities.

When we compare the regional and residual magnetic anomaly map, the strong positive magnetic anomaly values over the Awasa caldera is more evident in the regional one. This indicates that the source of anomaly should be found at a greater depth.

### 5.2.5 Residual magnetic field anomaly map

The residual magnetic anomaly map (Fig.5.16) of the study area was generated using Gaussian residual filter (cutoff wavelength 60 Km) using Geosoft OasisMontaj software. The prominent geological features observed in the residual magnetic anomaly map are generally preserved in the total magnetic anomaly maps (Fig.5.13). However, the residual magnetic anomaly map defines areas like Adami Tulu, Aluto volcanic center and Gademota caldera with very high magnetic anomalies as compared to the total magnetic anomaly map. The Munesa-Asela border faults, Lake Shala, Corbetti volcanic center and Awasa caldera complexes are also characterized by high magnetic anomaly values. All these high anomalous zones are concentrated within the WFB that runs parallel and close to the Munesa-Asela border faults. The area around Tora, which is very close to the SDZFZ also shows high residual magnetic anomaly. This indicates that the main sources of these magnetically anomalous zones found within or close to the WFB and SDZFZ are probably found at shallow depths.

Field observations indicate that the observed residual magnetic anomalies are also governed by the distribution of geologic materials and structural features. Areas covered by basaltic and scoriaceous rocks are associated with positive magnetic anomalies which may result from high remanent magnetization.

This phenomenon is evident at the locations of east of Lake Ziway, south of Lake Shala, west of Lake Awasa and east of Lake Langano which are covered by basaltic rocks and related scoriaceous materials (Fig. 2.3).

On the other hand, the central part of Lake Ziway, NE of Lake Ziway, areas associated with Lakes Abiata and Langano, west of Lake Abiata, north of Corbetti are dominated by low to very low magnetic anomalies. These zones are covered by thick Quaternary sediments (Fig. 2.3). The areas occupied by Kofele and west of Kulito which cover substantial part of the SE and SW parts of the highlands in the study area are characterized by low magnetic anomalies.

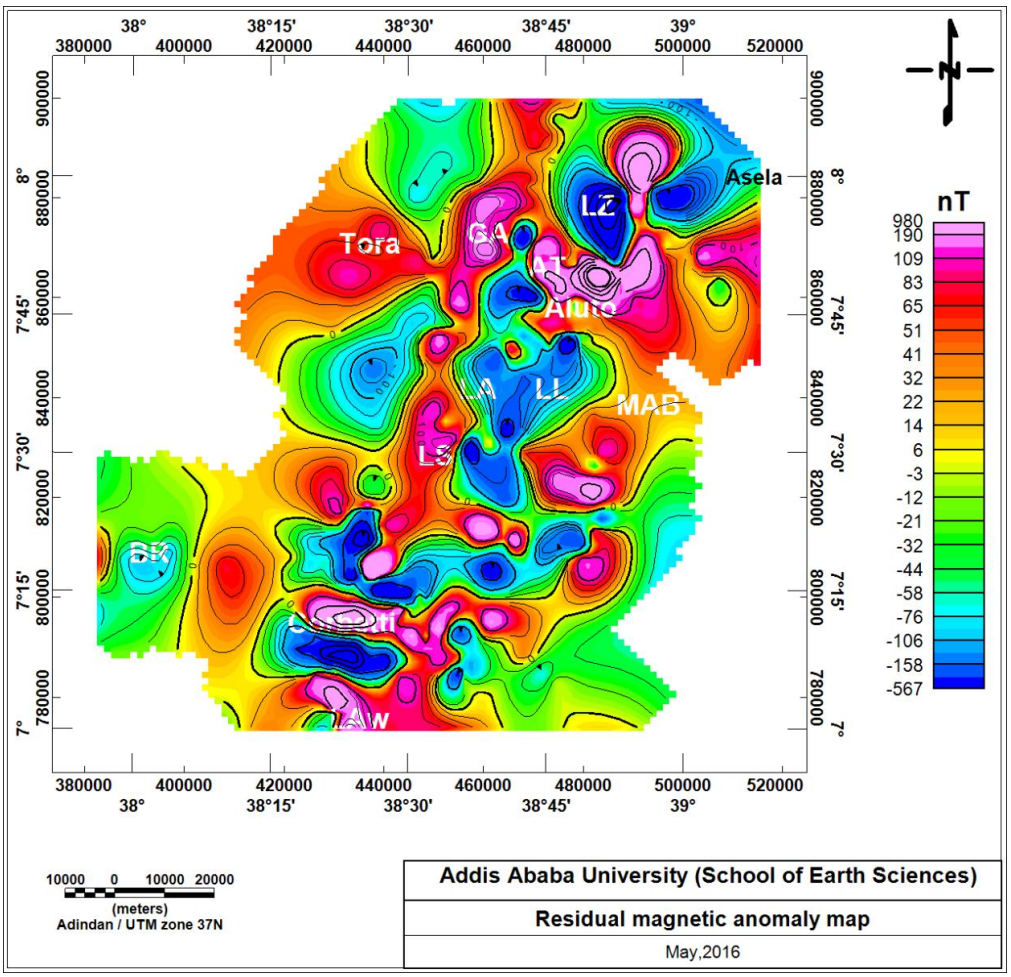


**Figure 5.16** Residual magnetic anomaly map of the study area. Where LZ (Lake Ziway), AT (Adami Tulu), LA (Lake Abiata), LL (Lake Langano), LS (Lake Shala), Law (Lake Awasa), BR (Bilate River), MAB (Munesa-Asela border fault).

Since the study area is located at low magnetic latitude (magnetic equatorial region), there exists an inverse relationship between nature of magnetic susceptibility of the geologic bodies/sources and their associated magnetic responses (anomalies). Therefore, the high to very high magnetic anomalies depicted over the volcanic centers are attributed to low magnetic susceptibility geologic materials beneath these silicic volcanic centers.

In contrary, the negative magnetic anomaly zone which covers most of the Lakes region and associated depressions and part of the highland are attributed to high magnetic susceptibility sediments derived from the neighboring volcanic rocks.

### 5.2.6 Magnetic analytical signal map

According to Dentith and Mudges (2014) the analytical signal map of a potential field is produced by combining the 3-directional gradients of the potential field at location in use and given by; $As(x, y, z) = \sqrt{(\frac{\partial f}{\partial x})^2 + (\frac{\partial f}{\partial y})^2 + (\frac{\partial f}{\partial z})^2}$ (3.16)

Where, *f* is the magnetic field (residual magnetic) considered in the computation.

Generally, the interpretation of magnetic data is difficult at low magnetic latitudes due to the complex nature of magnetic field at the equator/low latitude. However, the magnitude of analytical signal map reveals maximum value over magnetic contacts regardless of the direction of magnetization and is always positive.

The analytic signal map (Fig. 5.17) of the study area is obtained from the residual magnetic anomaly map using Geosoft Oasis Montaj. The map reveals magnetic anomalies that result from vertical and horizontal variations/contacts of geologic units/structures. As can be seen from the map, the observed maximum analytic values are generally coincident with the magnetic anomaly peaks observed in the residual magnetic anomaly map (Fig. 5.16).

Susceptibility contrasts in the basaltic units in contact result in large analytic signal gradients as compared with the surrounding sediments and low magnetic susceptibility rock units like ignimbrite, tuffs, rhyolite and other pyroclastic volcanic rocks.

This is evident on the east and SE of Lake Ziway where the Pleistocene basalt shows a high analytic signal value due to the high susceptibility contrast as compared with the surrounding units (Figs. 2.3 and 5.16).

The low magnetic anomalies of the Lakes Langano, Abiata and east of Shala observed in the residual anomaly map are now characterized by intermediate to high peaks of analytic signal values. These peaks are associated with the swarm of fault that pass between Lake Abiata and Lake Langano and continue along east of Lake Shala until it ends up in the east of Corbetti volcanic complexes.

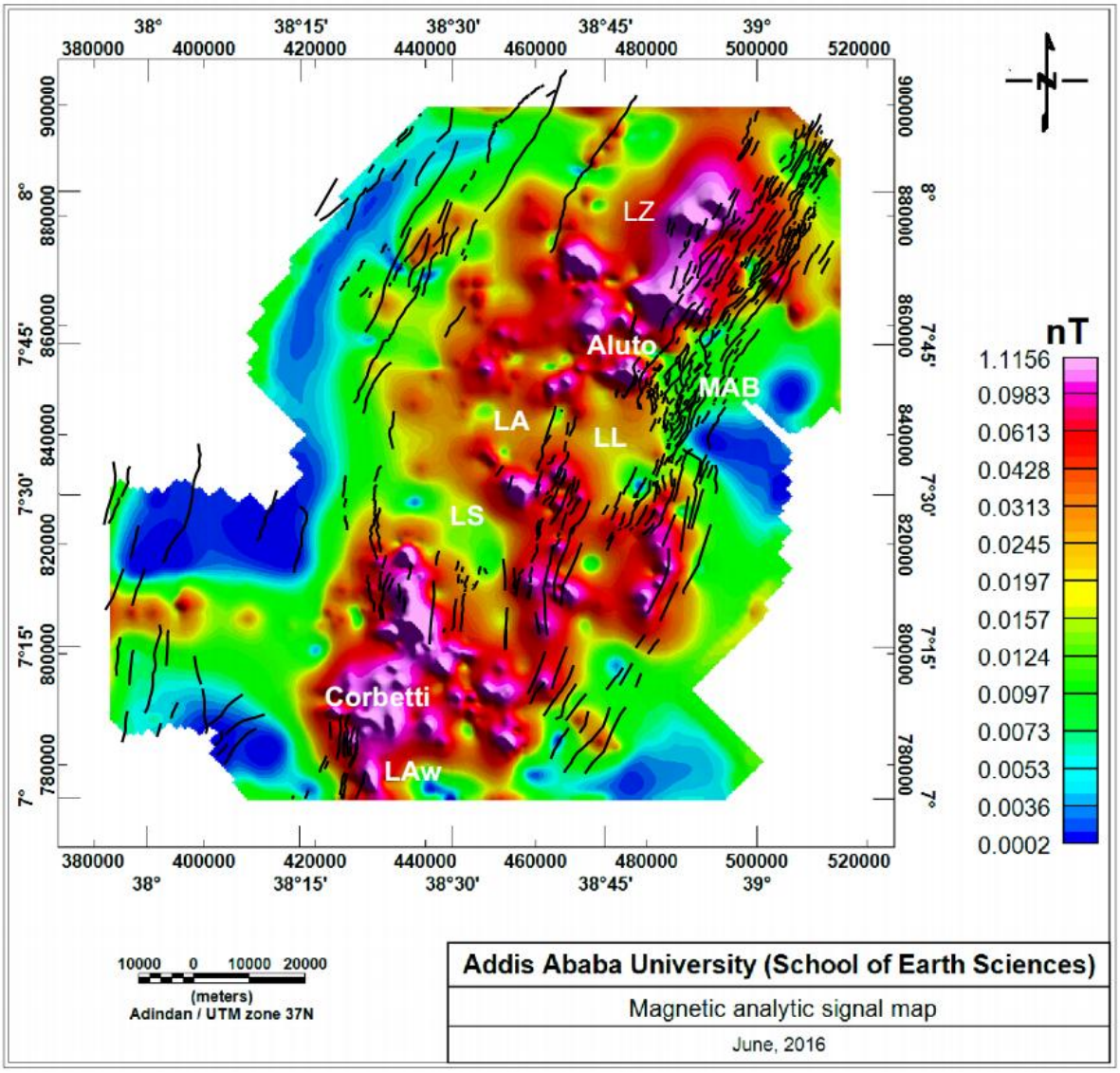


**Figure 5.17** Magnetic analytic signal map of the study area. The maps are superimposed with faults obtained from Corti, 2016. Black lines represent faults traced in the study area. LZ (Lake Ziway), LL (Lake Langano), LA (Lake Shala), Law (Lake Awasa), MAB (Munesa – Asela border fault).

Most of the structural contacts revealed by the analytic signal map in the study area generally follow N-S and NNE-SSW trends. In fact, there are also some contacts of lithologic units (basaltic units) exposed in the SE and south of the Lake Langano that are revealed by the analytic signal map. The Corbetti and Aluto volcanic centers are characterized by strong analytic signal gradients due to the contact between magmatic intrusions beneath the volcanic center and the surrounding rocks.

Therefore, the maximum values of the analytic signal map are concentrated on the rift floor close to the eastern rift escarpment, from Lake Ziway through Aluto, the lakes region up to Corbetti volcanic center and Awasa caldera. All these zones are correlated with the WFB which are characterized by intense faulting and magmatic intrusions. The Munesa-Asela border faults are characterized by intermediate to low analytic signal due to the low susceptibility rock units exposed in the area. These areas are mainly dominated by ignimbrite and tuff units. The low analytic signal over Lake Shala, SW, NW and SE peripheries of the study area is probably either due to thick sediments or low susceptibility rocks in contact with the surrounding rocks.

From the analytic signal map (Fig. 5.17), one can notice that all the faults mapped in the study area are not associated with high analytic signal gradients. Therefore, the geologic contacts are possibly attributed to the variation in the magnetic susceptibilities of the different geologic units (intrusive bodies, country rocks, structural contacts).

### 5.2.7 Magnetic tilt derivative map

The tilt derivative map (Fig. 5.18) of the study area is compiled by applying a tilt derivative filter to the magnetic analytical signal map using Geosoft OasisMontaj software. The map is supposed to easily identify the location of faults, contacts inorder to locate edges and geological boundaries in the study area. The tilt derivative map shows more detailed structural contacts/boundaries than the analytic signal map. It shows positive values over magnetic sources, cross through zero at or near the fault/contact locations and negative outside source zones.

Accordingly the study area is characterized by a set of numerous faults in the N-S, NE-SW and NW-SE directions. These directions are correlated with the general tectonic history of the study area with abundant N-S and NE-SW trending structures. Also there are some other trends in the study area with NW-SE orientation.

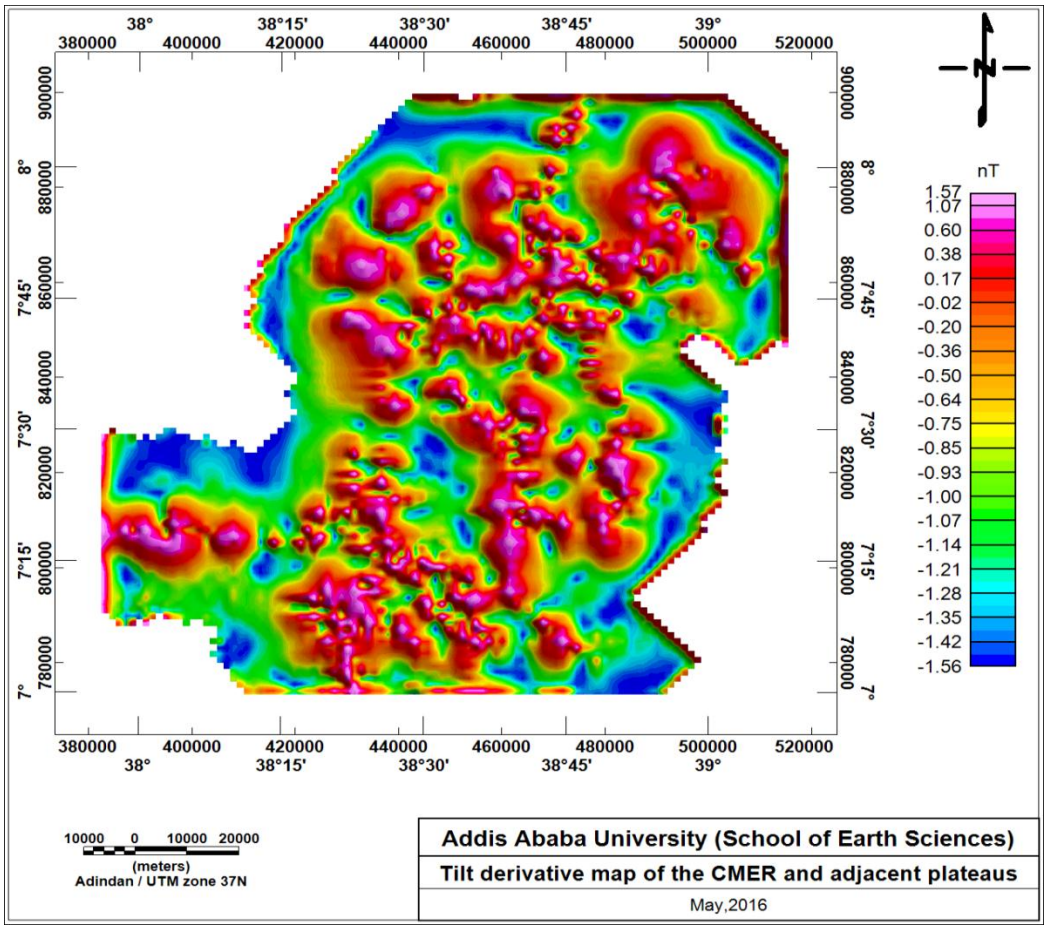


**Figure 5.18** Magnetic tilt derivative map of the study area

## 5.2.8 Euler deconvolution magnetic map

Euler deconvolution technique is applied to the residual magnetic anomaly in order to estimate the depth and location of the magnetic source. In standard Euler deconvolution process, each model contains solutions of a particular structural type defined by the structural parameter. From the principle of Euler deconvolution (GETECH manual), the structural index values 0, 1, 2, 3 represent geological features of contact, sill/dike, vertical pipe/horizontal cylinder and sphere respectively.

The Euler deconvolution map (Fig. 5.19) of the study area is compiled by applying a standard 3D Euler deconvolution filter using the Geosoft OasisMontaj software. The optimal structural index is selected by a visual inspection of maps which compiled using various structural indices until the best clustering of solutions is obtained.

Based on this procedure, a structural index of 1 was determined and applied to the residual magnetic anomaly map to derive the Euler deconvolution map. The map reveals magnetic sources of different depths marked by different colored symbols plotted on the map. These include a yellow circle indicating magnetic sources with depth less than 2 K. The red box indicates magnetic sources that range from 2 to 4 Km depth. The green triangles represent sources that range from 4 to 6 Km depth. The blue boxes represent sources that range from 6 to 8 Km depth. The light green inverted triangles represent sources that range from 8 to 10 Km depth. The letter 'x' represents sources that are greater than 10 Km.

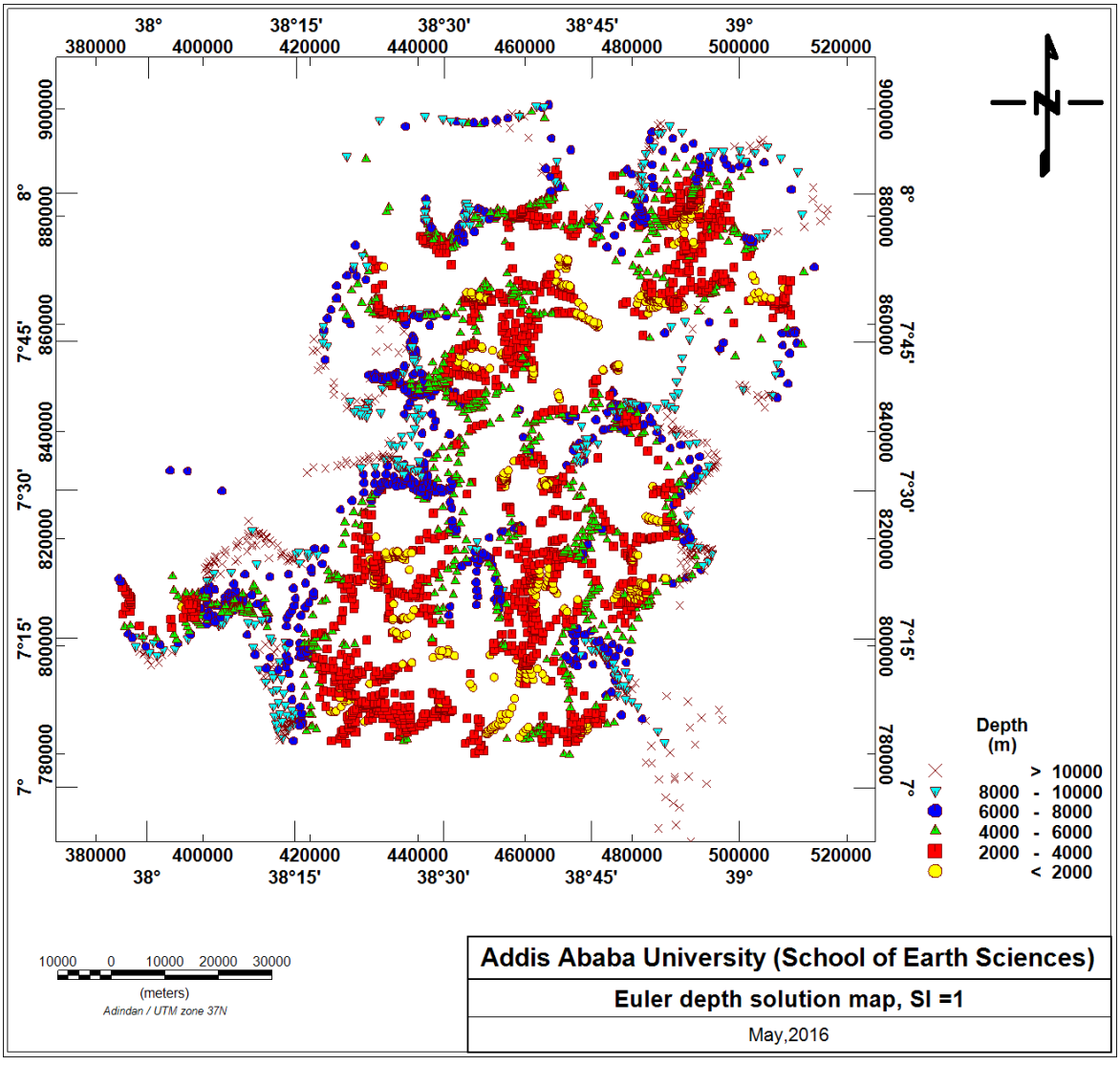


**Figure 5.19** Euler deconvolution magnetic map for SI = 1

The yellow and red boxes which represent relatively shallow sources are distributed along the WFB. In particular, they are densely concentrated over the locations of the Aluto, Shala and Corbetti volcanic complexes indicating that the magnetic sources there are of shallow origin. The letter ‘x’ which represents relatively deeper (> 10 Km) is mostly distributed over the shoulders of the SW and SE plateaus indicating the magnetic sources below the shoulders of the plateaus are relatively deeper.

The green triangles, blue boxes and light inverted triangles which represent relatively intermediate magnetic sources are concentrated over the areas dominated by thick sediments of the rift lakes and substantial parts of the SW and SE plateaus indicating that the sources there are at relatively intermediate depths.

The distribution of the sources (shallow, intermediate and depth sources) over the study area revealed by the Euler deconvolution magnetic map appear to be consistent with the distribution of the sources revealed by the regional magnetic anomaly map (Fig. 5.15) and the residual magnetic anomaly map (Fig. 5.16).

# CHAPTER SIX

# MOHO DEPTH AND GRAVITY MODELING

## 6.1 Moho depth map

In this section, crustal structure and probable depth to the Moho of the CMER and adjacent plateaus have been determined from receiver function analysis of broad band seismic data recorded by temporary deployments of seismic stations and surface wave dispersions in the MER, Afar depressions and the two uplifted plateaus. The compiled seismic data used in this study were collected by different authors and groups (Mulugeta Dugda et al., 2005; Stuart et al., 2006; Cornwell et al., 2010). Here, we used 73 data points/stations of Moho depth determined over different parts of the MER, the eastern and western plateaus separating the rift and the southern Afar depression. Even though these data points are not really sufficient, they can give clues regarding the Moho depth and crustal structure of the MER in general and the study area in particular. As shown in Figure 5.20, the seismic data stations considered for this MSc thesis work are not uniformly distributed throughout the MER, rather they are densely concentrated in the NMER with few data points in the CMER and SMER and the two plateaus. However, through the process of interpolation still we can deduce the general crustal structure and depth to Moho of the MER and specifically the study area.

In general, the map shows the different sectors of the MER including the major transversal offsets that cut the rift margin with an E-W structural trend. In particular, the YTVL which extends from ~$8.2^0$ – $9.0^0$ N cuts the MER at the NMER - CMER boundary and deflects west ward to accommodate an E-W trending orientation. This zone is considered to be active with a thinning crust (Keranen and Klemperer, 2008). The second one is the Goba-Bonga tectonic lineament intersecting the MER at the termination (boundary) of the CMER meeting the SMER. This zone is associated with a swarm of volcanic centers (Wagebeta volcanic complexes) giving rise to maximum gravity anomalies indicating that the crust there is thinning.

Generally, the crustal thickness (Moho depth) in the MER varies from ~34 km beneath the NMER adjacent to the CMER to ~38 km beneath the floor of the CMER.

This study shows the maximum possible crustal thickness of the SE plateau in the study area is estimated to be about 42 km, whereas, the crustal thickness beneath the SW plateau ranges from 36-40 km. Therefore, the crustal thickness (Moho depth) in the study area which is marked by broken red line (Fig. 5.20) is estimated to be about 36 – 40 km beneath SW plateau, 38 km in the rift floor and a maximum of 42 km beneath the SE plateau.

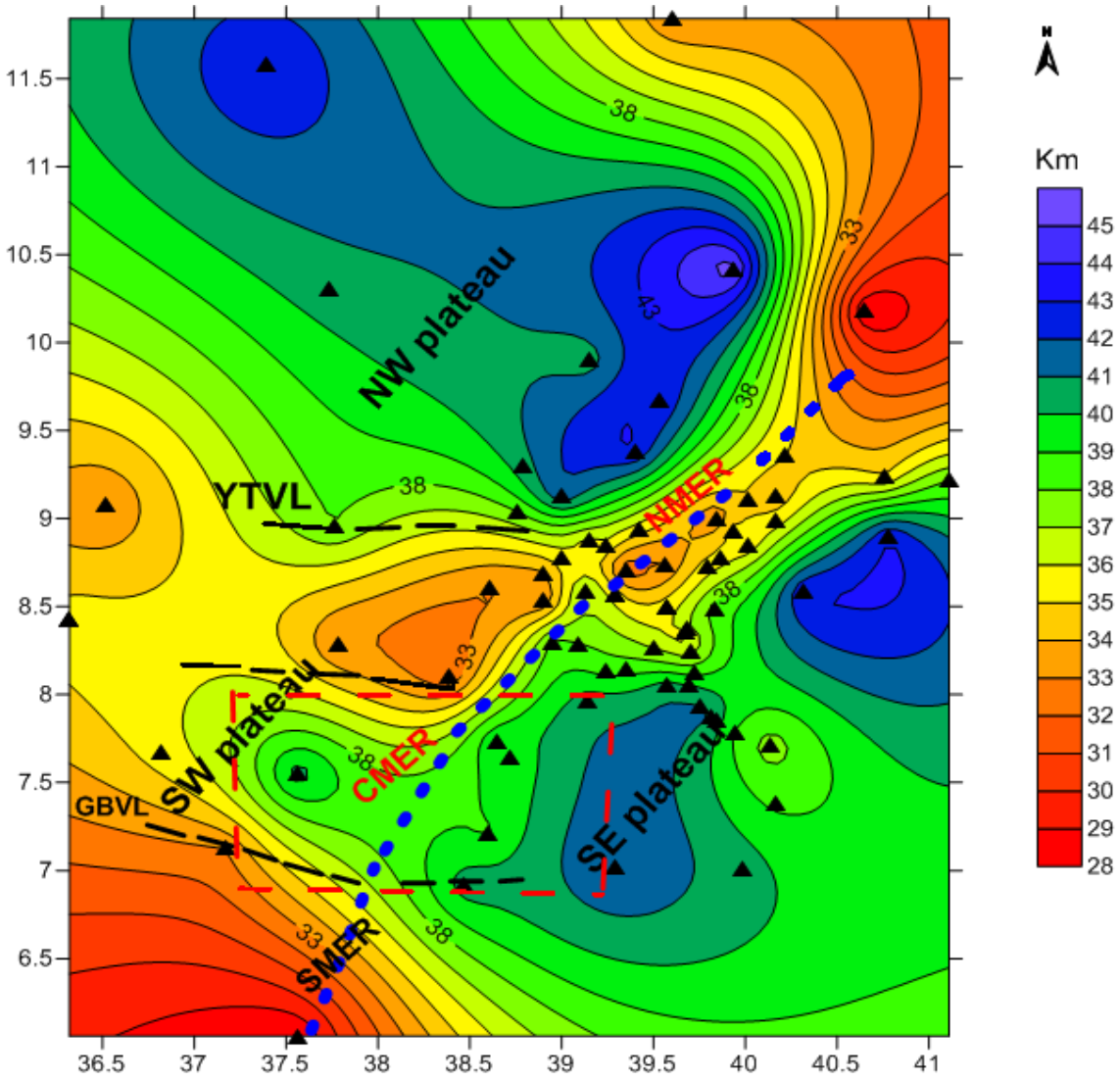


**Figure 5.20** Moho depth map of the MER and adjacent plateaus. Seismic data are from (Dugda et al., 2005; Stuart et al., 2006; Cornwell et al., 2010). The red rectangle indicates specific study area. The MER is highlighted with blue broken line, whereas the black broken line represents major transverse faults. Triangles represent stations used in this study. YTVL= Yerer Tulu Wellel volcano-tectonic lineament, GBVL= Goba Bonga tectonic lineament.

Furthermore, the observed Bouguer gravity anomalies are consistent with the seismically determined Moho depth. Specifically, the plateau shoulders coinciding with the maximum Moho depth (36 - 42 km) are sites of relatively low gravity anomalies (-215 to -260 mGal) and the rift floor zones coinciding with minimum Moho depth (~38 km) are sites of high gravity anomalies.

Mulugeta Dugda et al. (2005) has estimated the crustal thickness beneath the rift lakes ($7^0$ ~$8.5^0$ N) to be about 38 km which is fairly in agreement with the results obtained in this MSc thesis research work. The work of Keranen and Klemperer (2008) have also determined the crustal thickness to be about 36 – 38 km beneath the SE shoulder to 34 – 36 km beneath the SW shoulder and shows a slight variation with the results determined in this MSc thesis research work.

Moreover, the SMER which is outside of the present study area shows a very thin Moho depth which is assumed to be the result of two episodes of rifting, one from the Mesozoic rifting and the other from the Cenozoic rifting of the East Africa Rift System (Ameha Atnafu Muluneh et al., 2014 and references therein).

## 6.2 Gravity modeling

To investigate the general nature of the crustal structure beneath the central MER and adjacent plateaus a 2D vertical cross section was constructed across the rift along profile P1 and P2 (Fig. 5.21 and 5.22) shown on the Bouguer anomaly map (Fig. 5.4). The model was constructed from the anomaly values extracted from the Bouguer gravity anomaly map using 2D GM-SYS Geosoft OasisMontaj software. A starting density model was obtained from P-wave velocities of the 2-D seismic refraction model constructed from southern Afar to CMER following the MER axis from the works of Keller et al. (2004). This is done by converting the P-wave velocity of each layer to density using the relationship derived by Christensen and Mooney (1995).

Based on the P-wave velocity and the work of Mickus et al.(2007), the initial density assigned for the near surface volcanic rocks and sediments is about 2100 kg/$m^3$ and that of the Mesozoic sedimentary rocks that overlie the upper crust is about 2470 kg/$m^3$. The density of the upper crustal rocks is estimated to be 2670 kg/$m^3$ and the density of the lower crustal rocks is estimated to be 2870 kg/$m^3$. The density of the upper mantle is estimated to be about 3250 kg/$m^3$ and the density of the intrusive body that are intruding into the crust are considered to be 3000 kg/$m^3$.

Additional a-priori information was obtained from different previous geological (e.g., Gidey WoldeGabriel et al., 1990) and geophysical (e.g., Mickus et al., 2007) works conducted in the CMER in particular and MER as a whole.

Moreover, the possible crustal thickness (Moho depth) determined from the seismic data (data obtained from receiver function and surface wave dispersion) considered in this MSc thesis work (section 6.1) and from the P – wave velocity model (Keller et al., 2004) are used to constrain the initial model parameters.

The constructed crustal models across the CMER and adjacent plateaus are shown in Fig. 5.21 and 5.22. The crustal models are constructed in such a way that they cross the major structural units (SW plateau, rift floor and SE plateau) of the study area and hence enable us compare the variation of crustal thickness beneath the rift floor and the adjacent plateaus. The models are also constructed to cross the two major volcano-tectonically active zones of the SDZFZ and the WFB. Even though, the final model constructed is not unique, it satisfies the available geophysical and geological constraints considered in its construction.

## Profile P1 (W - E)

For the final gravity model (Fig. 5.21c) constructed along profile (P1) the error determined between the observed and calculated gravity values is 1.1 mGal. The final gravity model corresponding to layer 'A' consists of relatively low density near surface volcanic rocks and sediments with an average density value of about 2170 kg/m$^3$. The average thickness of this layer varies from less than 2 km over the rift floor to more than 4 km over the two plateaus. Within this layer there is a low density (~ 2100 kg/m$^3$) localized rock unit at the SW plateau coincident with one of the plateau volcanic centers that are modeled to obtain the best fit of the calculated and observed values. Layer 'B' with an average density value of 2480 kg/m$^3$ is interpreted to represent Paleozoic and Mesozoic sedimentary rocks combined with Oligocene flood basalts that unconformably overlay the basement rocks with an average thickness ranging from 2 – 4 km. This is in agreement with the work of Mickus et al. (2007) density model constructed along the MER rift axis from N – S who identified a thick (1.5 – 4 km) Paleozoic and Mesozoic sedimentary rocks that underlie the low density near surface volcanic rocks and sediments.

Moreover, Gidey WoldeGabriel et al. (1990) have also identified the presence of Mesozoic rocks that unconformably overlie the crystalline basement rocks at the SW rift margin (Guraghe area, Kella section).

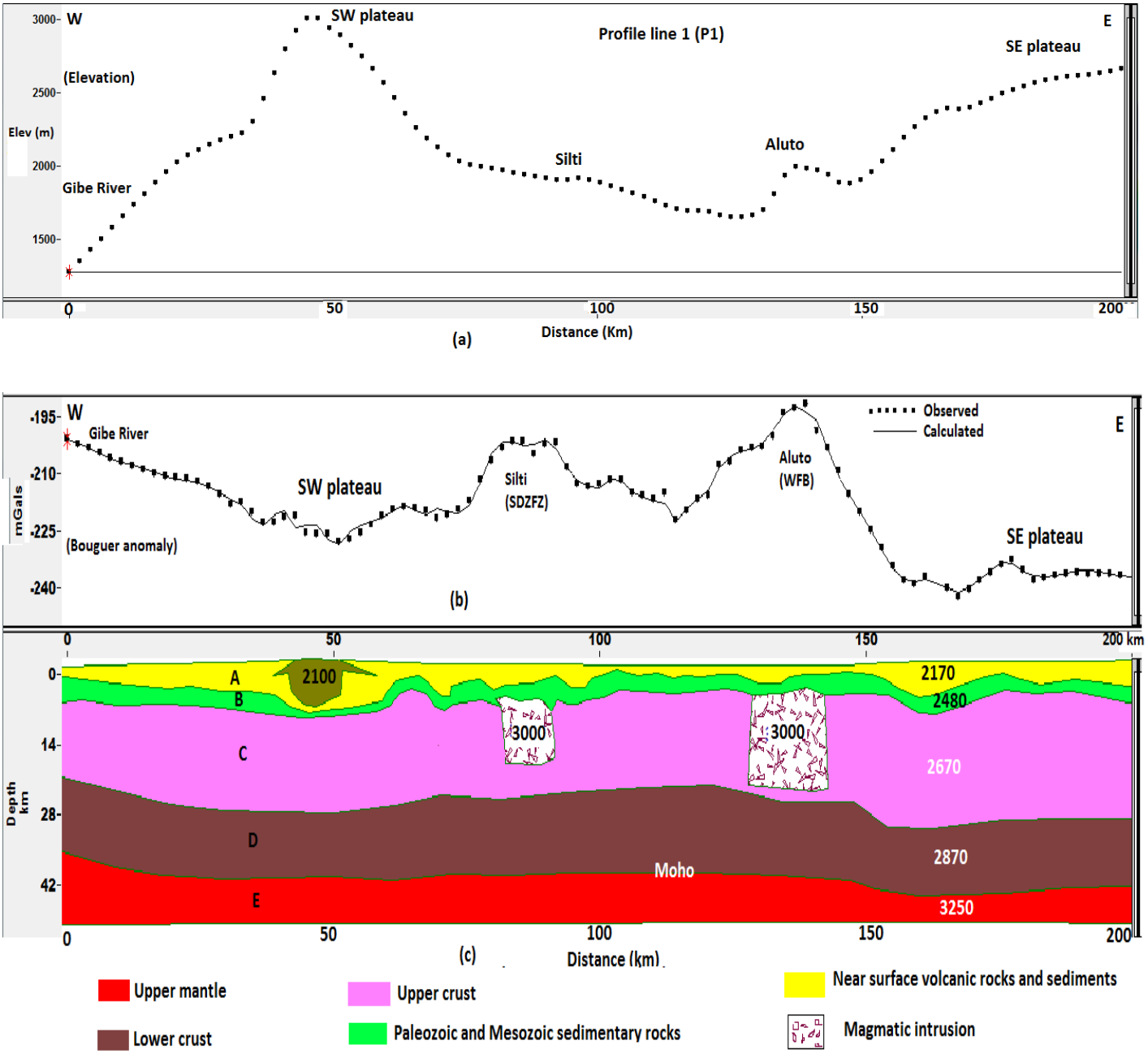


**Figure 5. 21** 2D Bouguer gravity anomaly modeling of the CMER and adjacent plateaus along profile P1. **(a)** Trend of topographic map, **(b)** observed (black dots) and calculated (black smooth line) of Bouguer gravity anomaly and **(c)** final density model. Density values are given in kg/m$^3$.

The third layer (layer 'C') represents upper crustal rocks with a density value of 2670 kg/m$^3$. Layer 'D' with a density value of 2870 kg/m$^3$ is thought to represent rocks of the lower crust. Layer 'E' represents rocks of the upper mantle and assigned a value of 3250 kg/m$^3$.

In order to obtain the best fit between the observed and calculated gravity field an intrusive body with a density of 3000 kg/m$^3$ in the upper crust is considered to exist beneath the SDZFZ (Silti) and WFB (Aluto).

The best fit between the observed and calculated gravity field is obtained by assuming a total crustal thickness (Moho depth) that ranges from 35 - 40 km beneath the SW plateau and 43 km beneath the SE plateau. The maximum crustal thickness beneath the rift floor is estimated to be about 39 km. Generally, these results are in close agreement with the crustal thickness values determined from receiver function and surface wave dispersions discussed in section 6.1.

## Profile P2 (W- E)

For the final 2D gravity model (Fig. 5.22c) constructed along profile (P2) the error determined between the observed and calculated gravity values is 1.98 mGal. The final gravity model corresponding to layer 'A' consists of relatively low density near surface volcanic rocks and sediments with an average density value of about 2150 kg/m$^3$. The average thickness of this layer varies from 2 km over the rift floor to more than 4 km over the two plateaus. Layer 'B' with an average density value of 2480 kg/m$^3$ is interpreted to represent Paleozoic and Mesozoic sedimentary rocks combined with Oligocene flood basalts and underlie the relatively low density near surface volcanic rocks and Quaternary sediments.

The third layer (layer 'C') is assigned a final density value of about 2670 kg/m$^3$ and is interpreted to represent the upper crustal basement rocks. Layer 'D' with a density value of 2870 kg/m$^3$ is thought to represent rocks of the lower crust. Layer 'E' represents rocks of the upper mantle and assigned a value of 3250 kg/m$^3$. In order to obtain the best fit between the observed and calculated gravity field an intrusive body with a density of 3000 kg/m$^3$ in the upper crust is considered to exist beneath the Corbetti volcanic center.

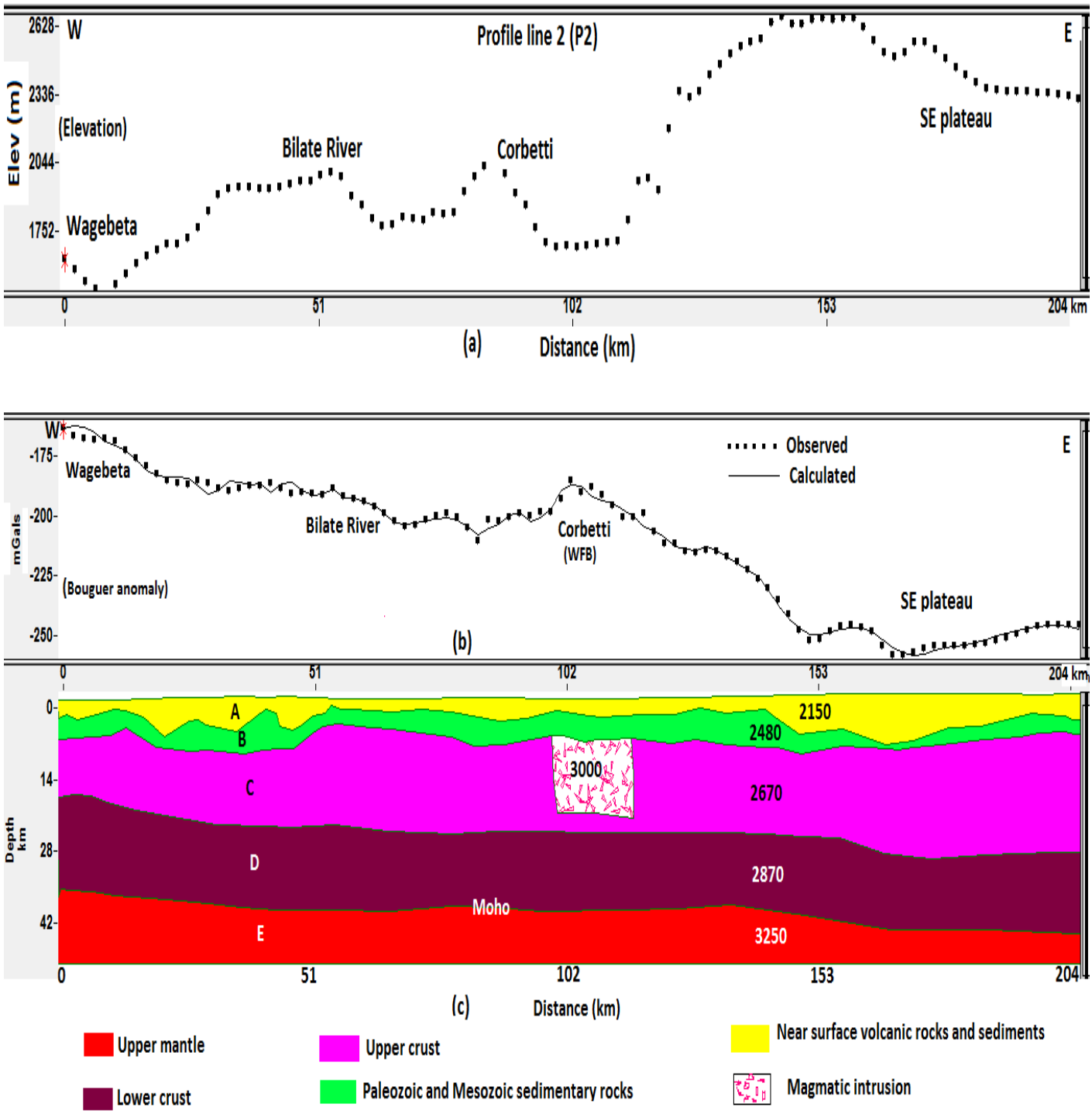


**Figure 5.22** 2D Bouguer gravity anomaly modeling of the CMER and adjacent plateaus along profile P1. **(a)** Trend of topographic map, **(b)** observed (black dots) and calculated (black smooth line) of Bouguer gravity anomaly and **(c)** final density model. Density values are given in kg/m$^3$.

The best fit between the observed and calculated gravity field is obtained by assuming a total crustal thickness (Moho depth) that ranges from 35 km beneath the Wagebeta caldera complexes to about 40 km beneath the Bilate River basin, while the maximum crustal thickness under the SE plateau is determined to be about 43 km. The maximum crustal thickness beneath the rift floor (e.g., beneath Corbetti volcanic center) is estimated to be about 39 km.

Generally, these results are in close agreement with the crustal thickness values determined from receiver function and surface wave dispersions discussed in section 6.1.

The gravity model constructed by Keller et al. (2004) and Mickus et al. (2007) showed that the crustal thickness under the rift floor (e.g., beneath Aluto volcanic center) was determined to about 40 km which is also consistent with the results of this MSc thesis research work. However, our interpretation results show a slight variation from the work of Keranen and Klemperer (2008) who determined that the crustal thickness varies from 34 – 36 km beneath the SW plateau and 36 – 38 km beneath the SE plateau.

# CHAPTER SEVEN

# DISCUSSION AND IMPLICATIONS

Results of the gravity, magnetic and seismic investigations of the central MER and adjacent plateaus considered in this MSc thesis study, have been translated into geologic in order to obtain the possible information about the structure, thickness and density distribution of the crust.

The topographic map (Fig. 5.1) and free-air anomaly map (Fig. 5.2) shows a clear physiographic variation between the rift floor and the adjoining plateaus, with minimum values (both elevation and free-air anomaly) over the rift floor and maximum values on the elevated platforms.

The intensity of the gravity and magnetic field is generally related with the main structural features of the study area. The intensity of gravity field increases with decreasing elevation. On the plateaus (SE and SW) the Bouguer gravity minimum coincides with areas of the highest elevation. Comparison of the observed Bouguer gravity anomaly over the SE plateau and SW plateau in the study area shows that the SE plateau is relatively dominated by lower Bouguer anomalies. A steep gravity gradient is observed by the SE escarpment of rift floor as compared to the lower gradient observed along the SW rift floor escarpment.

The minimum gravity anomalies observed over the plateaus are thought to be produced by the combined effect of crustal thickening and volcanic centers mapped on the plateaus (Fig. 2.3 and 5.8). The broad complete Bouguer gravity low located over the southeast and southwest plateau is also possibly due to deep Moho boundary. Previous geophysical works (Befkadu Oluma, 1986 and references therein) also suggests that this anomaly is attributed to either low density asthenospheric material at the base of the lithosphere or in the upper mantle beneath the SE plateau as isostatic compensation i.e. the SE plateau is compensated at depth by mass deficiencies. Moreover, it is also suggested that the whole of both plateaus is characterized by low complete Bouguer anomaly, suggesting the topographic relief is isostatically supported by deep crustal root (Abera Tessema and Antoine, 2004).

In contrary to the adjoining plateaus characterized by relatively low Bouguer gravity anomaly, the CMER floor is dominated by relatively narrow and high complete Bouguer and total magnetic field anomalies (Fig. 5.4 and 5.13).

This relatively narrow and high Bouguer gravity anomaly and the magnetic anomaly to some extent are classified into two separate and linear narrow zones with a general trend of NNE-SSW to N-S observed on the maps. The first one which runs parallel and close to the southeastern escarpment connects all the peralkaline volcanic complexes and/or calderas referred to the WFB and the second one that runs parallel and close to the south western rift margin corresponding to the SDZFZ.

At the SW part of the study area, there is a strong Bouguer gravity anomaly with a general trend of E-W corresponding to the location of the Goba-Bonga E-W oriented lineament and the associated Wagebeta caldera complexes. Several geological works have explained that the Wagebeta calderas and associated domes are arranged linearly transverse to the rift margin along the cross-rift Bonga lineaments (e.g., Gidey Woldegabriel et al., 1990 and references therein) (Fig. 5.8).

A comparison of the topographic profile (Fig. 5.3a), complete Bouguer gravity anomaly profile (Fig. 5.5a) and total magnetic anomaly profile (Fig. 5.14a) stacked together here (Fig. 5.23) show that the topographic and Bouguer gravity anomaly profiles show an inverse relationship, where minimum Bouguer gravity anomalies are observed over higher elevation and vice versa.

Correspondingly, due to the limited magnetic data distribution and the fact that magnetic anomalies do not vary with elevation a complete correlation of the topographic profile and the magnetic profile cannot be established. These findings are also consistent for the topographic, gravity and magnetic profiles constructed along different profiles considered along different latitudes.

Apart from the above correlations, a correlation of the Bouguer gravity and magnetic anomaly profiles (Fig. 5.23) and the other profiles not shown here but discussed in the relevant sections is strong and positive over the active volcanic centers.

Most of the features observed on the regional gravity and magnetic maps are also evident on the complete Bouguer gravity and total magnetic anomaly maps respectively.

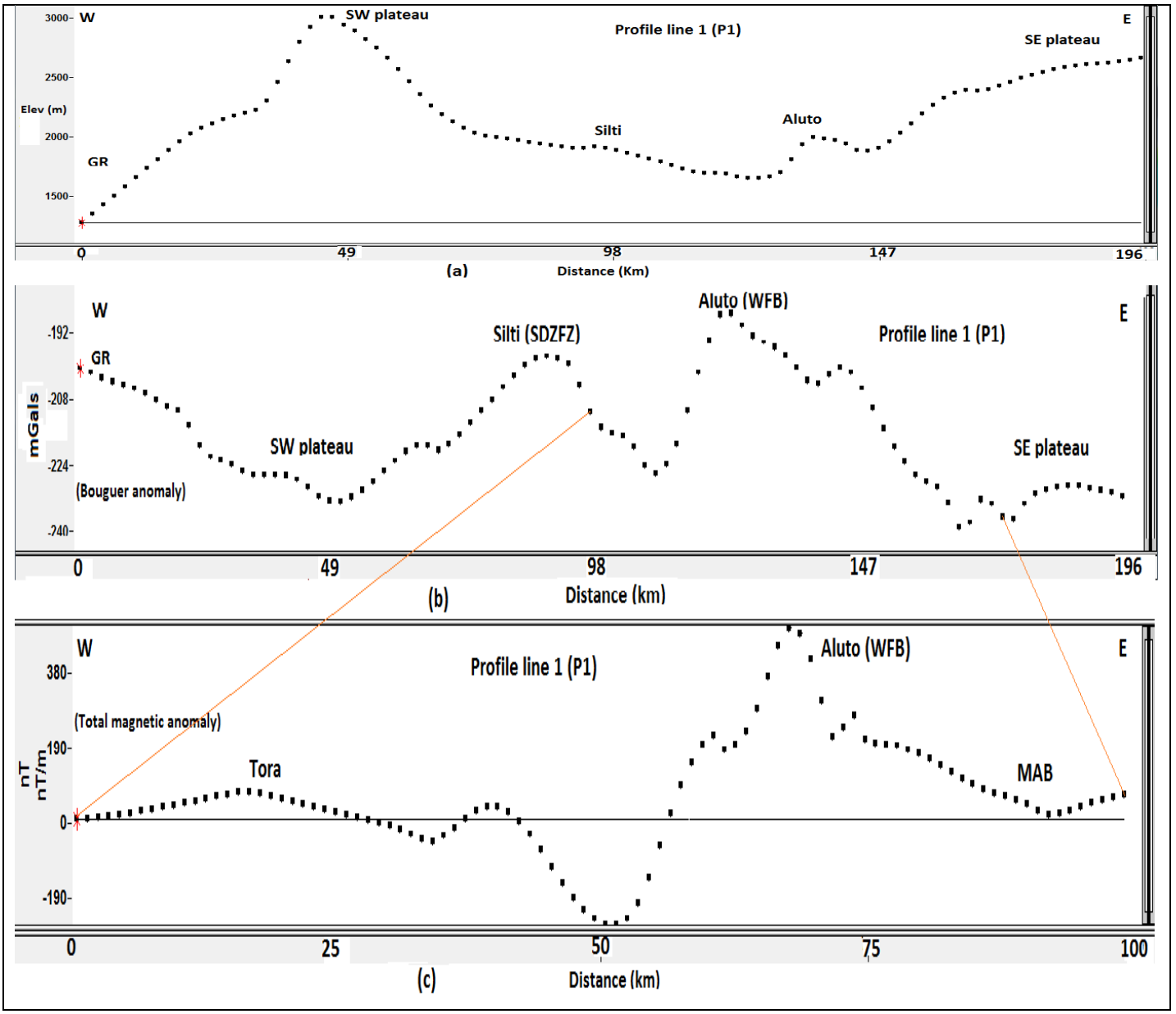


**Figure 5.23** Profile lines constructed from topographic (a), Bouguer gravity anomaly (b) and total magnetic anomaly (c) maps.

The regional gravity map and the regional magnetic map reveal that the long wavelength gravity and magnetic minima occur over the shoulders of the SE and SW plateaus. The gravity minimum is thought to indicate that the plateaus are underlain by either low density asthenosphere or a thick low density crust (deep Moho). This result is in close agreement with the thick crust (deep Moho 42 - 43 km under the SE plateau and 35 – 40 km under the SW plateau) determined from the 2D gravity modeling and seismic Moho depth map.

The major offset at the SW part of the study area with an E-W trending positive anomaly coincides with the Goba-Bonga tectonic lineament and it is more evident on the regional gravity anomaly map. It indicates that this major offset in association with the Wagebeta caldera complexes has possibly deep and regional sources and expected to play a significant role in rift extension. Different scholars have been explained the significance of this major offset in controlling rift propagation. For example, Bonini et al. (2005) noticed that the northward propagation of Kenya rift was possibly blocked by this major offset of Goba-Bonga tectonic lineament. Further, if we assume that rift evolution is propagating southward from the northern MER, the southern end of the CMER was blocked by the Goba-Bonga tectonic lineament and shifts from more wider rift in the CMER to narrow rift zone in the SMER.

As shown in the different residual gravity and magnetic anomaly maps, there are two distinct prominent features that correlate with positive anomalies over the rift axis and large negative values over the two adjoining plateaus. The low anomalies in the two plateaus are associated with different shield and composite volcanoes. The strong positive residual anomalies in the rift floor are correlated with the volcano tectonically active zones of the WFB and SDZFZ. The WFB that run close to the SE rift margin connects all the active volcanic centers of Bora, Aluto, Shala, Corbetti and Awasa caldera from north to south respectively. These anomalous zones are more evident on the residual gravity anomaly maps with NNE-SSW trend in the areas of Aluto and Lake Ziway and vary from NNE-SSW to N-S in the Shala, Corbetti and Awasa caldera complexes. At the NE of Lake Ziway and Asela area the anomaly direction changes to NE-SW. This change in direction has also been explained by several previous geological and geophysical works (e.g. Meyer et al., 1975; Rezene Mahatsente et al., 1999).

The SDZFZ defines the second positive residual anomaly that run close to the SW rift margin with a general orientation of NNE-SSW and its south ward propagation effect ends immediately at the west of Lake Abiata, whereas the WFB continues up to Corbetti volcanic center. In the study area this active zone connects several scoria cones aligned in NNE-SSW direction and basaltic rocks erupted following this weak zone.

Though the residual magnetic anomaly does not show strong structural pattern like the residual gravity anomaly map, it is characterized by strong positive residual magnetic anomalies over the volcanic centers.

The residual magnetic field shows an E-W trending anomaly over Corbetti volcanic center, which is unlikely as indicated from independent gravity and geological investigations. This difference is caused by the inherent problem of magnetic anomaly interpretation at low latitudes, where long N-S striking structures such as magmatic intrusions and/or dikes and contacts may be invisible, except where the structures are broken or terminate (Beard et al., 2000). Further, magnetic anomalies at low latitude tend to be stretched in an E-W direction.

Comparison of regional and residual gravity and magnetic anomaly shows that the strong positive anomaly zones associated with the WFB and SDZFZ are more evident on the residual than the regional field. This indicates that the sources of these anomalous zones are most probably found at sallow depths. Similar results have been deduced from the fault patterns affecting the study area by superimposing on the residual gravity anomaly and analytic signal map (Fig. 5.7 and 5.9). In this case the volcanic centers are not affected by active faults, rather the propagation of the fault system shifts away in either direction where they encounter the volcanic centers. This confirms the presence of hot magma chamber at shallow depth beneath these volcanic centers and behaves in a ductile manner than brittle deformation. The hot spring, fumaroles and alteration of volcanic rocks in the areas of Aluto, Corbetti and WondoGenet are also the surface manifestation of the presence of magmatic intrusions and magma chambers at shallow depths. Moreover, the compiled Euler deconvolution gravity map (Fig. 5.11) and Euler deconvolution magnetic map (Fig. 5.19) also show the existence of shallow sources beneath the rift floor and deep sources beneath the plateaus.

Therefore, both the Quaternary volcano tectonically active zones of the WFB and SDZFZ including the Goba - Bonga tectonic lineament are considered to be active zones of the CMER where tectonic and magmatic deformations are currently taking place.

# CHAPTER EIGHT

# CONCLUSIONS AND RECOMMENDATIONS

## 8.1 Conclusions

Based on the investigations made in this study the following conclusions and recommendations are forwarded.

The interpretation of new magnetic and existing gravity and magnetic data in combination with seismic data give us insight to constrain the nature of crustal structure, depth to Moho and density distribution within the crust of the CMER and the two adjacent plateaus. Based on our investigation results the intensity of gravity and magnetic fields are closely associated with the main structural features.

The study area is characterized by relatively low Bouguer anomalies over both the SE and SW plateaus, superimposed with relatively high gravity values over the rift floor. The minimum gravity anomaly coincides with areas of maximum elevation and generally the intensity of gravity field increases with decreasing elevation.

At the SW part of the study area there is a major offset intersecting the Guraghe border fault with an E-W and NW-SE trending anomaly zone. This coincides with the major offset of the Goba-Bonga tectonic lineament that intersects the MER at the CMER-SMER boundary and is interpreted to have deep and regional effect.

Comparison of regional and residual gravity and magnetic anomaly maps and enhancement techniques reveal that the Quaternary volcano-tectonically active zones of the WFB and SDZFZ are more evident on the residual anomalies indicating that they are underlain by shallow magmatic intrusions and/or magmatic chambers. The hot spring, fumaroles and alteration of volcanic rocks in the areas of Aluto, Corbetti and WondoGenet are also the surface manifestation of the presence of magmatic intrusions and magma chambers at shallow depths.

The analytic signal maps and Euler deconvolution maps compiled for the study area are consistent with the complete Bouguer anomaly map and its derivatives and total magnetic anomaly map and its derivatives in explaining the distribution of the anomaly sources over the

plateaus and the rift floor. These results are found to be in agreement with the volcano-tectonic map and geologic map of the study area.

2D gravity modeling across the CMER and adjacent plateaus constructed along two profiles shows that the crustal thickness varies from 35 – 40 km beneath the SW plateau to about 43 km beneath the SE plateau and it is estimated to be about 39 km under the rift floor. Seismic data from receiver function and surface wave dispersion indicates that the crustal thickness of the CMER floor is estimated to be about 38 km, whereas the crustal thickness varies from 36-40 km under the SW plateau to a maximum of 42 km beneath the SE plateau and is generally consistent with the 2D gravity modeling.

Our investigation results generally support the idea which suggests that rift extension and crustal deformation in the central Main Ethiopian Rift are currently concentrated over the Quaternary volcano-tectonically active zones of the Wonji Fault Belt, Silti DebreZeit Fault Zone and the Goba-Bonga tectonic lineaments and associated Wagebeta caldera complexes.

## 8.2 Recommendations

Even though we have processed sufficient gravity data, the numbers of magnetic data were limited to the rift floor and some parts of the highland. Therefore, to fully produce an integrated interpretation of gravity and magnetic survey over the CMER and adjacent plateaus, it is recommended to collect and fill the magnetic data coverage both on the rift floor and adjoining plateaus.

To understand and isolate the effect of deep and shallow sources of magnetic field, it is recommended to produce a general Curie isotherm map of the area which is non-existent at the moment.

The probable depth to Moho was determined by limited set of seismic data. Therefore, for detailed crustal structure and Moho depth undulation investigations detail seismic refraction survey will be required.

## REFERENCES


Abera Alemu (1983). Crustal Modeling from gravity data in the Ethiopian Rift. MSc Thesis. Addis Ababa University, Addis Ababa, Ethiopia.

Abera Alemu (1992). The Gravity Field and Crustal Structure of the Main Ethiopian Rift. Report **No. 26**. TRITA GEOD 1026. Stockholm, Sweden.

Abera Tessema, and Antoine, L.A.G. (2004). Processing and interpretation of the gravity field of the East African Rift: implication for crustal extension. Tectonophysics, **394**: 87–110.

Ameha Atnafu Muluneh (2014). Left-lateral transtension along the Ethiopian Rift and constrains on the mantle-reference plate motions.Tectonophysics, http://dx.doi.org/10.1016/j. tecto.2014.05.036.

Beard, L.P., Goitom, B. and Reidar, J.S. (2000). Interpretation of low latitude magnetic anomalies. NGU report. ISSN 0800 – 3416.

Befekadu Oluma, Abiy Hunegnaw, Mohammedberhan, A. and Ketsela Tadesse (1986). Geothermal Exploration Project Lakes: Corbetti Geothermal Prospect, Geophysical Exploration.

Bekele Abebe, Acocella, V., Tesfaye Korme and Dereje Ayalew (2007). Quaternary faulting and volcanism in the Main Ethiopian Rift. J. Afr. Earth Sci. **48**: 115–124.

Bendick, R., Bilham, R., Lakemariam Asfaw, and Klemperer, S. (2006). Distributed Nubia-Somalia relative motion and dyke intrusion in the Main Ethiopian Rift, Geophys. J. Int. **165:** 303–310, doi:10.1111/j.1365-246X.2006.02904.x.

Berckhemer, H., Baier, B., Bartelsen, H., Behle, A., Burckhardt, H., Gebrande, H., Makris, J., Menzel, H., Miller, H., Vees, R. (1975). Deep seismic soundings in the Afar region and on the highland of Ethiopia. Afar Depression of Ethiopia. 89–107.

Bilham, R., Bendick, R., Larson, K., Braun, J., Samson Tesfaye, Mohr, P., and Lakemariam Asfaw (1999). Secular and tidal strain across the Ethiopian rift, Geophysical Research Letters, **27**: 2789–2984.

Boccaletti, M., Mazzuoli, R., Bonini, M., Trua, T., and Bekele Abebe (1999). Plio-Quaternary volcanotectonic activity in the northern sector of the Main Ethiopian rift: Relationships with oblique rifting. Journal of African Earth Sciences, **29**: 679–698.

Boccaletti, M., Bonini, M., Mazzuoli, R., Bekele Abebe, Piccardi, L., Tortorici, L. (1998). Quaternary oblique extensional tectonics in the Ethiopian Rift (Horn of Africa). Tectonophysics, **287**: 97–116.

Bonini, M., Corti, G., Innocenti, F., Manetti, P., Mazzarini, F., Tsegaye Abebe, Pecskay, Z. (2005). Evolution of the Main Ethiopian Rift in the frame of Afar and Kenya rifts propagation. Tectonics 24, TC1007.

Buck, W.R. (2006). The role of magma in the development of the Afro-Arabian rift system. Geological Society of London, Special Publication, **259**: 43–54.

Cornwell, D., Maguire, P., England, R., Stuart, G. (2010). Imaging detailed crustal structure and magmatic intrusion across the Ethiopian Rift using a dense linear broadband array. Geochem. Geophys. Geosyst. 11. http://dx.doi.org/10.1029/2009GC002637.

Corti, G. (2009). Continental rift evolution: from rift initiation to incipient break-up in the Main Ethiopian Rift, East Africa. Earth Sci. Rev. **96**: 1-53.

Dobrin, M.B. and C.H. Savit (1988). Introduction to Geophysical Prospecting, 4th Edition, McGraw-Hill, London.

Ebinger, C. (2005). Continental breakup: the East African perspective. Astronomy and Geophysics, **46 (2)**: 16–2.21.

Ebinger, C. J., and Casey, M. (2001). Continental breakup in magmatic provinces: An Ethiopian example, Geology, **29**: 527–530.

Ebinger, C., Sleep, N.H. (1998). Cenozoic magmatism in central and east Africa resulting from impact of one large plume. Nature, **395**: 788–791.

Ebinger, C.J., Tilahun Yemane, Gidey WoldeGabriel, Aronson, J., Walter, R. (1993). Late Eocene-recent volcanism and faulting in the southern main Ethiopian rift system. J. Geol. Soc. (Lond.). **150**: 99–108.

Ebinger, C. (1991). Gravity data acquisition, reduction and error estimation. Interim Report to the Ethiopian Institute of Geological Surveys, Univ. Leeds. 9 pp.

EIGS (Ethiopian Institute of Geological Survey) (2012). Geology geochemistry and gravity survey of the Hosaena area. Unpublished technical report. Memoer **no 36.**

Fairhead, J.D. (1976). The structure of the lithosphere beneath the Eastern Rift, East Africa, deduced from gravity studies. Tectonophysics, **30**: 269 – 298.

Foulger, G. R. and Peirce, C. (). Geophysical methods in geology.

George, R., Rogers, N., and Kelley, S. (1998). Earliest magmatism in Ethiopia: Evidence for two mantle plumes in one flood basalt province: Geology, 923–926.

GETECH Group plc. (2007). Advanced processing and Interpretation of gravity and magnetic data.

Giday Woldegabriel, Aronson, J. L. and Walter, R. C. (1990). Geology, geochronology, and rift basin development in the central sector of the main Ethiopia rift. Geological Society of America Bulletin, **102(4)**: 439-458.

Gouin, P. (1970). Seismic and gravity data from Afar in relation to surrounding areas. Philos. Trans. Roy.Soc. Lond. Ser. **267**: 339-358.

Hayward, N.J., Ebinger, C.J. (1996). Variations in the along-axis segmentation of the Afar Rift system. Tectonics, **15**: 244–257.

Kazmin, V., Seife Michael Berhe, Nicoletti, M. and Petrucciani, C. (1980). Evolution of the northern part of the Ethiopian Rift. Accad. Naz. Lincei, Rome, **47**: 275–291.

Kearey, P. Brooks. M. and Hill, I. (2002). An Introduction to Geophysical Exploration, 3rd ed., Blackwell Science Ltd. 160 pp.

Keller, G., Harder, S., O'Reilly, B., Mickus, K., Ketsela Tadesse and Maguire, P. (2004). The Eagle Working Group. A preliminary analysis of crustal structure variations along the Ethiopian Rift.

Keranen, K. and Klemperer, S. (2008). Discontinuous and diachronous evolution of the Main Ethiopian Rift: Implications for the development of continental rifts, Earth Planet. Sci. Lett. **265 (1)**: 96–111, doi:10.1016/j. epsl.2007.09.038.

Lakemariam Asfaw, (1992). Constraining the African pole of rotation. Tectonophysics, **209**: 55–63.

Le Turdu, C., Tiercelin, J.J., Gibert, E., Travi, Y., Lezzar, K.E., Richert, J.P., Massault, M., Gasse, F., Bonnefille, R., Decobert, M., Gensous, B., Jeudy, V., Tamrat, E., Mohammed, M.U., Martens, K., Balemwal Atnafu, Tesfaye Cherent, Williamson, D. and Taieb, M. (1999). The Ziway– Shala Lake basin system, Main Ethiopian Rift: influence of volcanism, tectonics and climatic forcing on basin formation and sedimantation. Palaeogeography, Palaeoclimatology, Palaeoecology, **150**: 135–177.

Maguire, P.K.H., Keller, G.R., Klemperer, S.L., Mackenzie, G.D., Keranen, K., Harder, S., O'Reilly, B., Thybo, H., Lakemariam Asfaw, Khan, M.A., Mulugeta Amha (2006). Crustal structure of the Northern Main Ethiopian Rift from the EAGLE controlled source survey; a snapshot of incipient lithospheric break-up.

Maguire, P.K.H., Ebinger, C.J., Stuart, G.W., Mackenzie, G.D., Whaler, K.A., Kendall, J.-M., Khan, M.A., Fowler, C.M.R., Klemperer, S.L., Keller, G.R., Harder, S., Furman, T., Mickus, K., Lakemariam Asfaw, Atalay Ayele, and Bekele Abebe (2003). Geophysical project in Ethiopia studies continental breakup. EOS Trans. AGU. **84 (337)**: 342–343.

Makris, J., Henke, C.H., Egloff, F. and Akamaluk, T. (1991). The gravity field of the Red sea and East Africa. Tectonophysics, **198**: 369 - 381.

Makris, J., Menzel, H., Zimmermann, J. and Gouin, P. (1975). Gravity field and crustal structure of north Ethiopia. Afar Depression of Ethiopia. Schweizerbart, Stuttgart, 135–144.

Meyer, W., Pigler, A., Rosler, A. and Stets, J. (1975). Tectonic evolution of the Main Ethiopian Rift in southern Ethiopia. Schweizerbart, Stuttgart, 352–361.

Mickus, K., Ketsela Tadesse, Keller, G.R. and Befkadu Oluma (2007). Gravity analysis of the Main Ethiopian Rift. Journal of African Earth Sciences, **48**: 59–69.

Mohr, P. (1962). The Ethiopian Rift System. Bulletin of the Geophysical Observatory of Addis Ababa. **5**: 33–62.

Mulugeta Dugda, Nyblade, A.A., Julia, J., Langston, C.A., Ammon, C.J. and Simiyu, S. (2005). Crustal structure in Ethiopia and Kenya from receiver function analysis: implications for rift development in eastern Africa. J. Geophys. Res. 110, B01303, doi:10.1029/2004JB003065.

Reynolds, J.M. (1997). An Introduction to Applied and Environmental Geophysics. John Wiley and Sons limited, England, UK, 415-522 pp.

Rezene Mahatsente, Jentzsch, G. and Jahr, T. (1999). Crustal structure of the Main Ethiopian rift from gravity data: 3-dimensional modeling. Tectonophysics, 363–382.

Searl, R. and Gouin, P. (1972)**.** A gravity Survey of the central part of the Ethiopian Rift Valley. East African Rifts. Tectonophysics, **15 (1/2**): 41-52.

Stuart, G.W., Bastow, I.D. and Ebinger, C.J. (2006). Crustal Structure of the northern Main Ethiopian Rift from receiver function studies. The AfarVolcanic Province within the East African Rift System, SP259. Geol. Soc. Spec. Publ. 253–267.

Tadiwos Chernet, Hart, W. K., Aronson, J. L. and Walter, R. C. (1998). New age constraints on the timing of volcanism and tectonism in the northern main Ethiopian rift–southern Afar transition zone, Ethiopia. Journal of Volcanology and Geothermal Research, **80(3):** 267-280.

Telford, W.S**,** Geldart, L.P and Sheriff, R.E. (1990). Applied Geophysics**.** second edition Cambridge University Press, Cambridge, UK, 784 pp.

Tesfaye Korme, Acocella, V., and Bekele Abebe (2004). The role of pre-existing structures in the origin, propagation and architecture of faults in the Main Ethiopian Rift. Gondwana Res. **7**: 467–479.

Tiberi, C., C. Ebinger, V. Ballu, G. Stuart, and Befkadu Oluma (2005). Inverse models of gravity data from the Red Sea–Aden–East African rifts triple junction zone, Geophys. J. Int. **163**: 775–787, doi:10.1111/j.1365-246X.2005.02736.x.

Tsegaye Abebe, Balestrieri, M.L. and Bigazzi, G. (2010). The Central Main Ethiopian Rift is younger than 8 Ma: Confirmation through apatite fission – track thermochronology, Terra Nova, **22**: 470–476.

Tsegaye Abebe, Mazzarini F., Innocenti F. and Manetti, P. (1998). The Yerer - Tullu Wellel Volcanotectonic Lineament: A transtentional Structure in Central Ethiopia and the associated magmatic activity. J. Afr.Earth Sci. **26**: 135-150.

Tsegay Berhane (2015). Integrated geophysical investigations at the Corbetti-Shala-Aluto segment of the Main Ethiopian Rift: Implications for crustal structure, resources and volcanic hazards. Unpublished MSc Thesis, Addis Ababa University, Addis Ababa, Ethiopia, 118pp.

Ukstins, I., Renne, P., Wolfenden, E., Baker, J. and Menzies, M. (2002). Matching conjugate volcanic rifted margins: 40Ar/39Ar chronostratigraphy of pre- and syn-rift bimodal flood volcanism in Ethiopia and Yemen. Earth Planet. Sci. Lett. **198**: 289–306.

Wolfenden, E., Ebinger, C., Gezahegn Yirgu, Deino, A. and Dereje Ayale (2004). Evolution of the northern Main Ethiopian rift: birth of a triple junction. Earth and Planetary Science Letters, **224**: 213–228.

Wolfenden, E., Ebinger, C., Gezahegn Yirgu, Renne, P. and Kelley, S.P. (2005). Evolution of the southern Red Sea rift: birth of a magmatic margin. Geological Society of America Bulletin, **117**: 846–864.